# MEASUREMENT OF ELECTRIC QUADRUPOLE AND MAGNETIC OCTUPOLE SUSCEPTIBILITIES OF CERTAIN CUBIC PRAESODYMIUM-CONTAINING COMPOUNDS

STANFORD UNIVERSITY

MATTHEW SORENSEN

MARCH 2023

This dissertation is online at: https://purl.stanford.edu/pq544mv9689

I certify that I have read this dissertation and that, in my opinion, it is fully adequate in scope and quality as a dissertation for the degree of Doctor of Philosophy.

**Ian Fisher, Primary Adviser**

I certify that I have read this dissertation and that, in my opinion, it is fully adequate in scope and quality as a dissertation for the degree of Doctor of Philosophy.

**Harold Hwang**

I certify that I have read this dissertation and that, in my opinion, it is fully adequate in scope and quality as a dissertation for the degree of Doctor of Philosophy.

**Steven Kivelson**

Approved for the Stanford University Committee on Graduate Studies.

**Stacey F. Bent, Vice Provost for Graduate Education**

*This signature page was generated electronically upon submission of this dissertation in electronic format.*

# Abstract

Susceptibility, original developed experimentally in the context of magnetic systems, is here applied to the magnetic octupole and two-dimensional electric quadrupole. $PrV_2Al_{20}$ and $PrTi_2Al_{20}$ are motivated as model systems, realizations of electric quadrupole and magnetic octupole order without significant competing lower-order multipolar order (such as magnetic order). Basic methods to probe the susceptibilities are then discussed, with emphasis on the careful use of properties of cubic symmetry to isolate the desired multipolar moments.

A variety of experimental methods to probe the octupolar susceptibility are outlined, using combinations of strain and magnetic field to induce an octupolar moment. Limitations and advantages of each are noted. The AC elastocaloric effect, wherein oscillating strain is used to induce temperature oscillations in a material based on the entropy landscape thereof, is then motivated as a particularly powerful tool for probing the octupolar susceptibility. Experimental data using this technique on $PrV_2Al_{20}$, a system with realized magnetic octupolar order, is presented and analyzed, with a temperature-derivative of the octupolar susceptibility extracted. Lastly, the unique symmetry properties of the two-dimensional electric quadrupole and their implications are discussed in depth. Data is presented using the elastocaloric effect to probe the associated susceptibility in $PrTi_2Al_{20}$.

The efficacy of the techniques used, and limitations thereof, are then discussed, along with potential means of improvement. Further potential applications of the techniques herein developed are briefly noted.

# Acknowledgements

I would like to thank all the members of the Fisher Lab with whom I interacted for their support and patience. For more significant individual contributions, I note that Maja Bachmann and Linda Ye were instrumental in completion of the experimental work involved. Matthias Ikeda developed the primary experimental technique used herein, and engaged in helpful discussions besides. Johanna Palmstrom was particularly helpful at the beginning of my Ph.D. program in showing me around the lab, with Joshua Straquadine and Elliott Rosenberg helping to fill in additional gaps. Lastly, my principal investigator, Ian Fisher, receives my thanks for extraordinary (and perhaps unwise) patience.

My sincere apologies to any whose significant contributions I have forgotten to mention here; it has been a long 7 years.

# Contents

# List of Figures

# List of Tables

# Chapter 1

# Introduction

## 1.1 Motivation

### 1.1.1 Multipolar Order

Multipolar order is foundational to condensed matter physics, with all manner of magnetic (dipole) ordered states and interactions having been studied for decades. Higher-order multipoles, such as quadrupoles and octupoles, remain somewhat less studied, due to the smaller number of relevant materials and the relative difficulty in probing them. Nonetheless, they present a variety of interesting states that have drawn significant attention.

The simplest phenomenon of interest is the ordering of higher-order multipoles. While some quadrupolar systems are quite well characterized, other orders can be quite difficult to detect. Systems with 'hidden order', wherein thermodynamic signatures of a phase transition are discovered but the exact nature of the symmetry-breaking is elusive, have been proposed as candidates for very high-order multipoles [1, 2, 3]; $URu_2Si_2$ was proposed as an example of hexadecapole order, a fifth-order multipole [4].

The Kondo effect, first understood in the context of magnetic (dipole) impurities [5], also has generalizations to higher-order multipoles. Quadrupolar Kondo physics

remains an active area of study, with theoretical predictions regarding scaling behaviors still being realized [6]. Higher-order multipoles can also potentially offer a path to two-channel Kondo behaviors in bulk crystals [7].

The iron pnictide superconductor family often has a spin-density-wave ground state, but has also been noted to have a 'vestigial nematic' phase [8], wherein the rotational symmetry of the tetragonal lattice is broken before the onset of the spin density wave and the breaking of time-reversal and translational symmetries. As this vestigial nematic order, and associated nematic fluctuations, are considered potentially significant in the high-temperature superconductivity [9], the study of nematic order and fluctuations is then of interest in the study of superconductivity. Electric quadrupoles provide one of the simplest realizations of such order, via Jahn-Teller systems such as $TmVO_4$ [10]. Systems even exist containing quadrupolar order, i.e. nematic order, onsetting before a spin-density-wave [11], allowing nematic interactions in systems with magnetic order to be studied within more well-understood phase diagrams.

However, as evidenced by the mere existence of systems with 'hidden order', probing these higher order multipoles is generally not as simple as probing their lower-order magnetic analogues, with magnetization and other well-understood probes being inadequate to the task.

### 1.1.2 Development of Tools to Study Multipolar Order

All of these phenomena of interest then motivate development of new experimental tools that can probe the associated susceptibility of the higher rank multipole, a quantity with numerous benefits in the context of higher-order multipoles. First, it is finite for all temperatures; though it is potentially large only at lower temperatures, the temperature regime wherein it can be measured is nevertheless invariably larger than that of the corresponding ordered state. Next, the divergence of the susceptibility provides evidence for growing fluctuations, providing evidence for a given order parameter without needing to probe the ordered state directly. Finally, it can be measured for a variety of multipoles within the same material, and in the presence

of any order parameter, including simple magnetic order: quadrupolar and octupolar fluctuations can be probed even in systems which ultimately order via magnetic dipole, with strong fluctuations potentially demonstrating conditions that might allow realized quadrupolar/octupolar order within other materials.

To develop such tools, use of a relatively simple system is motivated. Here 4f ion systems are ideal, with their tendency toward localization and the potential $\Gamma_3$ doublet CEF ground state for cubic systems. For systems of this ground state, the doublet can be split by $\Gamma_3$ electric quadrupoles ($3J_z^2 - J^2$, $J_x^2 - J_y^2$) or a $\Gamma_2$ magnetic octupole ($\overline{J_x J_y J_z}$). In particular, the $Pr^3+$ ion is the most common host for such a ground state, with $PrTr_2Al_{20}$ compounds having been experimentally demonstrated to have this $\Gamma_3$ ground state [12]. $PrTi_2Al_{20}$ and $PrV_2Al_{20}$ are then of interest here, for their well-separated $\Gamma_3$ ground state ($40K$ between ground and first excited states [12]), electric quadrupole ordering at $2K$ (Ti) and $0.75K$ (V) [12], and potential octupolar ordering at $0.65K$ in higher-quality $PrV_2Al_{20}$ crystals [13]; these materials are then ideal testbeds to develop tools to study higher-order multipoles without the potential complications arising from lower-order interactions.

Here, we then seek to use $Pr(Ti,V)_2Al_{20}$ to test methods to probe susceptibilities of the magnetic octupole and the multi-dimensional electric quadrupole, via AC elastocaloric effect measurements.

## 1.2 Multipolar Order Background

Before discussing material and experimental methods, a brief discussion on generalized multipolar order is merited. First, the multipole expansion itself is outlined briefly, before specializing to 4f systems, including symmetry properties thereof and how they may be used in the pursuit of higher-order multipoles.

### 1.2.1 The Multipole Expansion

The multipole expansion represents a basis for describing a local electromagnetic charge distribution, representing it as a sum of simply-defined multipolar moments,

with each multipolar moment having separate electric and magnetic versions. The zeroth order multipole is the monopole, representing the mere existence of an electric or magnetic charge; it is then represented by a zeroth order tensor, or simply a scalar value. The first order multipole is then the dipole, representing linear gradients in electric or magnetic charge. It is represented by a vector, or three scalar components $(x, y, z)$, and gives rise to the traditional vector electric or magnetic field. The quadrupole is then represented by a second-order tensor, and represents the lowest-order correction to a distribution that cannot be described entirely via a dipole and monopole moment. n-th order multipoles (with prefixes corresponding to $2^n$) are then generally represented by an n-th order tensor, with the electric or magnetic multipolar moment then needing $2n + 1$ independent terms to be fully described. Figure 1.1 provides an illustration of such multipoles in terms of monopole charge distributions. The series provides a complete basis for describing a given (angular) charge distribution:

$$Q(\theta, \phi) = \sum_{l=0}^{\infty} \sum_{m=-l}^{l} C_l^m R_l^m \tag{1.1}$$

Here $C_l^m$ represents simply the magnitude of a given multipolar moment, with $l$ representing the order of the multipole (0 for monopole, 1 for dipole, etc.), and $m$ representing the $2l + 1$ independent/orthogonal components of that multipole. $R_l^m$ here represents the real spherical harmonics, sometimes called the tesseral spherical harmonics, each corresponding to a different (orthogonal) multipolar moment; they are defined by adding the standard spherical harmonics $Y_l^m$ with their complex conjugates $Y_l^{-m}$:

$$R_l^m = \begin{cases} \frac{1}{\sqrt{2}}(Y_l^{-m} + (-1)^m Y_l^m) & m > 0 \\ Y_l^m & m = 0 \\ \frac{i}{\sqrt{2}}(Y_l^m - (-1)^m Y_l^{-m}) & m < 0 \end{cases} \tag{1.2}$$

where phase is not physically significant, and chosen for visual clarity of Figure 1.1. Equation 1.2 can then represent either the electric or magnetic charge distribution, which, while related, are generally defined separately for convenience.

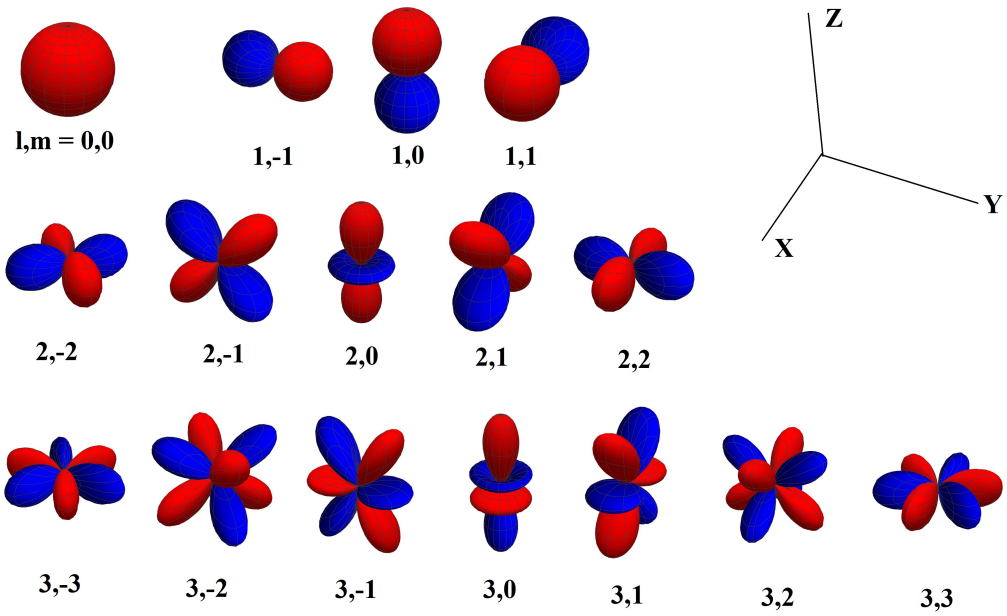


Figure 1.1: Multipolar moments up to 3rd order (octupolar), labeled via their real spherical harmonic $R_l^m$ (see text). Alternating colors then represent alternating magnetic or electric charge, where describing the distributions in terms of charge renders the multipoles visually equivalent.

Of brief note are the varying properties of the two multipole types (electric and magnetic) under inversion symmetry. As the electric field, and similarly the electric dipole, is a vector, and thus odd under inversion, inversion moves the monopole moments without altering them. This causes no change to even-order multipoles (monopole, quadrupole, etc.) while causing a sign change on odd-order multipoles (dipole, octupole, etc), as can be seen via Figure 1.1, where monopole charge is opposite the inversion center of identical or opposing monopole charge for even and odd order multipoles respectively. In contrast, given the magnetic field and dipole are pseudovectors, the magnetic dipole is instead the invariant moment under inversion, moving spatially but not changing sign; in a magnetic charge description, this is equivalent to the magnetic (monopole) charge changing sign under inversion. Thus, the even-order magnetic multipoles are affected by this sign change, while the variation in the odd-order multipoles cancels out with that caused by the spatial inversion itself, and odd-order magnetic multipoles are ultimately invariant under inversion. Here, we restrict ourselves to the more common inversion-invariant multipoles, including even-order electric multipoles (monopole, quadrupole, etc) and odd-order magnetic multipoles (dipole, octupole, etc.); these multipoles can then all be described in terms of $J^l$ operators (where $l$ is the order of the multipole), which will be of significant utility in later descriptions.

The multipole expansion can be viewed as a complete basis of potential symmetry-breaking order parameters. Magnetic dipole order, or simply magnetism, is a cornerstone of condensed-matter physics, but the material exemplars generally fall off as a function of order of the multipole, with the electric quadrupole being a somewhat less frequent subject of study, and the magnetic octupole and higher being quite minimally studied due to the relative rarity. Higher-order multipoles and their interactions are then in a sense a natural continuation from/generalization of the study of magnetism.

### 1.2.2 Utility of 4f Systems in the Study of Multipolar Order

Crystalline structures containing Lanthanide elements are of significant interest in the study of multipolar order for both their tendency to remain relatively localized

and the high angular momentum of 4f electrons. First, 4f electrons tend not to form bands, or only weakly hybridize with conduction electrons; this means that they can often be considered somewhat independently, with local 4f multipolar moments interacting through the lattice or conduction electrons but not forming more complicated Bloch states. Mean-field descriptions are then often particularly apt, and 4f electron behavior can frequently be conceptually described as single ions being acted on by or communicating with each other through some external field.

Next, higher-order multipolar moments require higher angular momentum values to exist, with angular momentum of 1 being required for quadrupolar polarization, for example. Spin-orbit coupling tends to be the dominant interaction, so the experimentally accessible states usually fall within a single $(2J + 1)$-fold degenerate $J$ manifold. With $J$ being a good quantum number, and being generally large ($J = 4$ for the $Pr^3+$ ion of interest here), large multipolar moments may be supported and adequately described by a single-ion Hamiltonian. The $2J + 1$ degeneracy is then often helpfully reduced by interactions with the surrounding crystalline electric field (CEF), leaving a reduced ground-state space of 1-6 states (depending on the ion and local crystal symmetry) to be dealt with, provided temperature is small relative to the CEF splitting. The CEF can then be used to find ground states that support only a limited, specific set of multipoles, which can occasionally allow higher-order multipoles to flourish, if the CEF splitting is large and dipole degrees of freedom are sequestered in energetically-disfavored states.

It should then be briefly noted that Actinides, with partially-filled 5f shells, often have similar properties, such as well-defined, large $J$ values and a tendency not to form bands. However, due to the larger radii of the 5f orbitals, hybridization with conduction electrons can be stronger. This can lead to states of significant physical interest, such as the aforementioned $URu_2Si_2$ [4], but of greater complexity than 4f counterparts; this is then less conducive to testing new methods for probing multipolar order. These electronic properties, combined with the radioactivity of all Actinide elements, leave Lanthanide ions a better candidate for the proposed measurements.

### 1.2.3 Group Theory and CEF Basics

The exact nature of the CEF splitting of a given rare-earth ion is best described in the context of group theory, as applied to crystalline solids. If the ions surrounding a given 4f ion create a symmetry corresponding to a specific point group at the ion site, then the CEF they generate, which splits the $2J + 1$ degeneracy, must maintain that symmetry. The corresponding Hamiltonian will respect the symmetries of this point group, and thus the energy eigenbasis will consist of states unchanged (to within a phase) by the symmetries of the point group, i.e., states belonging to irreducible representations of the point group, for integer values of $J$. Should the given $J$ value be half-integer, the physics of fermions demands the energy eigenstates instead belong to representations of the double group associated with said point group, and these and Kramers' theorem equivalently imply any potential CEF ground state must have a magnetic dipole degree of freedom, unless time reversal symmetry is already broken. Given the aforementioned tendency of magnetism to dominate, and the present interest in isolating higher-order interactions, ions with integer $J$ values are then of more interest, and shall be the focus of this discussion.

While coincidental near-degeneracies of different eigenstates can occur, it then follows that any true multiplet eigenstates, and thus multiplet ground states, can only arise from systems of sufficiently high symmetry, where the local point group symmetry of the 4f ion has at least one 2-dimensional irreducible representation. When such multiplets exist, generally only in systems of tetragonal or higher symmetry (hexagonal and cubic), the opportunity arises for spontaneous symmetry-breaking to reduce the degeneracy, which can then be described in terms of multipolar interactions. Group theory and symmetry then demand that multipolar moments that could arise to break this degeneracy belong to specific irreducible representations, i.e. break specific point group symmetries while preserving others. Given the underlying degeneracy arises from point group symmetries, rather than from time-reversal symmetry (Kramers' Theorem), the multipolar interactions which dominate are then often non-magnetic.

To illustrate with a relatively simple example, 4f ions (of integer $J$) experiencing a CEF of tetragonal $D_{2d}$ symmetry, such as the $Tm^{3+}$ of the aforementioned $TmVO_4$,

have only one symmetry option for a potential multiplet ground state, a doublet, as illustrated in Table 1.1. Any doublet ground state must then be of $\Gamma_5$ symmetry (singlet ground states have no degeneracy to allow for spontaneous symmetry-breaking multipolar order, and are not of interest here). In the case of point-group induced degeneracies, any multipole which would remove the degeneracy must belong to an irreducible representation arising from the product of the ground-state irreducible representation with itself, i.e.

$$\Gamma_5 \otimes \Gamma_5 = \Gamma_1 \oplus [\Gamma_2] \oplus \Gamma_3 \oplus \Gamma_4 \tag{1.3}$$

The $\Gamma_1$ component, a symmetry-preserving term present in all such irreducible representation products, represents multipoles such as the monopole, which cannot break the symmetry or the degeneracy, and can thus be safely ignored for the present discussion. Analogously to the case of a $\frac{1}{2}$ spin doublet, we then expect three multipoles, represented by 3 corresponding operators, to be capable of breaking the degeneracy, and potentially giving rise to an ordered state. For $\Gamma_2$, the irreducible representation product requires it be time-reversal-symmetry odd, for reasons best left to a dedicated group theory text. As can be seen in Table 1.1, the simplest multipole operator of this symmetry is $J_z$, corresponding to a magnetic dipole (along the $z$ axis). However, no such $J_i$ functions exist for $\Gamma_3$ and $\Gamma_4$, and the remaining magnetic analogues, $J_x$ and $J_y$, are of $\Gamma_5$ symmetry; as $\Gamma_5$ is not part of the sum composing $\Gamma_5 \otimes \Gamma_5$, the doublet states cannot support a magnetic dipole along these axes (should the energy splitting of the CEF be weak enough, or an applied magnetic field strong enough, magnetic interactions may occur via admixing of other, higher-energy CEF eigenstates). Hence, the other two operators capable of splitting the doublet, of $\Gamma_3$ and $\Gamma_4$ symmetries, are non-magnetic.

Specifically, the lowest-order (inversion-invariant) operators corresponding to $\Gamma_3$ and $\Gamma_4$ are $J_x^2 - J_y^2$ and $J_xJ_y + J_yJ_x$, corresponding to electric quadrupoles of the given symmetries. The three operators capable of splitting the doublet, in the pseudo-spin analogy, are the $\Gamma_2$ magnetic dipole along the c-axis $J_z$ and the electric quadrupoles of $\Gamma_3$ and $\Gamma_4$ symmetries, $J_x^2 - J_y^2$ and $J_xJ_y + J_yJ_x$ respectively. Which symmetry

| $D_{2d}$ | $E$ | $2S_4$ | $C_2(z)$ | $2C_2'$ | $2\sigma_d$ | Lowest-order Multipole |
|---|---|---|---|---|---|---|
| $\Gamma_1$ | $+1$ | $+1$ | $+1$ | $+1$ | $+1$ | $J^2$,$J_z^2$ |
| $\Gamma_2$ | $+1$ | $+1$ | $+1$ | $-1$ | $-1$ | $J_z$ |
| $\Gamma_3$ | $+1$ | $-1$ | $+1$ | $+1$ | $-1$ | $J_x^2 - J_y^2$ |
| $\Gamma_4$ | $+1$ | $-1$ | $+1$ | $-1$ | $+1$ | $\overline{J_x J_y}$ |
| $\Gamma_5$ | $+2$ | $0$ | $-2$ | $0$ | $0$ | $(J_x,\ J_y)$ |

Table 1.1: Character table for point group $D_{2d}$, with lowest-order (inversion-even) multipole via $J$ operators. Lines over operators represent symmetrized products thereof.

channel/operator ultimately orders is material-dependent, as is the relation between different $4f$ ions; $TmVO_4$ ultimately reduces the degeneracy via a cooperative Jahn-Teller effect breaking $\Gamma_4$ [10] symmetries, acquiring a ferro-quadrupolar order parameter. Other tetragonal materials could (and do [11]) order in the $\Gamma_2$ or $\Gamma_3$ channels, and could potentially order in an anti-ferro manner; the local ion symmetry has little to say on how ions interact with each other.

### 1.2.4 Conditions for Higher-Order Multipoles

To continue the tetragonal example, higher-order multipoles, such as octupoles, while not strictly forbidden, are unlikely; in whatever symmetry channel the system has a tendency to order in, there will be a lower-order multipole which the given higher-order multipole must out-compete, an unlikely prospect given the energy scales of multipolar interactions tend to decrease as the order of the multipole increases. To pursue more exotic multipoles, examining the generally less-studied systems of higher symmetry is then motivated.

Cubic symmetry, in particular, is an ideal candidate for the exploration of higher-order multipoles in 4f systems due to one potential CEF ground state. For the specific ion symmetry $T_d$, as can be seen in Table 1.2, there exist three potential multiplet ground states: $\Gamma_3$, $\Gamma_4$, and $\Gamma_5$. Magnetic dipoles here belong to the $\Gamma_4$ symmetry; as such, the $\Gamma_4$ and $\Gamma_5$ triplets are of less interest here, given their potential to support magnetic dipole moments:

| $T_d$ | $E$ | $8C_3$ | $3C_2$ | $6S_4$ | $6\sigma_d$ | Lowest-order Multipole |
|---|---|---|---|---|---|---|
| $\Gamma_1$ | +1 | +1 | +1 | +1 | +1 | $J^2$ |
| $\Gamma_2$ | +1 | +1 | +1 | −1 | −1 | $\overline{J_xJ_yJ_z}$ |
| $\Gamma_3$ | +2 | −1 | +2 | 0 | 0 | $(2J_z^2 - J_x^2 - J_y^2,\ J_x^2 - J_y^2)$ |
| $\Gamma_4$ | +3 | 0 | −1 | +1 | −1 | $(J_x, J_y, J_z)$ |
| $\Gamma_5$ | +3 | 0 | −1 | −1 | +1 | $(\overline{J_yJ_z},\ \overline{J_zJ_x},\ \overline{J_xJ_y})$ |

Table 1.2: Character table for point group $T_d$, with lowest-order (inversion-even) multipole via $J$ operators. Lines over operators represent symmetrized products thereof.

$$\Gamma_4 \otimes \Gamma_4 = \Gamma_5 \otimes \Gamma_5 = \Gamma_1 \oplus \Gamma_3 \oplus [\Gamma_4] \oplus \Gamma_5 \tag{1.4}$$

The $\Gamma_3$ doublet, however, offers a more limited potential slate of order parameters:

$$\Gamma_3 \otimes \Gamma_3 = \Gamma_1 \oplus [\Gamma_2] \oplus \Gamma_3 \tag{1.5}$$

The lowest-order multipoles in the available channels are then the magnetic octupole $\overline{J_xJ_yJ_z}$ in $\Gamma_2$ and the two-dimensional electric quadrupole space spanned by $3J_z^2 - J^2$ and $J_x^2 - J_y^2$ in $\Gamma_3$. The $\Gamma_3$ doublet is then a 'non-magnetic' doublet, in the sense that magnetic field cannot, to first order, split the doublet; the states cannot carry a magnetic dipole moment, and magnetic polarization requires admixture of other CEF eigenstates. This creates ideal conditions for higher-order multipolar interactions to dominate, provided the doublet is both the ground state and well-separated energetically from other eigenstates.

### 1.2.5 Associated Susceptibilities

With the quadrupole and octupole order parameters thus isolated via careful selection of CEF ground state, means to measure the susceptibility are of interest. Taken in a general sense, a susceptibility is the derivative of an order parameter ($\psi$) with respect to some conjugate field ($h$), evaluated at 0 field, i.e.

$$\chi_\psi = \left.\frac{d\psi}{dh}\right|_{h=0} \tag{1.6}$$

The two essential components to determining the susceptibility are then a conjugate field capable of coupling to the order parameter and a means of measuring the order parameter. To have a linear relationship with the order parameter, the field must be of identical symmetry; thus, the field must be of $\Gamma_2$ symmetry for the octupole, and $\Gamma_3$ symmetry for the quadrupole. As will be discussed in Chapters 3-5, this can be achieved via a $\Gamma_3$ strain for the quadrupole, or the careful combination of $\Gamma_4$ magnetic field and $\Gamma_5$ strain into a $\Gamma_2$ product field for the octupole. A variety of methods for measuring the octupole, specifically, are then discussed in chapter 3. The elastocaloric effect is then utilized to directly probe octupolar and quadrupolar susceptibilities in chapters 4 and 5 respectively. The fundamental mathematics of the experimental technique are outlined in chapter 2, and the details of its application to the order parameters in question covered in chapters 4 and 5. Briefly, the technique is capable of measuring the strain-derivative of entropy, $\frac{\partial S}{\partial \epsilon}$. Entropy can then be determined as a function of applied field, allowing the energetic splitting of the $\Gamma_3$ doublet states, and thus the magnitude of the induced order parameter, to be measured.

It is then of brief note that, given the elastocaloric effect measures $\frac{\partial S}{\partial \epsilon}$, it is effectively a probe of the temperature derivative of an associated elastic stiffness constant. Given the entropy can be defined via the Helmholtz free energy $F$, via $S = \frac{dF}{dT}\big|_V$, one can note that, in the limit of vanishing strain,

$$\frac{\partial S}{\partial \epsilon} = -\frac{\partial}{\partial \epsilon}\left(\frac{dF}{dT}\right) = -\frac{d}{dT}\left(\frac{\partial^2 F}{\partial \epsilon^2} d\epsilon\right) \tag{1.7}$$

where $\frac{\partial^2 F}{\partial \epsilon^2}$ is then the associated elastic stiffness component $C_{\epsilon,\epsilon}$ for the given strain component $\epsilon$, which may be any single strain-tensor component, expressed in an arbitrary basis.

## 1.3 $PrV_2Al_{20}$ and $PrTi_2Al_{20}$

### 1.3.1 $Pr^{3+}$ Ion

The $\Gamma_3$ doublet, thus motivated as an ideal ground state for probing higher-order multipoles, must then be found in a physical system. Beyond the aforementioned constraint of cubic symmetry, the ground state must then be $\Gamma_3$, rather than any other eigenstate, and would ideally be well-separated. As discussed earlier, $J$ is generally a good quantum number. Thus, CEF Hamiltonians of cubic symmetry can be constructed for a variety of (integer) $J$ values, and the CEF parameters varied so as to see which $J$ values lead to Hamiltonians that can achieve the desired ground state, or where the doublet ground state exists across the widest range of parameters. This calculation, performed by Lea, Leasq, and Wolfe [14], suggests $J = 4$ as the ideal candidate for such a system, with $J = 6, 8$ being alternative options wherein the doublet ground state is less well-separated from excited states and exists over a somewhat smaller Hamiltonian parameter space. Viewing the rare earth ions, $Pr^{3+}$ and $Pm^{3+}$, will generally take the $J = 4$ state. Given the radioactivity of $Pm^{3+}$, $Pr^{3+}$ becomes the preferred candidate.

With the focus thus narrowed to $Pr^{3+}$ materials, here we choose to focus on $PrTi_2Al_{20}$ and $PrV_2Al_{20}$. These compounds are notable for their cubic symmetry, $\Gamma_3$ ground state, quadrupolar ordering at 2K (Ti) and 0.75K (V), and proposed octupolar ordering at 0.65K in $PrV_2Al_{20}$.

### 1.3.2 Structure and Crystalline Electric Field

Both compounds share an identical structure, wherein the Pr and V or Ti ions are encased in Al Frank-Kasper shells [15]; see Figure 1.2. The Pr sublattice, in particular, forms a diamond structure, giving each Pr ion the aforementioned tetrahedral symmetry of point group $T_d$ (Al and Ti/V ions do not reduce this local symmetry). This gives rise to two distinct crystallographic sites for the Pr ion, and makes the crystal as a whole $O_h$ symmetry. The sites, being related by an inversion operation, could then potentially react differently to applied fields breaking inversion symmetry.

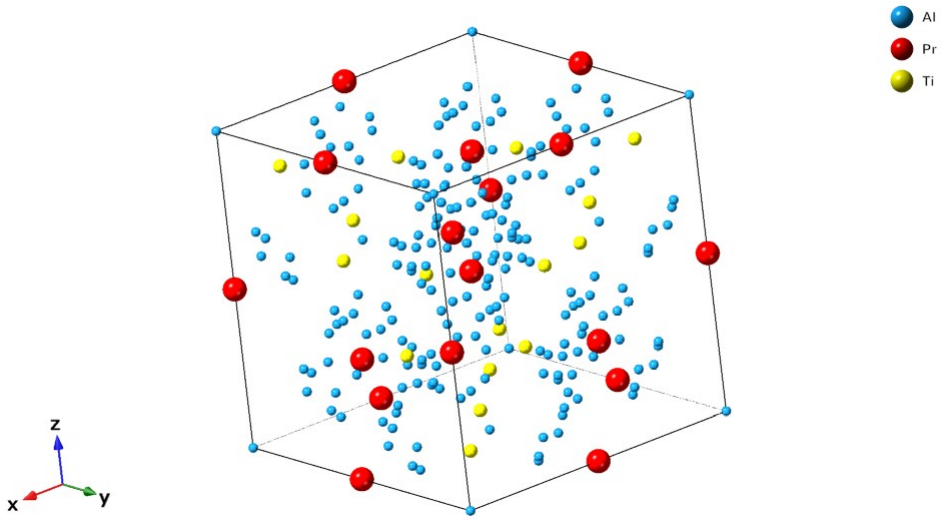


Figure 1.2: Structure of $PrTi_2Al_{20}$ via Okuyama et al [15]

Such fields are not of interest herein, and thus the sites can be considered identical for the purposes of discussing the related experiments. An inversion-even field will induce an equivalent distortion on all sites, and thus a ferro-type order parameter, in a manner well-described by a single-ion Hamiltonian with mean-field components.

The CEF splitting of the $J = 4$ manifold, via inelastic neutron scattering experiments [15], creates a $\Gamma_3$ ground state. Inelastic neutron scattering, heat capacity Schottky peaks [12], and magnetization anisotropy [17] suggest a first excited state of $\Gamma_4$ for Ti, separated by 60K, and $\Gamma_5$ for V, separated by 40K (Figure 1.3).

### 1.3.3 Ordered States and Related Properties

Both systems have quadrupolar order onset at low temperatures, with a ferro-quadrupolar phase transition in $PrTi_2Al_{20}$ at $\sim$ 2K, and an anti-ferro-quadrupolar phase transition in $PrV_2Al_{20}$ at $\sim$ 0.75K [12, 13], as shown in heat capacity data (Figure 1.4). Both phase transitions are necessarily first-order due to symmetry considerations. Softening of elastic modes associated with these quadrupolar phase transitions is minimal, suggesting the quadrupolar interactions are primarily mediated by conduction electrons, rather than the lattice [18]. $PrV_2Al_{20}$ additionally has a proposed octupolar phase transition at $\sim$ 0.65K [13], evidenced in heat capacity data (Figure 1.5). This

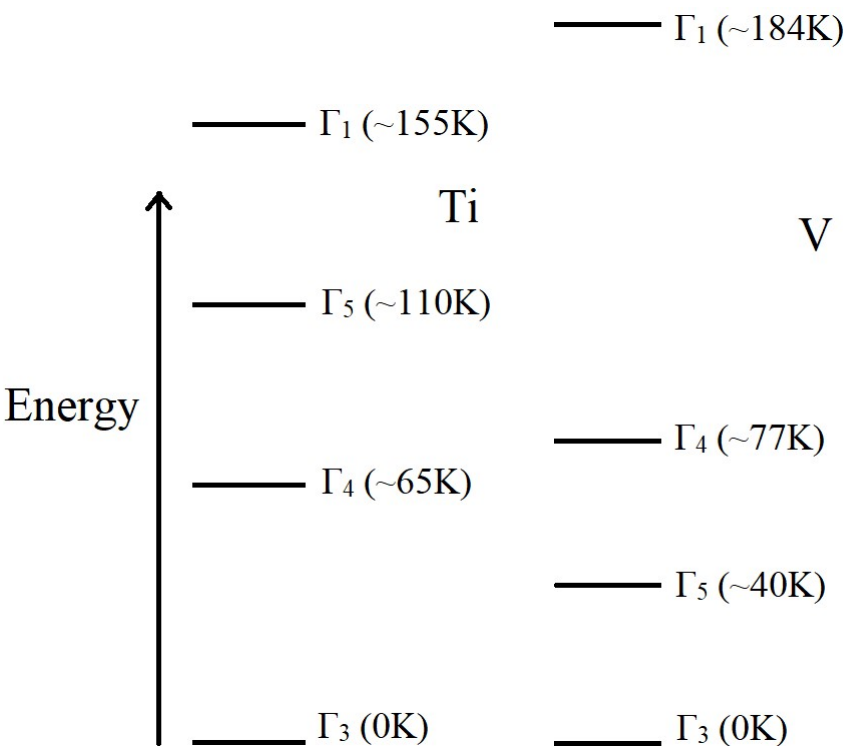


Figure 1.3: CEF Splitting for $PrTi_2Al_{20}$ (left) via Sato et al [16] and $PrTi_2Al_{20}$ (right) via Araki et al [17]

is, however, not observed in anything but the highest-quality crystals, as defined by residual resistivity ratio (RRR) [13], suggesting it is quite sensitive to disorder.

$PrV_2Al_{20}$ additionally has well-documented quadrupolar Kondo behavior [19], likely partially responsible for its relatively lower quadrupolar transition temperature [12]. Both systems also contain superconducting phase transitions, at 200mK for $PrTi_2Al_{20}$ [20] and 50mK for $PrV_2Al_{20}$ [21], notable for the potential role of quadrupolar and/or octupolar fluctuations. While the techniques herein developed may be of some interest in studying these phenomena, probing of Kondo behaviors and the superconducting states is outside the scope of the present work.

## 1.4 Summary

Higher-order multipolar interactions are of interest for a variety of reasons, from exotic interactions and ordered states to model nematic systems potentially relevant to superconductivity. They can be considered an extension or generalization of magnetic order, but with a substantially less developed set of experimental tools. Susceptibility, in particular, is then of interest in this context due to the extensive information it can provide about these interactions above, or even in the absence of, a phase transition.

The development of such tools is best achieved through comparatively simple model systems. Localized 4f systems provide a platform capable of supporting such higher-order multipoles, and, through the Crystalline Electric Field (CEF), materials that can have well-defined symmetry properties. The unique symmetry properties of cubic systems, and specifically the allowed $\Gamma_3$ doublet ground state, allow these higher-order multipoles to be energetically separated from lower-order multipolar interactions which would otherwise generally dominate. The combination of these concepts then presents a model system in the form of cubic $Pr^{3+}$ compounds.

$PrV_2Al_{20}$ and $PrTi_2Al_{20}$ then present themselves as realizations of the unique $\Gamma_3$ doublet ground state. Both compounds have realized quadrupolar ordering at low temperatures, with $PrV_2Al_{20}$ additionally having potential octupolar order at even lower temperatures. Both systems additionally have a variety of exotic behaviors associated with these ordered states, including Kondo effects and superconductivity. They

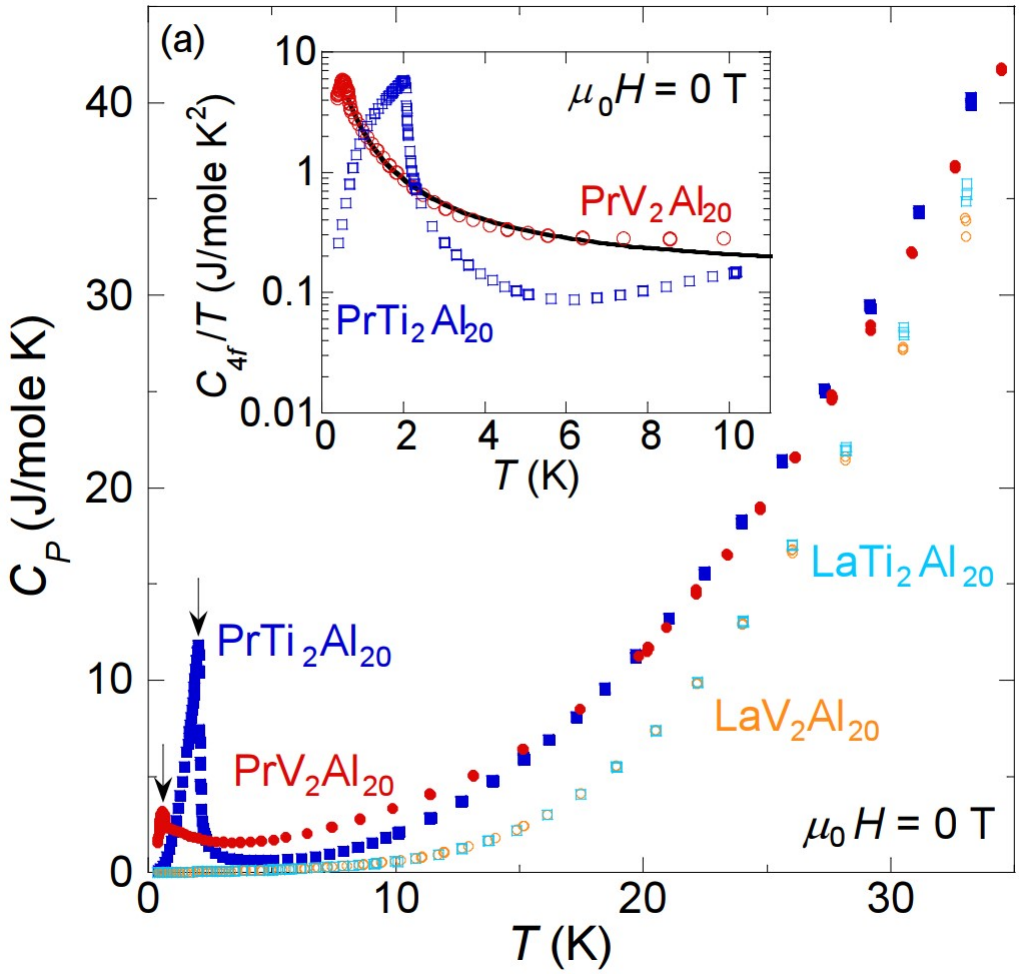


Figure 1.4: Heat Capacity for $PrTi_2Al_{20}$ and $PrV_2Al_{20}$, and their lanthanum analogues (with no 4f electrons). Reproduced from: Akito Sakai and Satoru Nakatsuji 2012 J. Phys.: Conf. Ser. **391** 012058. Used without modification under the terms of Creative Commons Attribution 3.0 (CC BY 3.0) license.

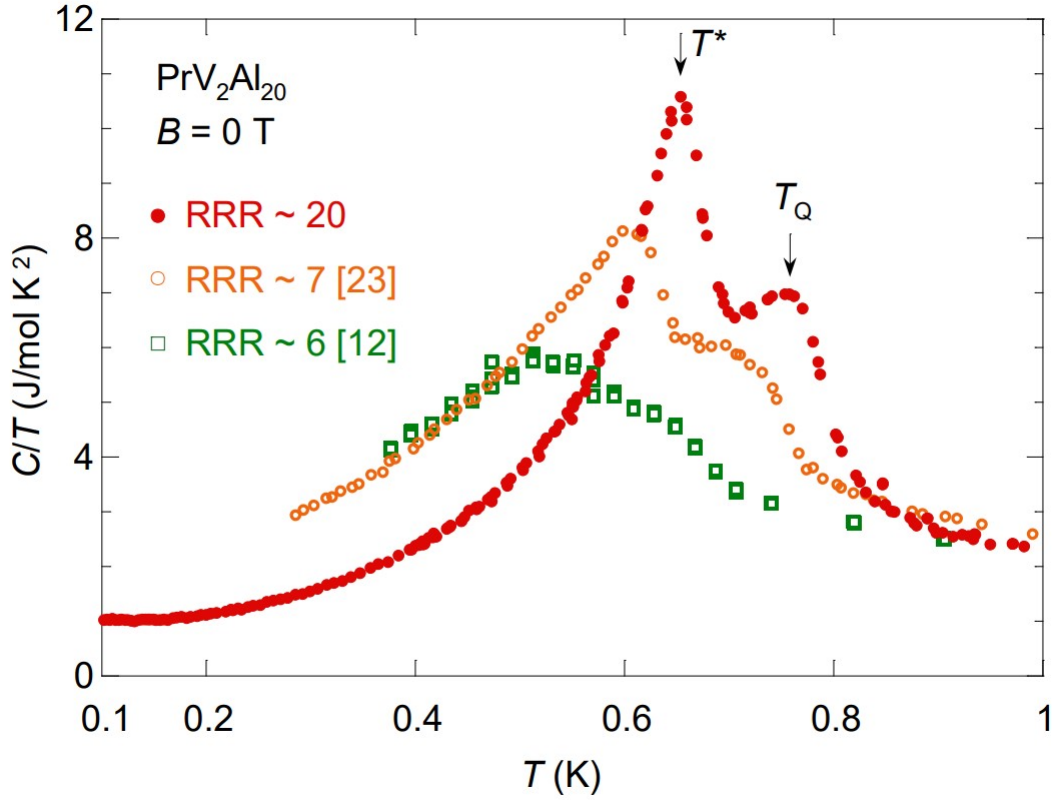


Figure 1.5: Heat Capacity for $PrV_2Al_{20}$ crystals of varying quality, as defined by RRR (residual resistivity ratio). Reproduced from: M Tsujimoto et al. Anomalous specific heat behaviour in the quadrupolar Kondo system PrV2Al20. 2015 J. Phys.: Conf. Ser. **592** 012023. Used without modification under the terms of Creative Commons Attribution 3.0 (CC BY 3.0) license.

are thus ideal candidates for susceptibility measurements, both as realizations of multipolar order wherein susceptibility techniques may be tested, and as systems where measuring susceptibilities, and thus fluctuation strength, could eventually provide a unique perspective on more exotic phenomena that are not as firmly understood.

## 1.5 Layout of this Dissertation

This dissertation consists primarily of three papers, chapters 3-5, in varying stages of publication, edited lightly for inclusion herein. Chapter 2 discusses the experimental methods used, including the AC elastocaloric effect, in more depth than the individual papers. Chapter 3 contains various potential methods for isolating and probing the octupolar susceptibility within cubic $Pr^{3+}$ compounds. Chapter 4 discusses utilizing the elastocaloric effect to probe $PrV_2Al_{20}$ and ultimately extract a quantity proportional to the octupolar susceptibility. Chapter 5 will explain some of the unique characteristics of quadrupolar order with multi-dimensional symmetry, before using the elastocaloric effect to probe quantities proportional to the quadrupolar susceptibility, and ultimately drawing conclusions on the form of these quadrupolar fluctuations in $PrTi_2Al_{20}$. Finally, chapter 6 will discuss broader conclusions from all 3 publications and briefly touch upon potential future directions for continuation of the work done thus far.

# Chapter 2

# Experimental Methods

## 2.1 Single-Crystal $PrV_2Al_{20}$ and $PrTi_2Al_{20}$

### 2.1.1 Crystal Growth

Crystals were grown via the self-flux method, as outlined by Sakai and Nakatsuji [12]. Aluminum shot (Puratronic, 99.999%), praesodymium chunk (Ames Laboratory, 99.99%), titanium sponge (Alfa Aesar, 99.95%), and vanadium pellets (ESPI Metals, 99.9%) were used. Elements were placed into 2mL alumina "Canfield" crucibles [22] (LSP Ceramics), consisting of two identical crucibles (13mm outer diameter, 25mm height) separated by a sieve, in ratios 97:2:1 Al:(Ti,V):Pr. The full crucibles were then placed in 2mm-thick quartz tubes (inner diameter 14mm) with one end sealed, with approximately 1 cm of quartz wool (gently compressed) placed above and below the crucibles. The unsealed end of the quartz tube was then narrowed via hydrogen torch just above the crucibles. The half-tubes of quartz were then placed under vacuum and purged three times by filling with argon gas (Ultra High Purity/UHP, 99.999%, Airgas) and reducing to vacuum each time (30mTorr base pressure), before filling again with approximately 0.4 barr argon and finally sealing the quartz tube. Extra-thick quartz and argon gas were used to reduce the effects of aluminum vapor attack on quartz.

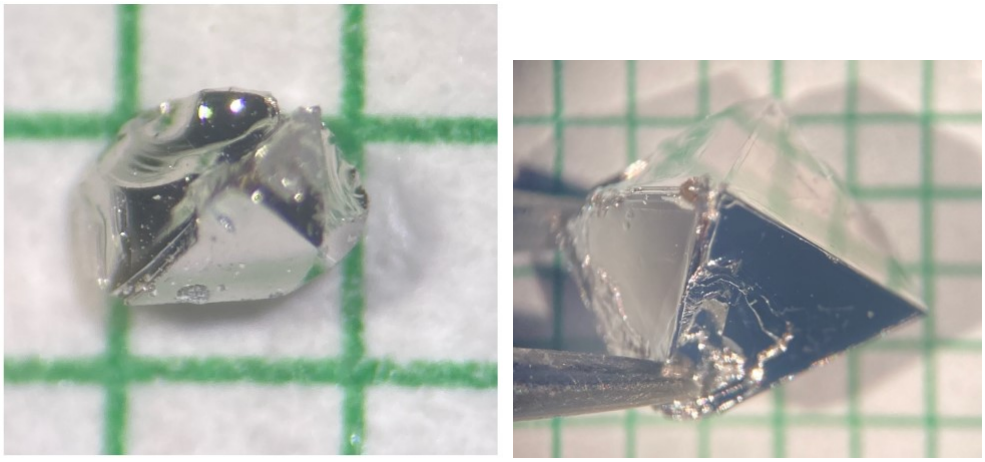

Figure 2.1: Typical $PrTi_2Al_{20}$ (left) and $PrV_2Al_{20}$ (right) crystals, on millimeter paper for scale, with triangular octahedron facets clearly visible.

The sealed ampoules were placed in high-temperature furnaces, with the element-containing crucible below the sieve and (upside-down) secondary crucible. Temperature was raised from room temperature to 1200C over approximately 12 hours, then held at 1200C for another 12 hours, to allow the praesodymium and vanadium or titanium to fully dissolve within the molten aluminum. Temperature was then reduced at a rate of 1C/.5C per hour (for $PrTi_2Al_{20}$ and $PrV_2Al_{20}$, respectively) to 1000C, at which point the quartz ampoules were removed from the furnaces as quickly as possible and placed into centrifuges, upside-down relative to their original/furnace orientation. The ampoules were then spun at 2k RPM (causing them to orient horizontally), with the centrifuges being disabled upon the centrifuge reaching the set spin-rate. This caused much of the molten aluminum to flow outward through the sieve to the secondary crucible, while any solids of adequate size were caught on said sieve and remained within their original crucible. The quartz was then broken with sufficient pressure, and the crystals gently chipped off of the sieve or crucible, which residual solidified aluminum had often attached them to.

### 2.1.2 Characterization

Crystals grew with an octahedral morphology, with varying degrees of perfection, with edge lengths ranging from .2-1mm for $PrTi_2Al_{20}$ or 1-5mm for $PrV_2Al_{20}$ (Figure 2.1). $PrV_2Al_{20}$ crystals generally grew as well-separated crystals, or as part of a twin, while $PrTi_2Al_{20}$ were occasionally found as single well-separated crystals but were generally more likely to grow in 'rafts,' wherein many crystals were joined together along a 2d plane. Structure was verified via powder x-ray, and composition via energy dispersive spectroscopy (EDS). No other phases were found within the $PrV_2Al_{20}$ growths, though crystals viewed under a scanning electron microscope had occasional microscopic inclusions of aluminum flux of diameter 1-50 $\mu m$. $PrTi_2Al_{20}$ growths were found to sometimes contain the contaminant $TiAl_3$ phase, which was identifiable by its tendency to grow in wide 2d plates, with very flat surfaces, rather than the 'pyramid' covered surfaces of $PrTi_2Al_{20}$ rafts. The contaminant phase could then be reliably avoided simply by choosing crystals based on crystal habit.

### 2.1.3 Preparation of Samples for Elastocaloric Effect Measurements

AC elastocaloric effect measurements generally required specific sample dimensions, with rectangular prism shapes being preferred. The need to secure the crystal in clamps, and further to attach thermometry to a region of the sample not covered by said clamps, imposed a minimum length requirement of 1mm, with additional length generally helping the process. The orthogonal dimensions were then limited by the blocking force of the piezoelectric mechanisms used to induce strain. Finite width was needed for attaching the aforementioned thermometry, so minimal thickness was preferred.

Crystals were thus prepared for measurement via polishing into bar shapes, generally 1.5-2mm in length, .5-1mm in width, and .05-.1mm thickness. Crystals were attached to a flat surface, usually a glass microscope slide, via wax. They were then polished with sandpaper of progressively higher grits until the bar was formed with thickness of 500 $\mu m$, at which point diamond lapping film of progressively smaller

sizes was used, culminating in .1 $\mu m$ lapping film being used to bring the bar to approximately 50 $\mu m$ in thickness, so as to reduce required force per unit strain.

The long axis was chosen to be either the [111] (octupolar measurement) or [110] (quadrupolar measurement) crystal axis. [111] was reliably chosen by constructing a bar with long axis perpendicular to a facet. This was generally done by attaching the facet to a glass microscope slide such that it hung over the edge, then polishing until a surface was created flush with the side of the glass slide. This surface then contained the desired long axis, and could be attached to another slide and polished down in the standard way into a bar shape. [110] was most easily achieved simply by constructing a bar whose long axis was parallel to an edge, and thus could be created simply by polishing down from any given triangular facet. The precise orientation of the plane perpendicular to the long axis of the bar was generally not significant and not controlled for, though its orientation was recorded. Orientation was confirmed by x-ray for [111] samples given their somewhat more involved process.

## 2.2 AC Elastocaloric Effect Measurements

Elastocaloric effect (ECE) measurements were carried out in a manner similar to that of Ikeda et al [23], using a commercial Razorbill CS-100 uniaxial strain cell. The process is reproduced here briefly for completeness.

### 2.2.1 Theory of Measurement

In materials with strong responses to strain of any given symmetry, be it a highly strain-dependent phase transition temperature or a strain-coupling order parameter, changes in strain must induce changes in entropy. However, if the strain is applied quickly enough, via an AC strain at a sufficiently high frequency, heat may not be able to flow fast enough to equilibrate, and for sufficiently high frequencies, the change in entropy must then be zero (see section 2.2.6). This implies that any strain-induced change in entropy must be converted into a temperature fluctuation:

$$dS = \frac{\partial S}{\partial \epsilon} d\epsilon + \frac{\partial S}{\partial T} dT = 0 \tag{2.1}$$

$$\left(\frac{dT}{d\epsilon}\right)_S = -\frac{\partial S}{\partial \epsilon}\left(\frac{\partial S}{\partial T}\right)^{-1} = -\frac{\partial S}{\partial \epsilon}\frac{T}{C_V} \tag{2.2}$$

It then follows that, should this adiabatic condition be achieved, the strain-dependence of the entropy, $\frac{\partial S}{\partial \epsilon}$, can be probed via this temperature fluctuation, provided the constant-volume heat capacity $C_V$ is known or can be approximated.

Here, we define the uniaxial strain via the deformation, $\epsilon = \frac{\Delta L}{L}$, where $L$ is the length of the sample along the primary strain axis. Strain is a second-rank tensor, and so there are 6 total independent components. Defining the primary strain axis as $x$ for convenience, the relations above then reflect the effects of $\epsilon_{xx}$; equation 5.3 is strictly accurate only when all 5 orthogonal strain tensor components ($\epsilon_{ij}$ for $i \neq j$, $\epsilon_{yy}$ $\epsilon_{zz}$) are held constant, though different strain bases may be used.

Experimentally, however, the actual thermodynamic constraint is instead that all orthogonal components of the stress tensor are held constant, i.e. $\sigma_{ii}$ for $i \neq x$ and $\sigma_{ij}$ for $i \neq j$ are held constant. This gives rise to a more complicated relation involving the experimentally-measured strain (stress is not directly probed):

$$dS = \frac{\partial S}{\partial \epsilon_{xx}} d\epsilon_{xx} + \frac{\partial S}{\partial \epsilon_{yy}} d\epsilon_{yy} + \frac{\partial S}{\partial \epsilon_{zz}} d\epsilon_{zz} + \frac{\partial S}{\partial T} dT = 0 \tag{2.3}$$

$$\left(\frac{dT}{d\epsilon_{xx}}\right)_S = -\left(\frac{\partial S}{\partial \epsilon_{xx}} + \frac{\partial S}{\partial \epsilon_{yy}}\frac{d\epsilon_{yy}}{d\epsilon_{xx}} + \frac{\partial S}{\partial \epsilon_{zz}}\frac{d\epsilon_{zz}}{d\epsilon_{xx}}\right)\left(\frac{\partial S}{\partial T}\right)^{-1} \tag{2.4}$$

The temperature fluctuation $dT$ then depends on multiple entropy derivatives in a slightly complicated fashion. However, when the partial derivative of the entropy with respect to one specific strain is significantly larger than the others, or otherwise distinguishable via unique dependencies, this can simplify to equation 5.3, though potentially with an additional multiplier in the form of a Poisson ratio. This comes with the caveat that dependencies of the Poisson ratios $\frac{d\epsilon_{yy}}{d\epsilon_{xx}}$ and $\frac{d\epsilon_{zz}}{d\epsilon_{xx}}$ on various factors, such as temperature, could then be introduced into the measured temperature fluctuation, given the measured $dT$ is normalized via a measured $d\epsilon_{xx}$, and $d\epsilon_{yy}$ and $d\epsilon_{zz}$ are

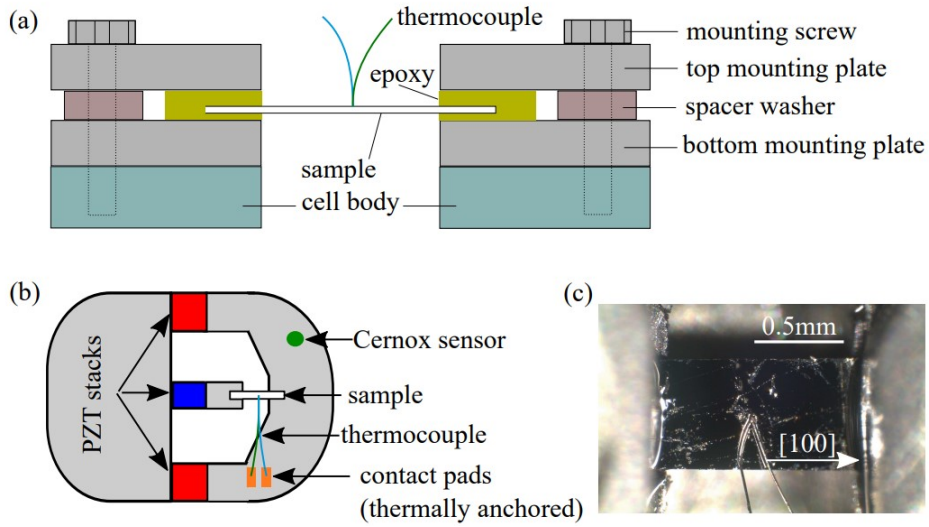


Figure 2.2: Schematic diagram of Razorbill CS-100 strain cell from profile (a) and top-down (b), with example sample of $BaFe_2As_2$ (c) for scale. Reprinted from M.S. Ikeda et al. "AC elastocaloric effect as a probe for thermodynamic signatures of continuous phase transitions". In: Rev. Sci. Instrum. 90 (2019), p. 083902, with the permission of AIP Publishing.

not measured; this is especially true if the entropy derivatives $\frac{\partial S}{\partial \epsilon_{ii}}$ are distinguished by functional form rather than by some having negligible amplitude, as will be the case in the experiments conducted in chapters 4 and 5 (although a different strain basis will be used, that of irreducible representations). This complication will be discussed in more depth in the relevant chapters, wherein the change of basis is introduced and justified, and the entropy derivatives distinguished within this alternative basis.

### 2.2.2 Experimental Setup

The Razorbill CS-100 commercial strain cell was utilized as the primary means of applying strain, used in the manner prescribed by Ikeda et al [23]. The cell is illustrated in figure 2.2. The three piezoelectric stacks are arranged so as to cancel the effects of their thermal contraction on the sample. The sample then experiences thermal-contraction-induced stress only via the difference between the natural thermal contraction of the sample and the titanium used in the construction of the cell

body; thermal contraction of the piezoelectric stacks does not affect the sample. The cell additionally contains flexures (not pictured) to reduce motion of the central island (wherein one side of the sample is mounted) towards either outer piezoelectric stack, and thus minimize stress on the sample along axes orthogonal to the piezoelectric stack axis.

A Quantum Design Physical Property Measurement System (PPMS), with 14T maximum magnetic field, was used to achieve cryogenic temperatures. The base temperature of the system was approximately 1.8K, meaning the transition temperatures of the $PrV_2Al_{20}$, $0.75K$ and $0.65K$ [12], were not accessible, and the ability to probe the transition of $PrTi_2Al_{20}$ at 2K [12] was limited. This was not considered a major drawback, given the purpose of the measurements described in this thesis was to study the relevant multipolar susceptibilities above the critical temperatures.

### 2.2.3 Sample Mounting

First, two of the Razorbill sample plates were secured to the cell body in their standard position, with Loctite Stycast 2850FT epoxy being added for additional stability. The sample was then secured to the sample plates via Stycast (Figure 2.3). The final two mounting plates were placed above and their respective mounting screws tightened, with additional stycast being added via the holes in the mounting plates to ensure the sample was well-connected mechanically with all mounting plates. Finally, a thermometer, anchored to the rest of the cell via gold wires, was gently manipulated into place, and a gold wire used to connect the sample to the thermometer. Connections between gold wires and thermometer/sample were secured with EPO-TEK H20E conductive epoxy. See 2.2.5 for more information on thermometry utilized.

### 2.2.4 Strain Application and Measurement

Strain was applied via the piezoelectric stacks of the CS-100 cell. Applying voltage to the three stacks caused each to apply stress, and by applying voltages of opposite signs to the inner stack and the outer stacks, the effects of multiple piezoelectric stacks could be effectively added together. DC voltage could then be applied to create large

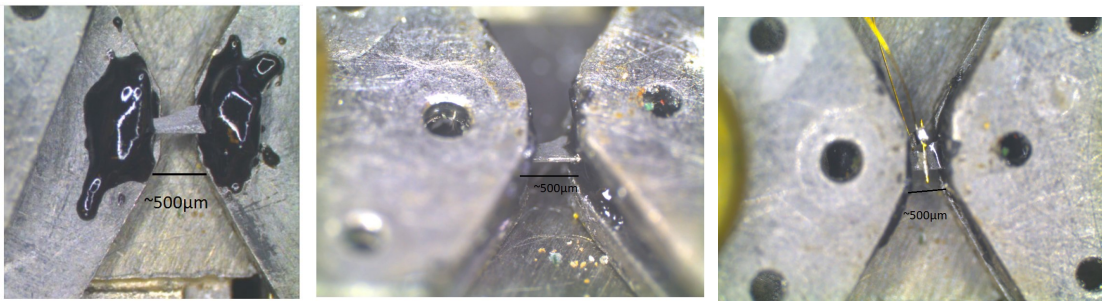


Figure 2.3: Photographs of a sample after being attached to the Razorbill Cell (left), with additional sample mounting plates on top (center), and with an attached thermometer (right).

constant uniaxial strains, while AC voltage could be applied to induce the oscillatory strains necessary for the technique. Stanford Research SR860 lock-in amplifiers were then used to drive the piezoelectric stacks. The two outer stacks were connected in parallel and received a DC voltage with a small AC component from the SR860 via a Tegam 2350 precision power amplifier, while the inner stack received a separate DC voltage, usually of opposite sign to that applied to the outer stacks, via a piezosystem jena SVR 350-1 bipolar voltage amplifier.

A capacitive sensor was then used to measure the resulting separation between the sample mounting plates, allowing calculation of $\frac{\Delta L}{L}$ for the portion of the sample between the two jaws of the strain cell. The changes in capacitance were measured via an Andeen-Hagerling AH2550A capacitance bridge.

As discussed in Ref. [23], strain will not necessarily be uniform throughout the sample, and some strain will relax through the adhesives used; thus, the capacitive sensor generally overestimated the applied strain, but in a consistent manner. Strain relaxation in the glue layer used to attach the sample to the cell reduces the strain $\epsilon_{xx}$ to approximately 70% of $\frac{\Delta L}{L}$, via finite element simulations done by Ikeda et al [23]. Additionally, strain in the sample itself is not generally uniform, relaxing near to the jaws over some finite distance. The thermometer was thus placed near the center of the sample, such that the region probed by the thermometer experienced as uniform a strain as possible.

### 2.2.5 Thermometry

Lakeshore Cernox resistive thermometers were used to measure both the sample temperature and the strain-dependent fluctuations thereof. Five Cernox thermometers, from the same manufacturing batch (so as to have similar resistances), were polished together to approximately 100 $\mu m$ thickness. One was then suspended from gold wires near the sample, as shown in Figure 2.3. These gold wires were anchored elsewhere on the cell body, far from the sample, and at their location a wheatstone bridge was constructed using the other 4 thermometers, with the sample thermometer serving as one of the legs. Current was then directed through the wheatstone bridge, usually of amplitude 50-100 $\mu A$ and frequency of 1-2 kHz. The sample thermometer was then probed directly with the SR860 lock-in amplifier, measuring at the frequency of the applied current, to determine the sample temperature itself. The central thermometer of the bridge was then used to more sensitively measure small variations in the sample thermometer's resistance; by using the dual-mode of the SR 860 lock-in, the sideband voltage across this thermometer was measured at the sum of the current and strain frequencies. Changes in the relative resistances of the legs occurring at the strain frequency, and thus temperature changes in the sample thermometer occurring at the strain frequency, could then be more precisely measured, allowing the temperature fluctuation to be determined with higher accuracy than could be achieved measuring the sample thermometer alone.

### 2.2.6 Adiabatic Condition

To briefly demonstrate how the adiabatic condition is considered and achieved, a simplified thermal model is presented from Ikeda et al [23] (Figure 2.4). This model includes the thermometer, the sample (representing the region of interest), and the thermal bath, representing unstrained parts of the sample (edges encased in glue) and the titanium cell body together. It can then be used to calculate the relationship between measured thermal fluctuations (via the thermometer) and the intrinsic thermal fluctuation, induced by AC strain and described by equation 2.2.

In this thermal model, two relevant timescales present themselves: the timescale of

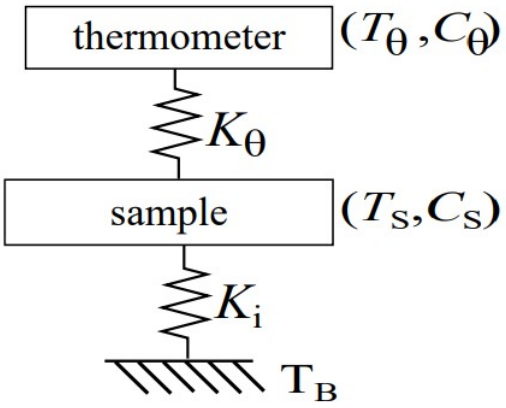


Figure 2.4: A heavily simplified thermal model for the elastocaloric effect, showing the sample ($S$), thermometer ($\theta$), and bath ($B$). $T$, $C$, and $K$ represent temperature, heat capacity, and thermal conductivity, respectively. Reprinted from M.S. Ikeda et al. "AC elastocaloric effect as a probe for thermodynamic signatures of continuous phase transitions". In: Rev. Sci. Instrum. 90 (2019), p. 083902, with the permission of AIP Publishing.

thermalization of the thermometer to the sample $\tau_\theta = \frac{C_\theta}{K_\theta}$ (where $C_\theta$ is thermometer heat capacity and $K_\theta$ is the thermal conductivity between thermometer and sample; see Figure 2.4) and the timescale of thermalization of the sample to unstrained portions of the sample, $\tau_i = \frac{C_S}{K_i}$ (where $C_S$ represents sample heat capacity and $K_i$ represents thermal conductance between portions of the sample). Assuming the strain-induced temperature fluctuation described earlier occurs within the sample, the thermometer will then read, as a function of frequency and the parameters of the thermal model [23]:

$$\begin{aligned} T_\theta(t) = T_B + \frac{E_0\epsilon}{\sqrt{a^2+b^2}} sin(\omega t + \phi) \\ \phi = arctan(\frac{a}{b}) \\ a = \frac{1}{\omega\tau_i} - \omega\tau_\theta \\ b = 1 + \frac{C_\theta}{C_S} + \frac{\tau_\theta}{\tau_i} \end{aligned} \tag{2.5}$$

Here $E_0$ represents the intrinsic temperature fluctuation described by equation 2.2, and $\epsilon$ represents the magnitude of the applied AC strain. As can be seen, the intrinsic signal is most fully realized (and thus the adiabatic condition most completely achieved) when the timescale $\omega^{-1}$ is significantly larger than $\tau_\theta$ and significantly smaller than $\tau_i$; this implies thermalization occurs without issue between the sample and thermometer, but is unable to occur quickly enough between the sample and the bath for significant heat to flow. As the timescale $\tau_i = \frac{C_S}{K_i}$ is determined primarily by the sample, this sets a lower bound on the frequency $\omega$ that can be used for the AC strain without significant signal loss due to heat flow. It is then desirable that the timescale $\tau_i$ be made as small as possible via minimization of the thermometer heat capacity and maximization of the thermal conductance between the thermometer and sample. In the limit that $\tau_\theta << \omega^{-1} << \tau_i$ and $C_\theta << C_S$, we then have $T_\theta(t) = T_B + E_0\epsilon sin(\omega t)$, where the measured temperature will be purely a function of the intrinsic temperature fluctuation of equation 2.2, $\frac{dT}{d\epsilon}$, and the amplitude of the applied AC strain $\epsilon$.

Failure to fully realize the adiabatic condition will then reduce the measured temperature fluctuations compared to the ideal fluctuations expected from the intrinsic properties of the sample. The reduction will then be a function of $C_S$, which in turn may depend heavily on temperature and strain, creating a complicated thermalization-based dependence of the measured signal on $T$ and $\epsilon$ in addition to any intrinsic dependence expected from Equation 2.2, and potentially rendering difficult or impossible the task of separating the intrinsic dependencies from the thermalization-based dependencies. These limitations are discussed individually for each measurement in chapters 4 and 5.

# Chapter 3

# Methods to Measure Octupolar Susceptibility

## 3.1 Preface

The following chapter was originally published as: M.E. Sorensen and I.R. Fisher. "Proposal for methods to measure the octupole susceptibility in certain cubic Pr compounds." Phys. Rev. B. **103**, 155106 (2021).  Light changes were made for inclusion herein, but the work is presented mostly as-published.

## 3.2 Abstract

Direct means of measuring the susceptibility towards an octupole order parameter are proposed via a sixth-rank tensor property. Equivalent derivatives of more conventionally measured tensor properties, including elastic stiffness, magnetic susceptibility, and elastoresistivity, are written in full, as constrained by the symmetry of the experimentally-motivated $O_h$ point group. For simplicity, we consider the specific case of $Pr^{3+}$ ions in a cubic point symmetry with a $\Gamma_3$ crystal field ground state, but the ideas are somewhat general. Experimental feasibility of measuring these various derivatives of tensor quantities is discussed.

## 3.3 Introduction

Quantum states of localized electrons can have a variety of well-defined electromagnetic multipole moments; indeed, within higher angular-momentum states, particularly those that often arise from f-orbitals, higher-order multipolar moments frequently have some non-zero expectation value in the presence of simple magnetic (dipole) order. Of course, multipolar moments are subject to higher-order interactions amongst themselves, and can thus order independently of any dipole moment, but this is uncommon: the dipole typically dominates in energy scale whenever a variety of multipoles are present or allowed. This motivates the use of the associated multipole susceptibility as a powerful tool for analyzing these higher-order multipoles, as the strength and character of specific multipolar interactions can be probed without requiring a simple ordered state of such a multipole. For higher-rank multipoles, however, it is a non-trivial task to relate the multipole susceptibility to physically measurable quantities.

It is well established that a ($q = 0$) magnetic susceptibility may be measured via an applied uniform magnetic field. Specifically, a magnetic field couples bilinearly to the magnetization (magnetic dipole moments per unit volume), and hence is an appropriate conjugate field. Similarly, antisymmetric strain couples bilinearly to electric quadrupoles, providing access to the quadrupole strain susceptibility [11]. Here, we focus on the magnetic octupole, the next in the multipole series [1].

Magnetic octupole order has been proposed for many f-orbital systems, but is often hard to verify or probe directly[1, 2, 3]. Given the time-reversal symmetry breaking inherent in a magnetic moment (of any rank), a bilinear coupling of an octupole to strain, like that of the electric quadrupole, is not possible; similarly, a magnetic field will couple bilinearly only to the magnetic dipole moments, with symmetry forbidding a bilinear octupole coupling. As shown in the work of A.S. Patri et. al. [24], however, the combination of the two provides a conjugate field which, by symmetry, can couple

[1] The electric dipole, magnetic quadrupole, and electric octupole break inversion symmetry, and are thus less common: Crystalline Electric Field ground states that preserve inversion do not include these multipoles as degrees of freedom, leaving them often (but not always) high-energy excited states in 4f systems, rather than potentially ordered ground states

directly to the octupole, allowing one to define and measure a susceptibility. This susceptibility most naturally manifests itself in a 6th-rank tensor, in contrast to the 2nd-rank (magnetic susceptibility) tensor for dipoles and the various 4th-rank tensor components representative of quadrupole susceptibilities; the octupole susceptibility can thus be measured independently of the behavior of the lower-order multipoles in the system, at least under certain restrictions.

Measurement of an octupole susceptibility is then possible whenever the specifics of the system render it finite, but possibly quite difficult if lower-order multipoles are present. In particular, lower-order terms in a material's tensor properties invoking the strain or magnetic field individually could potentially drown out any higher-order effects associated with the octupolar degrees of freedom. Thus, the use of Neumann's principle [2] to significantly constrain the symmetry-allowed tensor terms is motivated, as terms can potentially be identified which have fewer lower-order components or other possible experimental impediments.

Furthermore, we choose to restrict our focus to intermetallic compounds with $Pr^{3+}$ ions in a cubic point symmetry, and for which the crystalline electric field ground state is a $\Gamma_3$ doublet. The specific symmetries of this system forbid all magnetic dipoles and three of the five electric quadrupoles, allowing the octupole's conjugate field to be applied without inducing any lower-order multipoles. This system has been theoretically shown to allow and potentially favor an octupole order parameter [24], and has been experimentally shown to order in a manner suggestive of an octupole order parameter [24, 25], making a measurement of the octupole susceptibility almost certainly feasible.

Thus, herein we propose and elucidate upon the measurement of various tensor components to identify the associated susceptibility of a given octupole, separating it from the susceptibilities of other multipoles and probing interaction strengths of the octupole directly.

[2] Neumann's principle essentially states that a crystal's physical properties must be invariant under the symmetry operations of the crystal

Table 3.1: Effects of various mirror planes ($\sigma$) and rotations ($C$) contained in $O_h$ on a generic 2nd-rank tensor

| Symmetry | Effect(s) | Implied Equality |
|---|---|---|
| $\sigma_i$ | $i \to -i$ | $F_{ij} = -F_{ij} (= 0)$ |
| $\sigma_{i=\pm j}$ | $i \to \mp j \to i$ | $F_{ij} = F_{ji}$ |
| $C_{4k}$ | $i \to j \to -i$ | $F_{ij} = -F_{ji}$ |
| $C_{3(111)}$ | $i \to j \to k \to i$ | $F_{ij} = F_{jk}$ |

### 3.3.1 Background

#### Introduction to the $O_h$ Point Group

While any cubic point group can give rise to a $\Gamma_3$ doublet ground state, the most prominent experimentally realized case for an octupole order parameter has an $O_h$ point group [25, 15]. The $O_h$ point group, being the most highly symmetric cubic point group, contains 48 symmetry elements, many of which are redundant in constraining the various tensor properties (see Appendix A for full list of symmetries via a character table). A convenient, less redundant basis to work in is then shown in Table 3.1, where $\sigma_i$ represents a mirror plane defined by the $i$ axis, $C_{xi}$ represents an x-fold rotation about the $i$ axis, and $F_{ij}$ represents some generic 2nd-rank material property tensor.

These symmetry elements of the point group place constraints on tensor properties of the material via Neumann's principle: the tensor properties must be invariant under the symmetry operations of the point group. In the absence of perturbative fields, these are calculated trivially by applying the symmetries to a given tensor element and observing how they affect the various indices; for example, under $C_{3(111)}$ rotation, $x \to y$, so

$$\begin{aligned} F_{xx} = C_{3(111)} F_{xx} &= F_{yy} \\ F_{xx} &= F_{yy} \end{aligned} \tag{3.1}$$

Additional examples are shown in Table 3.1. The presence of additional perturbative fields, such as magnetic field in the elastic tensors or elastic strains in the magnetic susceptibility, breaks the symmetries of the material and allows otherwise forbidden

terms. This can be accounted for by simply incorporating the symmetry transformations of the perturbative fields [26].The symmetries of the strain tensor and magnetic field are then relevant to all other tensors, and worth some brief discussion. The strain tensor is defined in a manifestly symmetric manner,

$$\epsilon_{ij} \equiv \frac{\partial \mu_i}{\partial x_j} + \frac{\partial \mu_j}{\partial x_i} \tag{3.2}$$

where $\mu_i$ represents the displacement of an atom along the $i$ axis from the unstrained position $x_i$. The inherent symmetry of the strain tensor then requires $\epsilon_{ij} = \epsilon_{ji}$, but otherwise elements of the strain tensor will transform similarly to any other tensor, via applications of the symmetry operations to their indices [3]. Magnetic field, on the other hand, is a pseudovector, invariant under inversion; thus, it transforms as expected under the various rotations, but under mirror planes, which can be considered as a combined rotation and inversion, it effectively experiences only the rotation. Hence, $\sigma_x(H_x, H_y, H_z)$ yields $(H_x, -H_y, -H_z)$, for example, in contrast to an arbitrary normal vector $\sigma_x(A_x, A_y, A_z) = (-A_x, A_y, A_z)$. One can see the effect of these external fields with a brief example: without magnetic field, for instance, one sees

$$\begin{aligned} F_{xy} = C_{4z} F_{xy} &= -F_{yx} \\ F_{xy} &= -F_{yx} \\ \sigma_{x=y} F_{xy} = \sigma_{x=y}(-F_{yx}) &= -F_{xy} \\ F_{xy} = -F_{xy} &= 0 \end{aligned} \tag{3.3}$$

i.e. $\chi_{xy}$ (and, by similar symmetries, all $\chi_{ij}$ terms for $i \neq j$) is constrained to be 0.

[3]Herein, all proposed measurements treat strain as an extrinsic property, controllable via application of external force; as such, it is not constrained by Neumann's principle

However, introducing a magnetic-field dependency to these terms yields

$$\begin{aligned} C_{4z}F_{xy}(H_z) &= -F_{yx}(H_z) \\ \sigma_{x=y}(-F_{yx}(H_z)) &= -F_{xy}(-H_z) \\ \sigma_{x=y}C_{4z}F_{xy}(H_z) = F_{xy}(H_z) &= -F_{xy}(-H_z) \end{aligned} \tag{3.4}$$

Thus, $F_{xy}$ is no longer constrained to be zero, but merely constrained to be odd in $H_z$, the external field that breaks the symmetry ($\sigma_{x=y}$) that constrained it to be zero. Terms constrained to be equal in the absence of perturbative fields can have dependencies in fields with slight variation in sign and ordering, but will maintain identical sets of coefficients; for example, while $F_{xy} = F_{yz}$ without field, $F_{yz}(H_x)$ need not be identical $F_{xy}(H_x)$, but must instead be identical to $F_{xy}(H_z)$ (via $C_{3(111)}$), leaving the two terms with identical, if differently ordered, sets of coefficients. Similarly, using the above example, $F_{xy}(H_z) = -F_{yx}(H_z)$, implying $F_{xy}$ and $F_{yx}$ will have the same linear $H_z$ coefficients, but with opposite sign. These symmetry principles will be used in section 3.4 to determine allowed terms in several higher rank tensors. Complete descriptions of how these symmetries apply to the various tensors examined in the text can be found in Appendix B.

### 3.3.2 The $\Gamma_3$ Doublet

While strong spin-orbit coupling among local 4f electrons often makes $J$ a good quantum number, the crystalline electric field (CEF) splitting in 4f materials can substantially reduce the number of available states within a given $J$ multiplet, at least in a low-temperature regime. One of these CEF eigenstates, the $\Gamma_3$ doublet, is generally present in cubic systems, but is rarely the ground state, meaning it cannot often be experimentally isolated. However, calculations have shown that in the special case $J = 4$, associated with the $Pr^{3+}$ ion (with $4f^2$ orbital) [4], the doublet is a potential ground state [14].

[4]Using the Russell-Saunders coupling scheme, $U^{4+}$ ($5f^2$) can also manifest a J=4 state. However, the extended nature of $5f$ orbitals often smears out the CEF eigenstates. Furthermore, in some cases j-j coupling is more appropriate. Hence, $Pr^{3+}$ is the clearest manifestation of a J=4 state

The $Pr^{3+}$ ions in the most prominent octupole case exist on a diamond lattice [15], so the symmetry of the CEF eigenstates is determined by the $T_d$ point group, as this is the local symmetry an individual ion experiences. The $\Gamma_3$ doublet, with basis states (in $J = 4$), is then given by,

$$\Gamma_3^{(1)} = \frac{1}{2}(\sqrt{\frac{7}{6}}\,|4\rangle - \sqrt{\frac{5}{3}}\,|0\rangle + \sqrt{\frac{7}{6}}\,|-4\rangle)$$
$$\Gamma_3^{(2)} = \frac{1}{\sqrt{(2)}}(|2\rangle + |-2\rangle) \tag{3.5}$$

As a two-state space, this can be treated as a pseudo-spin [24], and analogously three operators can potentially split the doublet and create a finite order parameter. Group theory decomposition of the doublet in $T_d$ suggests the symmetry of the allowed operators:

$$\Gamma_3 \otimes \Gamma_3 = \Gamma_3 \oplus \Gamma_2 \oplus \Gamma_1 \tag{3.6}$$

Thus, of the three operators that would act as Pauli matrices in this pseudo-half-spin two-state space, two have the symmetry of $\Gamma_3$ ($E$) and one has the $\Gamma_2$ ($A_2$) symmetry. One might thus expect one of these operators to break time-reversal symmetry analogously to the Pauli $S_y$ matrix, and indeed the lowest-order multipole of $\Gamma_2$ symmetry is then time-reversal odd. Thus, from the angular-momentum operators $J_x, J_y, J_z$ and their various products (the Stevens operators), the allowed order parameters are represented by two time-reversal-even quadrupole operators of $\Gamma_3$ symmetry

$$O_2^2 = \frac{\sqrt{3}}{2}(J_x^2 - J_y^2)$$
$$O_2^0 = \frac{1}{2}(2J_z^2 - J_x^2 - J_y^2) \tag{3.7}$$

and one time-reversal-odd octupole operator of $A_2$ symmetry

$$\tau_{xyz} = \frac{\sqrt{15}}{6}\overline{J_x J_y J_z} \tag{3.8}$$

where $\overline{J_x J_y J_z}$ denotes all permutations of the indices $x, y, z$, i.e. a six-term object. In typical pseudo-spin fashion, one can note the eigenstates of the three operators in the aforementioned basis: $\Gamma_3^{(1)}$ and $\Gamma_3^{(2)}$ for $O_2^0$, $\Gamma_3^{(1)} \pm \Gamma_3^{(2)}$ for $O_2^2$, and $\Gamma_3^{(1)} \pm i\Gamma_3^{(2)}$ for $\tau_{xyz}$. It can then be noted that none of these three operators represent and/or commute with a magnetic dipole operator. Indeed, in $T_d$ and other cubic point groups, magnetic dipoles belong to a triply-degenerate $\Gamma_4$ ($T_1$) irreducible representation, an object that, as seen in the group theory decomposition, one cannot construct from the two $\Gamma_3$ ($E$) basis states. More intuitively, this can be explained by the $\Gamma_3$ doublet basis states $\Gamma_3^{(1)}$ and $\Gamma_3^{(2)}$ both having three (primary-axis) $C_2$ rotational symmetries, which are universally broken by a dipole order parameter. Thus, cubic praseodymium compounds are of particular interest in the study of higher-order multipoles, as they provide the opportunity to directly probe time-reversal-odd octupolar signatures without (magnetic) dipole signatures; dipole moments are forbidden, to the extent that the energy separation between the $\Gamma_3$ CEF ground state and any triplet excited states is large relative to the temperature and/or magnetic field.

### 3.3.3 Defining an Octupole Susceptibility

Given the presence of a potential octupolar moment, the natural question is how best to access it experimentally. As was noted by A.S. Patri et. al. [24], an octupolar susceptibility can easily be defined for a variety of potential order parameters. Here we choose to focus on a $q = 0$ order parameter, as this presents the most experimentally accessible possibility. It is also, however, of interest for a broader set of potential order parameters; analogously to the magnetic case, finite-q octupole order parameters would likely appear via a sharp feature of some kind in the $q = 0$ octupole susceptibility at or near the relevant ordering temperature.

Based on the symmetry properties of the $\tau_{xyz}$ octupole, one can quickly note that a time-reversal-odd conjugate field would be necessary to couple to it. Utilizing two experimentally-common external fields, strain and magnetic field, it can couple bilinearly to two objects, $H_x\epsilon_{yz} + H_y\epsilon_{zx} + H_z\epsilon_{xy}$ and $H_x H_y H_z$[5] (here these are considered

[5]Looking to a character table quickly shows these two objects to be of $A_2$ symmetry in $T_d$, when $H$ is properly acknowledged as a pseudovector

uniform, but a finite-q order parameter could be coupled to via similar but staggered fields). Choosing to focus on the former for the moment, one might then expect application of this field

$$H\epsilon \equiv H_x\epsilon_{yz} + H_y\epsilon_{zx} + H_z\epsilon_{xy} \tag{3.9}$$

could induce a finite octupolar moment in an originally unordered state,

$$O \equiv < \tau_{xyz} > \tag{3.10}$$

and one could thus define a susceptibility

$$\chi_O \equiv \frac{\partial O}{\partial(H\epsilon)} \tag{3.11}$$

Here it is worth noting that the octupole has thus far been examined in the $T_d$ point group corresponding to the local symmetry of the $4f$ ion, while discussion on material properties has centered on the $O_h$ point group of the specific material (wherein the $Pr$ sites sit on a diamond lattice [15]), which defines the symmetries of the material's tensor properties. Given the chosen coupling field will only induce a ferro-octupolar order parameter, one can note that, while an individual octupole has $\Gamma_2$ symmetry in $T_d$, a pair of aligned octupoles on the two independent ion sites in the greater $O_h$ unit cell correspond to a $\Gamma_2^+$ symmetry[6]. Thus, for $O_h$ and for a susceptibility as has been described, the order parameter and conjugate field can be more specifically defined as being $\Gamma_2^+$. More broadly, it can be seen that, given the basis states are invariant under inversion (to within an overall phase), and all three operators are similarly invariant, any ferro-aligned $\Gamma_3$ order parameter in $T_d$ will couple as $\Gamma_3^+$ in the larger $O_h$ unit cell [7] ($\Gamma_3^-$ objects can couple bilinearly only to non-ferro-aligned $\Gamma_3$ order parameters, which break the inversion symmetry of the

[6]The magnetic octupole is itself invariant under inversion symmetry, while inversion swaps the two independent ion sites in the broader $O_h$ unit cell (equivalent to the two diamond sublattices); thus, if the local octupoles are aligned identically on the two sites, i.e. a ferro-octupolar configuration, the system is invariant under inversion symmetry ($\Gamma_2^+$ in $O_h$ has the same symmetries as $\Gamma_2$ in $T_d$, plus inversion, owing to $T_d$ being a subgroup of $O_h$).

[7]analogously to the $\Gamma_2$ case, $\Gamma_3^+$ in $O_h$ is equivalent to $\Gamma_3$ in $T_d$ with added inversion symmetry

larger $O_h$ cell).

### 3.3.4 Basic Landau Theory

With this $H\epsilon$-type conjugate field, a motivational, simplified model can be established by looking purely at a potential octupolar order parameter. This choice of longitudinal field does leave the aforementioned issues: strain, a second rank tensor, can couple to a quadrupole moment, while magnetic field can couple to a magnetic dipole, leaving any octupole interactions potentially masked. Here we again take advantage of the $\Gamma_3$ doublet: the two $\Gamma_3$ quadrupole moments couple bilinearly only to the two $\Gamma_3$ strains, $\epsilon_{xx} - \epsilon_{yy}$ and $2\epsilon_{zz} - \epsilon_{xx} - \epsilon_{yy}$, while the $\epsilon_{ij}$ strains present in the octupole conjugate field are of $\Gamma_5^+$ type; they can couple to quadrupoles, but only to the $\Gamma_5^+$-type quadrupoles, which are, like the aforementioned magnetic dipoles, forbidden to the extent that the CEF gap is large relative to temperature and strain. Thus, no CEF-allowed multipoles will couple with any of the objects within the octupole conjugate field, allowing one to safely write a lowest-order free energy for just the octupole moment without ignoring any cross-coupling terms not already 'forbidden' by the CEF splitting:

$$F = \frac{a}{2}O^2 - \lambda(H\epsilon)O + \frac{C_{44}^0}{2}(\epsilon_{xy}^2 + \epsilon_{yz}^2 + \epsilon_{zx}^2) \tag{3.12}$$

where $a$ is then assumed to be of the standard form $a_0(T - \theta)$, so as to allow for a continuous octupole phase transition, and $C_{44}^0$ is the un-renormalized elastic stiffness.

Assuming the case of a controlled conjugate field [8], one can then note that minimizing free energy requires a finite order parameter,

$$O = \frac{\lambda H\epsilon}{a} \tag{3.13}$$

[8]Strain is a thermodynamic quantity and the material will adopt a value that minimizes the free energy subject to a given set of stresses. However, experimental configurations can be established in which stresses are applied such that given (measured) strains are established. From a thermodynamic perspective, this is equivalent to a Legendre transformation in which strain now becomes a forced (controllable) parameter.

thus allowing one to solve for the octupole susceptibility

$$\chi_O \equiv \left.\frac{dO}{d(H\epsilon)}\right|_{H\epsilon=0} = \frac{\lambda}{a_0(T-\theta)} \tag{3.14}$$

Presuming a temperature-independent coupling of the moment and the field $\lambda$, the octupole susceptibility may then follow a simple Curie-Weiss functional form, particularly in systems with a tendency toward an explicit octupole ordering. More generally (i.e. beyond just $\Gamma_3$ doublet cases), this can be taken as the primary proof-of-existence of a measurable octupole susceptibility: more complicated temperature dependencies will naturally arise from higher-order terms, but can do so both in systems with and without an independent octupole, given other allowed terms invoking other (biquadratic) multipole couplings. Any free-energy term of the form $H^2\epsilon^2$ (after minimization with respect to the various order parameters) must either invoke the octupole or a product of order parameters (a biquadratic dipole-quadrupole coupling, for instance), and thus will have a more complicated lowest-order temperature dependence, excepting coincidental cancellations. The $\Gamma_3$ case is, of course, already simplified by the necessary components of such a composite term, the three magnetic dipoles and the $xy/yz/zx$ quadrupoles, requiring excited CEF states. A simple $1/(T-\theta)$ dependence in the relevant free energy term is then a reliable indicator of an independent octupolar order parameter, or one with a tendency to order in the absence of competing phases.

One can then note that the octupole susceptibility, to within some proportionality constant, can be extracted by taking appropriate derivatives of the free energy:

$$\left.\frac{\partial^2 F}{\partial(H\epsilon)^2}\right|_{H\epsilon\to 0} = -\frac{\lambda^2}{a} \tag{3.15}$$

This presents the octupolar susceptibility as being proportional to a term in a sixth-rank magneto-elastic tensor. Of course, simpler and similar quantities also present themselves; one can quickly note that a similar quantity (off by a factor of

2) could be found by taking the derivatives separately, and that $\frac{\partial^2 F}{\partial \epsilon^2}$ corresponds to the elastic stiffness tensor, while $\frac{\partial^2 F}{\partial H^2}$ corresponds to a magnetic susceptibility. We therefore propose measuring the relevant sixth-rank tensor term, and thus the $(q = 0)$ octupole susceptibility, via field and/or strain derivatives of more commonly measured tensor quantities; in doing so, the more complicated sixth-rank tensor term can be accessed by well-established and understood experimental methods designed for various second- and fourth-rank tensor quantities.

## 3.4 Thermodynamic Tensors

Thermodynamic quantities, quantities explicitly representative of derivatives of the free energy, are the most direct potential measurements to capture the octupolar susceptibility. Thus, the most obvious tensor quantities involving strain and magnetic field, elastic stiffness and magnetic susceptibility, are herein enumerated.

It should be noted that all tensors herein are general for the $O_h$ point group; while a given term within a tensor may be of specific interest for the octupole here, the allowed and disallowed terms, and their equalities, are a function solely of the point group (and the definitions of the tensors), and not the details of any given system. The symmetric constraints which allow and/or disallow various terms are detailed in Appendix B. Additionally, it should be noted that none of the coefficients are implied to be equal across tensors, with the exception of a handful of identically-labelled coefficients between the elastic stiffness and (strain-dependent) magnetic susceptibility tensors.

### 3.4.1 Elastic Stiffness Tensor

The elastic stiffness tensor, defined by $C_{ij,kl} \equiv \frac{\partial^2 F}{\partial \epsilon_{ij} \partial \epsilon_{kl}}$, represents the stress (i.e. force) necessary to produce a given set of strains in a material. It inherits several symmetries from its definition and that of the strain tensor, $\epsilon_{ij} \equiv \frac{\partial \mu_i}{\partial x_j} + \frac{\partial \mu_j}{\partial x_i}$. Namely, the definition of the strain tensor requires $\epsilon_{ij}$, and thus $C_{ij,kl}$, is invariant under exchange of $i$ and $j$ (or $k$ and $l$), while the definition of $C_{ij,kl}$ requires it be invariant under exchange

Table 3.2: The full elastic stiffness tensor in $O_h$, in compactified Voigt notation and to second order in magnetic field, color-coded to indicate which terms are identical.

| | $xx$ | $yy$ | $zz$ | $yz$ | $zx$ | $xy$ |
|---|---|---|---|---|---|---|
| $xx$ | $C_{11}^{(0)} + A_1 H_x^2 + A_2(H_y^2 + H_z^2)$ | $C_{12}^{(0)} + A_4 H_z^2 + A_3(H_x^2 + H_y^2)$ | $C_{12}^{(0)} + A_4 H_y^2 + A_3(H_x^2 + H_z^2)$ | $+D_1 H_y H_z$ | $B_1 H_y + D_2 H_z H_x$ | $-B_1 H_z + D_2 H_x H_y$ |
| $yy$ | $C_{12}^{(0)} + A_4 H_z^2 + A_3(H_y^2 + H_x^2)$ | $C_{11}^{(0)} + A_1 H_y^2 + A_2(H_z^2 + H_x^2)$ | $C_{12}^{(0)} + A_4 H_x^2 + A_3(H_y^2 + H_z^2)$ | $-B_1 H_x + D_2 H_y H_z$ | $+D_1 H_z H_x$ | $B_1 H_z + D_2 H_x H_y$ |
| $zz$ | $C_{12}^{(0)} + A_4 H_y^2 + A_3(H_z^2 + H_x^2)$ | $C_{12}^{(0)} + A_4 H_x^2 + A_3(H_z^2 + H_y^2)$ | $C_{11}^{(0)} + A_1 H_z^2 + A_2(H_x^2 + H_y^2)$ | $B_1 H_x + D_2 H_y H_z$ | $-B_1 H_y + D_2 H_z H_x$ | $+D_1 H_x H_y$ |
| $yz$ | $+D_1 H_y H_z$ | $-B_1 H_x + D_2 H_y H_z$ | $B_1 H_x + D_2 H_y H_z$ | $C_{44}^{(0)} + A_5 H_x^2 + A_6(H_y^2 + H_z^2)$ | $+D_3 H_x H_y$ | $+D_3 H_z H_x$ |
| $zx$ | $B_1 H_y + D_2 H_z H_x$ | $+D_1 H_z H_x$ | $-B_1 H_y + D_2 H_z H_x$ | $+D_3 H_x H_y$ | $C_{44}^{(0)} + A_5 H_y^2 + A_6(H_z^2 + H_x^2)$ | $+D_3 H_y H_z$ |
| $xy$ | $-B_1 H_z + D_2 H_x H_y$ | $B_1 H_z + D_2 H_x H_y$ | $+D_1 H_x H_y$ | $+D_3 H_z H_x$ | $+D_3 H_y H_z$ | $C_{44}^{(0)} + A_5 H_z^2 + A_6(H_x^2 + H_y^2)$ |

of $ij$ and $kl$. These taken together motivate the use of compactified Voigt notation rather than a full 9x9 matrix, as many terms are exactly identical to their neighbors in such a full construct (e.g. $C_{xy,xy} = C_{xy,yx} = C_{yx,xy} = C_{yx,yx}$).

Taking two field derivatives then reconstructs the desired $\chi_O \equiv \frac{\partial O}{\partial(H\epsilon)} \propto \frac{\partial^2 F}{\partial(H\epsilon)^2}$, and thus the field-dependence of the tensor is the primary point of interest. The aforementioned inherent symmetries combined with those of the point group leave 3 independent non-zero terms in the absence of magnetic field, with arbitrary magnetic fields breaking the point-group symmetries and allowing 10 additional independent coefficients (to second order in field), as can be seen in Table 3.2. The $A_5$ (yellow, diagonal boxes) and $D_3$ (blue, off-diagonal boxes) coefficients would then represent the desired direct probe of octupolar susceptibility:

$$A_5 = \frac{\partial^2 F}{\partial^2(H_i \epsilon_{jk})} \propto \chi_O \tag{3.16}$$

$$D_3 = \frac{\partial^2 F}{\partial(H_i \epsilon_{jk})\partial(H_j \epsilon_{ki})} \propto \chi_O \tag{3.17}$$

### Practical Considerations

A number of considerations present themselves in potential measurements of the relevant coefficients [9]. First, it should be noted that while $A_5$ is unconstrained in its sign by symmetry, the octupole contribution to $A_5$ would necessarily be negative, or correspond to a softening of the lattice:

$$F = -\frac{\lambda^2(H\epsilon)^2}{2a} + \frac{C_{44}^0}{2}(\epsilon_{xy}^2 + \epsilon_{yz}^2 + \epsilon_{zx}^2)$$
$$C_{44} = \frac{\partial^2 F}{\partial \epsilon_{ij}^2} = C_{44}^0 - \frac{\lambda^2 H_k^2}{a} \tag{3.18}$$

In short, a finite field allows a finite octupole moment, and thus a finite shear strain, to reduce the free energy, reducing the energy cost associated with strain via the $C_{44}^0$ term and thus making the lattice more susceptible to said strain, or softer.

As far as conducting the measurement, a [111] oriented field could be used to measure a combination of $A_5$ and $D_3$ via intermixing the 9 terms in the lower-right quadrant. The $A_6$ coefficient would be induced, but is likely small, as it corresponds to the lowest-order interaction of CEF-forbidden octupoles, or a higher-order interaction invoking CEF-forbidden quadrupoles and dipoles. Alternatively, a [001] aligned magnetic field could be used for measuring a specific elastic constant for the orthogonal shear plane. This, however, would break the degeneracy typical of these three coefficients, inducing the $A_5$ term within only one ($C_{xyxy}$ for $H_z$), meaning the measurement may need to distinguish a newly-differentiated $C_{ijij}$ from the still-equal $C_{jkjk}$ and $C_{ikik}$.

Generally, associated changes in sound velocities/resonant frequencies would likely invoke nearly all $C$ and $D$ coefficients from Table 3.2. However, assuming a [111]-oriented magnetic field, all (field-dependent) contributions associated with the allowed $\Gamma_3$ quadrupoles would cancel (the allowed couplings to field would be to $H_x^2 - H_y^2$ and $2H_z^2 - H_x^2 - H_y^2$). Thus, the remaining coefficients would correspond to CEF-forbidden

[9] Many experimental methods are available to probe such a quantity, and the specific method of choice is of little import to the statements made here. The elastocaloric effect, however, presents one such method, and will be discussed in greater detail in chapter 4, wherein it will be used to measure the specific coefficients of interest

multipoles, and would likely be small. In contrast, a field aligned along a single principle axis would have a symmetry-allowed coupling to an allowed quadrupole, though the coupling of this quadrupole and the field to shear strains specifically would be higher order and not likely to be significant. Field-independent effects from the $\Gamma_3$ quadrupoles would naturally remain, which would manifest via $C_{11} - C_{12}$, or $C_{11}^{(0)} - C_{12}^{(0)}$ using coefficients from Table 3.2.

Lastly, it should be noted that the $B_1$ coefficients are constrained to be time-reversal odd/imaginary, and thus linear contaminants would likely be either absent or out-of-phase (and thus easily filtered).

### 3.4.2 Magnetic Susceptibility Tensor

Magnetic susceptibility, herein defined (in slight contrast to convention, and for para-/diamagnetic states) via

$$\chi_{ij} \equiv \left.\frac{\partial^2 F}{\partial H_i \partial H_j}\right|_{H\to 0} \propto -\frac{\partial M_i}{\partial H_j} = -\frac{\partial M_j}{\partial H_i} \tag{3.19}$$

is a frequently measured quantity, characterizing the linear response of induced magnetic moment to external magnetic field. While the octupole would not produce the simple dipole response typically dominant in susceptibility, the dependence of magnetic susceptibility (quadratically) on strain would give an effective $H\epsilon$ conjugate field and recover $\chi_O \equiv \frac{\partial O}{\partial (H\epsilon)} \propto \frac{\partial^2 F}{\partial (H\epsilon)^2}$, similarly to the aforementioned tensors.

For $O_h$ symmetry, there is a single independent (non-zero) term in the susceptibility tensor in the absence of strain, $\chi_{ii}^0$. Externally induced strains introduce 12 additional independent coefficients (to second order in strain). Thus, for $i \neq j$

$$\chi_{ii} = \chi_{ii}^{(0)} + E\epsilon_{ii} + F(\epsilon_{jj} + \epsilon_{kk}) + A_1\epsilon_{ii}^2 + A_2(\epsilon_{jj}^2 + \epsilon_{kk}^2) + A_3\epsilon_{ii}(\epsilon_{jj} + \epsilon_{kk}) + A_4\epsilon_{jj}\epsilon_{kk} + A_6(\epsilon_{ij}^2 + \epsilon_{ik}^2) + A_5\epsilon_{jk}^2 \tag{3.20}$$

$$\chi_{ij} = G\epsilon_{ij} + D_3\epsilon_{ik}\epsilon_{jk} + D_1\epsilon_{ij}\epsilon_{kk} + D_2\epsilon_{ij}(\epsilon_{ii} + \epsilon_{jj}) \tag{3.21}$$

where $A_5$ and $D_3$ again represent the desired coefficients proportional to the octupole susceptibility, $\frac{\partial^2 F}{\partial(H_i\epsilon_{jk})^2}$ and $\frac{\partial^2 F}{\partial(H_i\epsilon_{jk})\partial(H_j\epsilon_{ik})}$ respectively. As implied by the labeling, many coefficients here are constrained by the definition of the tensors (as derivatives of free energy) to be identical to counterparts in the elastic stiffness tensor.

### Practical Considerations

Two experimental configurations are suggested. First, to recover the $A_5$ coefficient, susceptibility could be measured along any principal axis, while a shear strain is applied in a plane perpendicular to said axis. The likely application of a net compressive or tensile strain, as opposed to pure shear strain, would induce several other coefficients. The $E$ and $F$ coefficients, in particular, would correspond to allowed bilinear couplings of the $\Gamma_3$ quadrupoles, but are easily experimentally distinguished by their representing linear strain dependencies (as opposed to quadratic). The rest are unlikely to be large, given they do not represent the lowest-order allowed coupling to either allowed quadrupole.

Alternatively, the $D_3$ coefficient could potentially be measured by applying two simultaneous shear strains, and measuring the transverse susceptibility using the two axes perpendicular to said shear strains. In practice, a simpler method would be to use a [111]-aligned magnetic field and a [111] uniaxial stress, inducing all three shear strains simultaneously to measure a combination of $A_5$ and $D_3$. Unfortunately this would likely induce all the coefficients simultaneously, but, again, they would likely

be small compared to $A_5$ and $D_3$ given their connection to no multipoles and/or CEF-forbidden multipoles (excepting potentially $E$ and $F$, which would again distinguish themselves from the terms of interest by their linearity in strain).

Many common measurements for magnetic susceptibility involve centering a sample in a detection solenoid and varying field (AC), or setting a field and moving a sample through a detection solenoid (DC), to measure its moment via the response in said solenoid. In either case, unexpected sample movement relative to the detector would generate a spurious signal. Thus, the use of DC strains is motivated, as effects of AC strains would be very difficult to decouple from the effects of sample movements (relative to a detector) that most strain-applying techniques are likely to produce. Unfortunately, this means the susceptibility would have to be measured as a function of strain, with the zero-strain term presenting itself as a constant background; measuring only the strain-dependent term, rather than its sum with the zero-strain susceptibility, would require AC strains. However, with the $\Gamma_3$ doublet being non-magnetic, the strain-independent term should be both generally small and not strongly enhanced by low temperatures, potentially allowing easily-realized strains to drive the octupolar contribution to dominance over any background. Experimental apparatus capable of measuring magnetic moments while compensating for the effects of sample movement, via careful strain application or a detector with significant positional tolerance (perhaps an optical probe or a detector mounted on the strain cell, for instance), may then further apply AC strain and AC magnetic field; an octupole susceptibility could then be isolated from much of the background by measuring the component of the magnetic moment varying with the sum or difference frequency of the strain and magnetic field frequencies.

Lastly, it should be noted that controlling strain would be a potential difficulty, as a measurable octupole susceptibility would lead to a softening of the shear mode with field. Thus, application of constant stress would lead to increasing strain with increasing field. Careful and direct measurement of strain, or the use of a fairly small AC magnetic field for susceptibility measurements, could help mitigate this softening.

### 3.4.3 Non-Linear Magnetic Susceptibility

While not the primary focus of this paper, the aforementioned $H\epsilon$ product is not the unique lowest-order object the octupole can couple to within the limits of strain and magnetic field; an object of identical symmetry can be constructed simply with a cubic magnetic field term, $H_xH_yH_z$ [10]. Thus, higher-order magnetization effects can often capture the same information as strain dependencies. Using the same susceptibility definition (albeit without the $H \to 0$ limit), but expanding in magnetic field rather than in strain, this introduces 5 new independent terms to 4th order; for $i \neq j$,

$$\begin{aligned} \chi_{ii}^{(0)} + AH_i^2 + B(H_j^2 + H_k^2) + \\ CH_i^4 + D(H_j^4 + H_k^4) + \\ +6DH_i^2(H_j^2 + H_k^2) + EH_j^2H_k^2 \end{aligned} \tag{3.22}$$

$$\begin{aligned} \chi_{ij} = 2BH_iH_j + 2EH_iH_jH_k^2 \\ +4DH_iH_j(H_i^2 + H_j^2) \end{aligned} \tag{3.23}$$

where the E coefficient represents the desired $\frac{\partial^2 F}{\partial (H_xH_yH_z)^2}$. None of these coefficients are implied by symmetry to be identical to any from the previous tensors.

#### Practical Considerations

Experimentally, the obvious complication is that the high fields potentially necessary to accurately fit a quartic or higher function could render the higher CEF states relevant to the result. Magnetic energy would become comparable to the gap for fields of ∼15T-30T depending on the material (likely ∼.42T/K for a given CEF gap, which are in the 40-60K range [25]).

Two methods present themselves: a simple magnetization-vs-field measurement for a [111]-aligned field and thus [111]-aligned magnetization, and a simple [100] susceptibility measurement with a secondary transverse field along an [011]-type axis.

[10] though microscopics may vary, in pure symmetry terms, $\epsilon_{ii}$ and $\epsilon_{ij}$ transform equivalently to $H_i^2$ and $H_iH_j$ respectively; $H_i$ belongs to a $T_1$ representation, and the product of two different field components $H_iH_j$ creates a $T_2$ object symmetrically analogous to a shear strain

In the [111] case, magnetization would be expected to be $\propto H^5$, or $\frac{dM}{dH} \propto H^4$. Thus, magnetization would have to be sensitively plotted against a fairly wide field range, with a background from the simple dipolar susceptibility being present (but again, likely small for appropriately low field strengths and temperatures, given the CEF splitting). Alternatively, this method would also potentially lend itself to an AC measurement scheme; an AC magnetic field could be applied and the magnetization measured at the fifth harmonic, potentially providing a dramatic improvement in signal-to-background ratio for the octupolar signal.

The alternative [100] case may represent a simpler measurement with a more complicated apparatus. If a strong field could be applied along the [011] axis, a traditional magnetic susceptibility measurement could then be performed along the [100] axis, with the results plotted against $H_{011}$ and fit to a quartic function. Using an AC technique for the [100] susceptibility measurement would eliminate much of the contamination from field misalignment, though background susceptibility from non-octupolar sources would remain a potential issue; in particular, a quadratic dependence on field could potentially arise from a coupling to the $O_2^2$ quadrupole, forbidden with the previous alignment scheme but potentially induced here.

## 3.5 Resistivity

Resistivity is not a thermodynamic quantity, but terms in the resistivity tensor can nevertheless contain information about the onset of order parameters. Appropriate derivatives of resisitivity tensor elements can then sometimes capture information similar to that in derivatives of the free energy, i.e. thermodynamic probes [26]. In particular, perturbations that break symmetries of the crystallographic point group can induce changes in resistivity tensor terms, should the perturbation(s) or some product thereof belong to the same irreducible representation as a given resistivity tensor term. Should the applied perturbation also then match the irreducible representation of the order parameter, a term in the change in resistivity will then be linearly proportional to the order parameter, allowing the change in the resistivity to reflect the associated susceptibility to within some proportionality constant.

Thus, higher rank tensors describing derivatives of resistivity often contain information regarding susceptibility toward symmetry-breaking instabilities, to within some coupling constant. This constant can potentially depend on temperature, or allow certain order parameters to more strongly influence resistivity than others. These complications are generally not insurmountable in extracting the dependence of the underlying order parameter on strain/field. This, combined with the fact that resistivity is, generally, more easily accessed experimentally than many thermodynamic quantities, particularly when trying to measure in a symmetry-selective way, motivates a thorough evaluation.

In the specific context of the $\tau_{xyz}$ octupole allowed in the $\Gamma_3$ doublet, the cyclic permutations of $H_z\epsilon_{xy}$ can couple bilinearly to the octupole, but both of these objects are of $\Gamma_2^+$ symmetry in $O_h$, a symmetry that cannot be constructed purely via elements of the resistivity tensor ($\Gamma_2^+$ has no quadratic basis functions in $O_h$). However, expanding a $\Gamma_5$-type term in the resistivity tensor $\rho_{xy}$, one can note that two objects already present, $H_z$ and $\tau_{xyz}$, together form an object of of appropriate $\Gamma_5$ symmetry. The symmetry-allowed dependency is therefore

$$\begin{aligned} \Delta\rho_{xy}(H_z, \epsilon_{xy}) &\propto H_z\tau_{xyz} \\ \Delta\rho_{xy}(H_z, \epsilon_{xy}) &\propto H_z^2\epsilon_{xy}\chi_O \end{aligned} \tag{3.24}$$

and thus, the object of relevance is a first derivative with respect to strain and second derivative with respect to magnetic field of a resistivity tensor term, i.e. a term in a 6th rank tensor. This object is most easily approached by considering either the second field derivative of the 4th rank elastoresistivity tensor, or the first strain derivative of the 4th rank second-order magnetoresistance tensor. We focus here primarily on the former.

### 3.5.1 Elastoresistivity Tensor

Elastoresistivity is defined via [26]

$$m_{ij,kl} \equiv \frac{\partial(\frac{\Delta\rho}{\rho})_{ij}}{\partial\epsilon_{kl}} \tag{3.25}$$

Herein the normalized resistivity tensor is defined in a manifestly symmetric manner for convenience, $(\frac{\Delta\rho}{\rho}) = \rho^{-1/2}(\Delta\rho)\rho^{-1/2}$[26], enabling the use of the symmetry $(\frac{\Delta\rho}{\rho})_{ij}(H) = (\frac{\Delta\rho}{\rho})_{ji}(-H)$. Thus, the overall tensor is similar, but not identical to, the elastic stiffness tensor; for example, it is not symmetric under exchange of $ij$ and $kl$, and purely dynamic contaminants such as the simple Hall Effect appear in several terms. The full tensor is shown in Table 3.3, to second order in magnetic field; there are only 3 allowed unique field-independent terms, with an additional 15 being induced by applied field. The use of compactified Voigt notation is motivated by this high level of symmetry; excluded terms have identical coefficients to those included on the table, but may have some sign differences, which can be calculated trivially via the symmetries of $\rho_{ij}$ (switching coefficients adds a sign change to each $H$ term) and $\epsilon_{ij}$ (switching coefficients changes nothing); e.g. via the symmetry of $\rho_{ij}$, $m_{zyyy}$ would be $-B_2H_x + D_2H_yH_z$, in slight contrast to $m_{yzyy} = +B_2H_x + D_2H_yH_z$. The $A_6$ (yellow boxes) and $D_5$ (blue boxes) coefficients then represent the desired susceptibility:

$$A_6 = \frac{\partial^2 m_{ij,ij}}{\partial H_k^2} \propto \chi_O \tag{3.26}$$

$$D_5 = \frac{\partial^2 m_{ij,jk}}{\partial H_k \partial H_i} \propto \chi_O \tag{3.27}$$

It should be further noted that similar notation to previous tensors was chosen for convenience, but that none of these coefficients are constrained by symmetry to have any relationship with those in any of the thermodynamic tensors.

Table 3.3: The full elastoresistivity tensor in $O_h$ in compactified Voigt notation, color-coded to indicate which terms have identical or differing coefficients

| | $xx$ | $yy$ | $zz$ | $yz$ | $zx$ | $xy$ |
|---|---|---|---|---|---|---|
| $xx$ | $m_{11}^{(0)} + A_1 H_x^2 + A_2(H_y^2 + H_z^2)$ | $m_{12}^{(0)} + A_3 H_z^2 + A_4 H_x^2 + A_5 H_y^2$ | $m_{12}^{(0)} + A_3 H_y^2 + A_4 H_x^2 + A_5 H_z^2$ | $D_1 H_y H_z$ | $D_2 H_z H_x$ | $D_2 H_x H_y$ |
| $yy$ | $m_{12}^{(0)} + A_3 H_z^2 + A_4 H_y^2 + A_5 H_x^2$ | $m_{11}^{(0)} + A_1 H_y^2 + A_2(H_z^2 + H_x^2)$ | $m_{12}^{(0)} + A_3 H_x^2 + A_4 H_y^2 + A_5 H_z^2$ | $D_2 H_y H_z$ | $D_1 H_z H_x$ | $D_2 H_x H_y$ |
| $zz$ | $m_{12}^{(0)} + A_3 H_y^2 + A_4 H_z^2 + A_5 H_x^2$ | $m_{12}^{(0)} + A_3 H_x^2 + A_4 H_z^2 + A_5 H_y^2$ | $m_{11}^{(0)} + A_1 H_z^2 + A_2(H_x^2 + H_y^2)$ | $D_2 H_y H_z$ | $D_2 H_z H_x$ | $D_1 H_x H_y$ |
| $yz$ | $B_1 H_x + D_3 H_y H_z$ | $B_2 H_x + D_4 H_y H_z$ | $B_2 H_x + D_4 H_y H_z$ | $m_{44}^{(0)} + A_6 H_x^2 + A_7(H_y^2 + H_z^2)$ | $B_3 H_z + D_5 H_x H_y$ | $B_3 H_y + D_5 H_z H_x$ |
| $zx$ | $B_2 H_y + D_4 H_z H_x$ | $B_1 H_y + D_3 H_z H_x$ | $B_2 H_y + D_4 H_z H_x$ | $B_3 H_z + D_5 H_x H_y$ | $m_{44}^{(0)} + A_6 H_y^2 + A_7(H_z^2 + H_x^2)$ | $B_3 H_x + D_5 H_y H_z$ |
| $xy$ | $B_2 H_z + D_4 H_x H_y$ | $B_2 H_z + D_4 H_x H_y$ | $B_1 H_z + D_3 H_x H_y$ | $B_3 H_y + D_5 H_z H_x$ | $B_3 H_x + D_5 H_y H_z$ | $m_{44}^{(0)} + A_6 H_z^2 + A_7(H_x^2 + H_y^2)$ |

### Practical Considerations

The tensor presents several obvious experimental opportunities and challenges. First, inspection of the yellow boxes in Table 3.3 makes clear that the $m_{xyxy}$ elastoresistivity coefficient is even in $H_z$, and hence that measurement of the $A_6$ coefficient is possible without a linear-in-field contaminant, meaning that it could potentially be extracted as the sole fit parameter of elastoresistivity vs field data. This, in turn, would mean that the coefficient could potentially be extracted with a fairly limited field range, limiting issues arising from high fields (i.e. non-negligible mixing of CEF states).

Most experimental methods of probing elastoresistivity, however, do not apply pure shear strains, but also induce normal strains $\epsilon_{xx}$, $\epsilon_{yy}$, $\epsilon_{zz}$. The associated symmetry-preserving strain component couples directly to a simple Hall Effect via changing the carrier density; with small strains, charge carrier count would remain constant against an increasing/decreasing volume. Thus, even without a linear-in-field term in the desired $m_{ijij}$ elastoresistivity term, a successful measurement would likely still show a strain-dependent Hall Effect that would need to be accounted for via the traditional methods (this would correspond to an admixture of the $B_1$ and $B_2$ coefficients in the table). For fields aligned precisely along one of the crystal axes $k$, measurement of $\rho_{ij}$ in positive and negative fields would, in principle, allow cancellation of this linear contaminant. Contact misalignment, which can result in admixture

of $\rho_{ii}$ in an attempt to measure $\rho_{ij}$, can be subtracted using ideas developed earlier in Ref. [27].

Perhaps more importantly, elastoresistivity requires controlling/measuring the strain experienced by a crystal. If an experiment failed to hold strain constant as a function of field, the octupole susceptibility would not be faithfully measured. An example would be the case where stress is held fixed, i.e. a piezoresistance measurement. Given the octupole susceptibility can manifest in the elastic stiffness (see section 3.4.1), the very application of field would change the stiffness independently of temperature, thus changing the strain under conditions of constant stress. Such an effect can be minimized via the use of a strain-applying apparatus that is very stiff relative to the sample, or nearly eliminated by directly measuring and controlling for strain. Appropriate experimental apparatus for such a task have been developed [28].

It should be further noted that Table 3.3 represents a general compilation of terms allowed in an expansion of resistivity in terms of strain and magnetic field (to first order in strain, second order in field); the order of derivatives is not particularly relevant, and thus strain dependencies of the magnetoresistance would draw from the same set of allowed terms, though high fields (or high strains) would potentially render relevant higher terms than those contemplated here.

## 3.6 Conclusion

The $\Gamma_3$ doublet ground state for local 4f orbitals in a cubic point symmetry was motivated as an ideal system to study octupole order parameters and their associated susceptibility, given the allowed $\tau_{xyz}$ octupole and the energetic disfavoring of magnetic dipoles. Considering the allowed couplings of such an order parameter, several commonly-measured tensor quantities in which it might appear were discussed. These were fully elucidated in the $O_h$ point group, the point group of potential experimental realizations of an octupolar order parameter [25, 15]. Specific terms within external-field-dependent elastic stiffness, elastoresistivity, and magnetic susceptibility tensors which would be linearly proportional to a potential $\tau_{xyz}$ octupole susceptibility were identified. Potential measurements, and complications arising from contaminant

terms, were discussed for each individual tensor, with several octupole-isolating experiments ultimately proposed.

More broadly, similar ideas could be used to isolate contributions of a variety of higher-order local multipoles and in any number of material systems. The chosen system was convenient for both being relatively simple (a doublet ground state) and having no overlap in conjugate fields (the strain component of the octupole conjugate field coupled to no other order parameters allowed by the CEF ground state). Nonetheless, the core idea of isolating specific multipolar contributions to potentially rich phase diagrams via higher-rank tensor properties is applicable to a variety of localized 4f systems.

### 3.6.1 Acknowledgements

The authors would like to thank M.C. Shapiro, E.W. Rosenberg, R.M. Fernandes, and B.J. Ramshaw for helpful conversations. We particularly thank R.M. Fernandes for pointing out the possibility to measure the octupole susceptibility via the 5th harmonic of the AC magnetic susceptibility. This work was supported by the Gordon and Betty Moore Foundation EPiQS Initiative, through Grant GBMF9068. M.E.S. was supported by a NSF Graduate Research Fellowship (Grant No. DGE-114747).

## 3.A Character Table

See Table 3.4. For convenience, a series of symmetrized cubic rotation products have been added. These have the same spatial symmetries as the magnetic octupole, and thus indicate the irreducible representations of the various possible magnetic octupole moments.

## 3.B Table Symmetries

Herein, terms are defined by "types," where a given type is defined by having a unique index composition (i.e. $ii, ii$ vs $ii, jj$), and $i \neq j \neq k$ holds for all types. A type then

| $O_h$ | | $E$ | $8C_3$ | $6C_2$ | $6C_4$ | $3(C_4)^2$ | $i$ | $6S_4$ | $8S_6$ | $3\sigma_h$ | $6\sigma_d$ | linear functions and rotations | quadratic functions | cubic functions and cubic rotation products |
|---|---|---|---|---|---|---|---|---|---|---|---|---|---|---|
| $\Gamma_1^+$ | $A_{1g}$ | +1 | +1 | +1 | +1 | +1 | +1 | +1 | +1 | +1 | +1 | - | $x^2+y^2+z^2$ | - |
| $\Gamma_2^+$ | $A_{2g}$ | +1 | +1 | -1 | -1 | +1 | +1 | -1 | +1 | +1 | -1 | - | - | $\overline{R_xR_yR_z}$ |
| $\Gamma_3^+$ | $E_g$ | +2 | -1 | 0 | 0 | +2 | +2 | 0 | -1 | +2 | 0 | - | $(2z^2-x^2-y^2,$ $x^2-y^2)$ | - |
| $\Gamma_4^+$ | $T_{1g}$ | +3 | 0 | -1 | +1 | -1 | +3 | -1 | 0 | -1 | -1 | $(R_x, R_y, R_z)$ | - | $(R_x^3, R_y^3, R_z^3)$ $(\overline{R_xR_z^2}+\overline{R_xR_y^2}, \overline{R_yR_z^2}+\overline{R_yR_z^2},$ $\overline{R_zR_y^2}+\overline{R_zR_x^2})$ |
| $\Gamma_5^+$ | $T_{2g}$ | +3 | 0 | +1 | -1 | -1 | +3 | -1 | 0 | -1 | +1 | - | $(yz, zx, xy)$ | $(\overline{R_xR_z^2}-\overline{R_xR_y^2}, \overline{R_yR_x^2}-\overline{R_yR_z^2},$ $\overline{R_zR_y^2}-\overline{R_zR_x^2})$ |
| $\Gamma_1^-$ | $A_{1u}$ | +1 | +1 | +1 | +1 | +1 | -1 | -1 | -1 | -1 | -1 | - | - | - |
| $\Gamma_2^-$ | $A_{2u}$ | +1 | +1 | -1 | -1 | +1 | -1 | +1 | -1 | -1 | +1 | - | - | xyz |
| $\Gamma_3^-$ | $E_u$ | +2 | -1 | 0 | 0 | +2 | -2 | 0 | +1 | -2 | 0 | - | - | - |
| $\Gamma_4^-$ | $T_{1u}$ | +3 | 0 | -1 | +1 | -1 | -3 | -1 | 0 | +1 | +1 | $(x, y, z)$ | - | $(x^3, y^3, z^3)$ $(xz^2+xy^2, yx^2+yz^2, zy^2+zx^2)$ |
| $\Gamma_5^-$ | $T_{2u}$ | +3 | 0 | +1 | -1 | -1 | -3 | +1 | 0 | +1 | -1 | - | - | $(xz^2-xy^2, yx^2-yz^2, zy^2-zx^2)$ |

Table 3.4: $O_h$ Character Table

constitutes a term and all terms that can be generated from that (arbitrary) original term by various symmetries, which can be simplified to include only the symmetries of a given tensor, the 3-fold rotational symmetry, and the various 4-fold rotations. For example, Type II for the elastic stiffness tensor, $C_{ii,jj}$, includes $C_{xx,yy}$, $C_{yy,xx}$ (owing to the symmetry of the tensor; see relevant section below), $C_{yy,zz}$, etc. The wording "sign change" is used to indicate the operation $(x) \rightarrow (-x)$ for a given variable a tensor depends on, such as magnetic field.

### 3.B.1 Elastic Stiffness

Here the $C$ symmetry is defined as that which exchanges the two subsets of indices (i.e. $C_{ab,cd} \rightarrow C_{cd,ab}$), while the $\epsilon$ symmetry is defined as that which switches indices within a subset ($C_{ab,cd} \rightarrow C_{ba,cd}$).

**Type I**: $C_{ii,ii}$ (Red Boxes in Table 3.2)

1. Invariant under simultaneous sign change of any two field components ($\sigma_i/\sigma_j/\sigma_k$)

2. Invariant under simultaneous exchange of $H_j$ and $H_k$ and sign change of $H_i$ ($\sigma_{j=k}$)

Final Form: $C_{11}^0 + A_1H_i^2 + A_2(H_j^2 + H_k^2)$

**Type II**: $C_{ii,jj}$ (Green Boxes in Table 3.2)

1. Invariant under simultaneous sign change of any two field components ($\sigma_i/\sigma_j/\sigma_k$)

2. Invariant under simultaneous exchange of $H_i$ and $H_j$ and sign change of $H_k$ ($\sigma_{i=j}$,$C$)

Final Form: $C_{12}^0 + A_3(H_i^2 + H_j^2) + A_4(H_k^2)$

**Type III**: $C_{ij,ij}$ (Yellow Boxes in Table 3.2)

1. Invariant under simultaneous sign change of any two field components ($\sigma_i/\sigma_j/\sigma_k$)
2. Invariant under simultaneous exchange of $H_i$ and $H_j$ and sign change of $H_k$ ($\sigma_{i=j}$,$\epsilon$)
Final Form: $C_{44}^0 + A_6(H_i^2 + H_j^2) + A_5(H_k^2)$
**Type IV**: $C_{ii,ij}$ (Orange Boxes in Table 3.2)
1. Zero in the absence of symmetry-breaking field, magnetic or otherwise ($\sigma_i$ or $\sigma_j$)
2. Antisymmetric under simultaneous sign change of $H_k$ and $H_j/H_i$ ($\sigma_i/\sigma_j$)
Final Form: $B_1H_k + D_2H_iH_j$
**Type V**: $C_{ij,kk}$ (Purple Boxes in Table 3.2)
1. Zero in the absence of symmetry-breaking field, magnetic or otherwise ($\sigma_i$ or $\sigma_j$)
2. Invariant under simultaneous exchange of $H_i$ and $H_j$ and sign change of $H_k$ ($\sigma_{j=k}$,$\epsilon$)
3. Antisymmetric under exchange of $H_i$ and $H_j$ followed by sign change of $H_i$ ($C_{4k}$,$\epsilon$)
Final Form: $D_1H_iH_j$
**Type VI**: $C_{ij,jk}$ (Blue Boxes in Table 3.2)
1. Zero in the absence of symmetry-breaking field, magnetic or otherwise ($\sigma_i$ or $\sigma_k$)
2. Invariant under simultaneous exchange of $H_i$ and $H_k$ and sign change of $H_j$ ($\sigma_{i=k}$,$C$,$\epsilon$)
3. Antisymmetric under exchange of $H_i$ and $H_k$ followed by sign change of $H_i$ ($C_{4j}$, $C$)
Final Form: $D_3H_iH_k$

### 3.B.2 Strain-dependent Magnetic Susceptibility

The magnetic susceptibility tensor, again defined by

$$\chi_{ij} \equiv \left.\frac{\partial^2 F}{\partial H_i \partial H_j}\right|_{H\to 0} \propto -\frac{\partial M_i}{\partial H_j} = -\frac{\partial M_j}{\partial H_i} \tag{3.28}$$

has one obvious symmetry. This symmetry, herein defined as "$\chi$" symmetry, implies invariance under simple exchange of indices, i.e. $\chi_{ij} \to \chi_{ji}$
**Type I**: $\chi_{ii}$
1. Invariant under sign-change of $i/j/k$ indices ($\sigma_i/\sigma_j/\sigma_k$)
2. Symmetric under exchange of $j$ and $k$ indices ($\sigma_{j=-k}$)

Final Form: $\chi_{ii} = \chi_{ii}^{(0)} + A\epsilon_{ii} + B(\epsilon_{jj} + \epsilon_{kk}) + C\epsilon_{ii}^2 +$
$D(\epsilon_{jj}^2 + \epsilon_{kk}^2) + E\epsilon_{ii}(\epsilon_{jj} + \epsilon_{kk}) +$
$F\epsilon_{jj}\epsilon_{kk} + G(\epsilon_{ij}^2 + \epsilon_{ik}^2) + L\epsilon_{jk}^2$

**Type II**: $\chi_{ij}$

1. Zero in the absence of symmetry-breaking field, strain or otherwise ($\sigma_i$ or $\sigma_j$)
2. Antisymmetric under sign change of $i/j$ ($\sigma_i/\sigma_j$)
3. Invariant under exchange of $i$ and $j$ coefficients ($\sigma_{i=-j}.\ \chi$)

Final Form: $M\epsilon_{ij} + N\epsilon_{ik}\epsilon_{jk} + O\epsilon_{ij}\epsilon_{kk} + P\epsilon_{ij}(\epsilon_{ii} + \epsilon_{jj})$

It can then be noted that, given the definition of $C$ and the definition of $\chi$, each of these terms corresponds to some allowed term in the free energy, and the terms which give rise to many of the $C$ tensor terms are identical to many that give rise to the strain-dependent $\chi$ tensor terms. Thus, the terms can be rewritten as
$\chi_{ii} = \chi_{ii}^{(0)} + E\epsilon_{ii} + F(\epsilon_{jj} + \epsilon_{kk}) + A_1\epsilon_{ii}^2 + A_2(\epsilon_{jj}^2 + \epsilon_{kk}^2) + A_3\epsilon_{ii}(\epsilon_{jj} + \epsilon_{kk}) + A_4\epsilon_{jj}\epsilon_{kk} +$
$A_6(\epsilon_{ij}^2 + \epsilon_{ik}^2) + A_5\epsilon_{jk}^2$
$\chi_{ij} = G\epsilon_{ij} + D_3\epsilon_{ik}\epsilon_{jk} + D_1\epsilon_{ij}\epsilon_{kk} + D_2\epsilon_{ij}(\epsilon_{ii} + \epsilon_{jj})$

### 3.B.3 Non-linear Magnetic Susceptibility

The inherent symmetry of the tensor here remains $\chi_{ij} \to \chi_{ji}$, as in the previous case.

**Type I**:$\chi_{ii}$

1. Invariant under simultaneous sign change of any two field components ($\sigma_i/\sigma_j/\sigma_k$)
2. Invariant under simultaneous exchange of $H_j$,$H_k$ and sign change of $H_i$ ($\sigma_{j=-k}$)

Final Form: $\chi_{ii}^{(0)} + AH_i^2 + B(H_j^2 + H_k^2) + CH_i^4 + D(H_j^4 + H_k^4) + EH_i^2(H_j^2 + H_k^2) + FH_j^2H_k^2$

**Type II**:$\chi_{ij}$

1. Zero in the absence of symmetry-breaking field, magnetic or otherwise ($\sigma_i$ or $\sigma_j$)
2. Invariant under simultaneous sign change of $H_i$,$H_j$ ($\sigma_k$)
2. Antisymmetric under simultaneous sign change of $H_j$,$H_k/H_k$,$H_i$ ($\sigma_i/\sigma_j$)
3. Invariant under simultaneous exchange of $H_i$,$H_j$ and sign change of $H_k$ ($\sigma_{i=-j}$,$\chi$)

Final Form: $\chi_{ij} = GH_iH_j + LH_iH_jH_k^2 + NH_iH_j(H_i^2 + H_j^2) + OH_k(H_i^2 - H_j^2)$

Furthermore, moving beyond Neumann's Principle, it can be noted that the aforementioned definition of magnetic susceptibility implies each term derives from a corresponding term in the free energy. Some of these $\chi$ tensor terms are then implied to derive from the same allowed term within the free energy, and are thus constrained to be equal, to within a numerical factor (given different derivative orders). Additionally, one term allowed by Neumann's principle in $\chi_{ij}$, $OH_k(H_i^2 - H_j^2)$, implies a term in $\chi_{ii}$, $H_iH_jH_k$, that is forbidden, and is thus not allowed (alternatively, the free-energy term implied by $OH_k(H_i^2 - H_j^2)$ is found to cancel if the equivalent free-energy terms from $\chi_{ij}$,$\chi_{jk}$, and $\chi_{ki}$ are added together, yielding $H_iH_jH_k(H_i^2 - H_j^2 + H_j^2 - H_k^2 + H_k^2 - H_i^2)$.

Thus, the allowed terms can be further simplified to:
$\chi_{ii}^{(0)} + AH_i^2 + B(H_j^2 + H_k^2) + CH_i^4 + D(H_j^4 + H_k^4) + 6DH_i^2(H_j^2 + H_k^2) + EH_j^2H_k^2$
$\chi_{ij} = 2BH_iH_j + 2EH_iH_jH_k^2 + 4DH_iH_j(H_i^2 + H_j^2)$

### 3.B.4 Elastoresistivity

Elastoresistivity, defined again by

$$m_{ij,kl} \equiv \frac{\partial(\frac{\Delta\rho}{\rho})_{ij}}{\partial\epsilon_{kl}}$$

does not admit the exchange of the index pairs, i.e. $m_{ij,kl} \rightarrow m_{kl,ij}$. Thus, the symmetries of the constituent components are the only major symmetries of the tensor itself. First, the inherent "$\epsilon$" symmetry implies invariance under $m_{ij,kl} \rightarrow m_{ij,lk}$. Next, the symmetry of the normalized resistivity tensor, defined here (for the purposes of symmetry [26]) via

$$(\frac{\Delta\rho}{\rho}) = \rho^{-1/2}(\Delta\rho)\rho^{-1/2} \tag{3.29}$$

implies invariance under the "$\rho$" symmetry operation, $m_{ij,kl} \rightarrow -m_{ji,kl}$, as noted in the relevant section above.

**Type I**: $m_{ii,ii}$ (Red Boxes in Table 3.3)
1. Even in $H_i/H_j/H_k$ ($\sigma_i/\sigma_j/\sigma_k$,$\rho$)
2. Invariant under exchange of $H_j$,$H_k$ ($\sigma_{j=k}$,$\rho$)
Final Form: $m_{11}^0 + A_1 H_i^2 + A_2(H_j^2 + H_k^2)$
**Type II**: $m_{ii,jj}$ (Green Boxes in Table 3.3)
1. Even in $H_i/H_j/H_k$ ($\sigma_i/\sigma_j/\sigma_k$,$\rho$)
Final Form: $m_{12}^0 + A_3 H_k^2 + A_4 H_i^2 + A_5 H_j^2$
**Type III**: $m_{ij,ij}$ (Yellow Boxes in Table 3.3) 1. Invariant under simultaneous sign change of any two field components ($\sigma_i/\sigma_j/\sigma_k$)
2. Invariant under exchange of $H_i$,$H_j$ ($\sigma_{i=-j}$,$\rho$,$\epsilon$)
Final Form: $m_{44}^0 + A_6 H_k^2 + A_7(H_i^2 + H_j^2)$
**Type IV**: $m_{ii,ij}$ (Peach Boxes in Table 3.3)
1. Zero in the absence of symmetry-breaking field, magnetic or otherwise ($\sigma_i$ or $\sigma_j$)
2. Antisymmetric under simultaneous sign change of $H_j$,$H_k/H_k$,$H_i$ ($\sigma_i/\sigma_j$)
3. Invariant under simultaneous sign change of $H_i$,$H_j$ ($\sigma_k$)
4. Invariant under simultaneous sign change of $H_i$,$H_j$,$H_k$ ($\rho$)
Final Form: $D_2 H_i H_j$
**Type V**: $m_{ij,jj}$ (Orange Boxes in Table 3.3)
1. Zero in the absence of symmetry-breaking field, magnetic or otherwise ($\sigma_i$ or $\sigma_j$)
2. Antisymmetric under simultaneous sign change of $H_j$,$H_k/H_k$,$H_i$ ($\sigma_i/\sigma_j$)
3. Invariant under simultaneous sign change of $H_i$,$H_j$ ($\sigma_k$)
Final Form: $B_2 H_k + D_4 H_i H_j$
**Type VI**:$m_{ij,kk}$ (Purple Boxes in Table 3.3)
1. Zero in the absence of symmetry-breaking field, magnetic or otherwise ($\sigma_i$ or $\sigma_j$)
2. Antisymmetric under simultaneous sign change of $H_j$,$H_k/H_k$,$H_i$ ($\sigma_i/\sigma_j$)
3. Invariant under simultaneous sign change of $H_i$,$H_j$ ($\sigma_k$)
4. Invariant under exchange of $H_i$,$H_j$ ($\sigma_{x=-y}$,$\rho$)
Final Form: $B_1 H_k + D_3 H_i H_j$
**Type VII**: $m_{ii,jk}$ (Violet Boxes in Table 3.3)
1. Zero in the absence of symmetry-breaking field, magnetic or otherwise ($\sigma_j$ or $\sigma_k$)
2. Odd in $H_j/H_k$ ($\sigma_j/\sigma_k$,$\rho$)

3. Even in $H_i$ ($\sigma_i$,$\rho$)

Final Form:$D_1 H_j H_k$

**Class VIII**: $m_{ij,jk}$ (Blue Boxes in Table 3.3)

1. Zero in the absence of symmetry-breaking field, magnetic or otherwise ($\sigma_i$ or $\sigma_k$)
2. Antisymmetric under simultaneous sign change of $H_j$,$H_k$/$H_i$,$H_j$ ($\sigma_i/\sigma_k$)
3. Invariant under simultaneous sign change of $H_i$,$H_k$ ($\sigma_j$)

Final Form: $B_3 H_j + D_5 H_k H_i$

# Chapter 4

# ECE Measurements of Octupolar Susceptibility

## 4.1 Preface

The following chapter represents an as-yet unpublished paper in the process of publication, titled "Measurement of the magnetic octupole susceptibility of $PrV_2Al_{20}$." The authorship includes Linda Ye, Matthew E. Sorensen, Maja Bachmann, and Ian R. Fisher, with Linda Ye and Matthew Sorensen having contributed equally to this work.

## 4.2 Abstract

AC elastocaloric effect measurements under magnetic field were used to probe the octupolar susceptibility of single crystals of $PrV_2Al_{20}$, a cubic system proposed to have a non-Kramers doublet ground state and realized magnetic octupolar order [12, 13, 29]. Through carefully chosen geometry, magnetic field and strain were applied so as to couple to a magnetic octupolar moment and split the ground state doublet. AC elastocaloric effect was then measured across a range of strains, magnetic fields, and temperatures. A simple Landau model was used to fit data, with fits to functions of magnetic field and strain allowing for the extraction of a quantity proportional to the

octupolar susceptibility. The extracted $\frac{d\chi_O}{dT}$ was then presented as a thermodynamic property of the material, dependent only on temperature, and plotted for a number of temperatures.

## 4.3 Introduction

A wide variety of ordered electronic/magnetic states have been observed, characterized within the Landau paradigm by the symmetries that they break. Considering ordered states based on local atomic orbitals, various types of ordered states based on magnetic dipoles (ferromagnets, ferrimagnets, and antiferromagnets of all sorts) are extremely common. While ordered states between higher rank multipoles are also possible, interactions fall off progressively more rapidly for successively higher rank multipoles, such that while there are numerous examples of quadrupole order, there are relatively few candidates for yet higher rank order, including octupolar. Furthermore, identifying such 'hidden order' states can itself be a challenge, since the specific broken symmetry can be challenging to identify/determine. Such systems, if they can be correctly identified, would not only be of interest due to their rather unique and subtle order, but also because such states, when allowed to interact with conduction electrons, have been shown theoretically to be connect to novel types of non-Fermi liquid behavior [30] and unconventional superconductivity [31].

All of these points of interest motivate development of new experimental tools that can probe the associated susceptibility of the higher rank multipole – a quantity that (a) is finite for all temperatures (though possibly only large at low T), even above Tc, (b) the divergence of which directly attests to the presence of growing fluctuations, (c) and which can be directly compared to other competing symmetry channels (i.e. even in cases where a lower rank multipole 'wins', identifying the presence of strong fluctuations of the competing higher rank multipole state can help determine pathways to realizing such a state in other related materials). Here we experimentally identify strong octupolar fluctuations in the cubic compound $PrV_2Al_{20}$, by measuring the temperature-dependence of the octupolar susceptibility.

While appropriate conjugate fields for uniform magnetic and quadrupolar moments can be readily obtained, for higher order multipoles, such as the magnetic octupole, simple/single conjugate fields do not exist. In such cases, multiple external fields may be necessary to adequately simulate the higher-order octupolar field. For example, the magnetic octupole can generally couple to the product of magnetic field and strain, as discussed in Ref. [32], via multiple fields. The susceptibilities associated with any individual constituent field then become of concern, however.

To sidestep this and other complications, 4f ion systems are ideal, with their tendency toward localization and the potential $\Gamma_3$ doublet CEF ground state for cubic systems. For systems of this ground state, the doublet can be split by $\Gamma_3$ electric quadrupoles ($3J_z^2 - J^2$, $J_x^2 - J_y^2$) or a $\Gamma_2$ magnetic octupole ($\overline{J_x J_y J_z}$). In particular, the $Pr^3+$ ion is the most common host for such a ground state, with $PrTr_2Al_{20}$ compounds having been experimentally demonstrated to have this $\Gamma_3$ ground state [12]. $PrV_2Al_{20}$ is chosen here, for its noted, well-separated $\Gamma_3$ ground state ($40K$ between ground and first excited states [12]), its electric quadrupole ordering at $0.75K$ [12], and its octupolar ordering at $0.65K$ in higher-quality crystals [13]; it is then ideal for susceptibility measurements, which can potentially identify octupolar fluctuations a) at higher temperatures, b) despite the dominant/higher energy quadrupolar ordering and interactions and c) in crystals where disorder may prevent the octupolar ordering from manifesting at all.

### 4.3.1 Coupling Considerations

As pointed out by Yong-Baek Kim et al [24], one potential conjugate field for the octupole here, $H_i\epsilon_{jk}$, incorporates a $\Gamma_4$ magnetic field ($H_i$) and a $\Gamma_5$ strain ($\epsilon_{jk}$), where $i, j, k \in x, y, z$ and $i \neq j \neq k$. The corresponding order parameters for these two fields on their own, the $\Gamma_4$ magnetic dipole and $\Gamma_5$ electric quadrupole ($xy$, $yz$ and $zx$ symmetries), then do not split the $\Gamma_3$ doublet ground state to lowest order, and are effectively forbidden so long as the energy gap between the CEF ground state and excited states is large relative to the coupling energy.

While the idea of creating an 'octupolar field' to couple with the octupolar moment of the $\Gamma_3$ doublet may imply miniscule energy scales, an 'octupolar field' is not the most accurate description of the coupling involved. It is perhaps more insightful to consider the interaction of the octupolar moment with either one of the fields individually. Taking the magnetic field as the first example, if we apply a magnetic field (of $\Gamma_4$ symmetry) of arbitrary direction, the interaction with the octupolar moment ($\Gamma_2$ symmetry) will then indicate $\Gamma_4 \otimes \Gamma_2 = \Gamma_5$. In other words, the octupolar moment, of positive or negative sign, will interact with a (magnetic field) vector in the $\Gamma_4$ manifold to generate an object characterized by a vector in the $\Gamma_5$ manifold, in this case a quadrupolar moment. The same effect can be applied in reverse, as $\Gamma_5 \otimes \Gamma_2 = \Gamma_4$.

Thus, while either field (magnetic or quadrupolar) individually may not bilinearly couple to the octupole, either field will distort the two (positive and negative) octupolar moments carried by the $\Gamma_3$ states to give them moments (quadrupolar or magnetic, respectively) of opposite sign that the other field (strain or magnetic, respectively) can then couple to bilinearly to split the doublet (see Figure 4.1a). As seen in Figure 4.1b, this means the energy of the ground state doublet splits quite dramatically in the presence of both fields, but relatively minimally in the presence of only one. We then restrict ourselves to the case of 111 magnetic field and uniaxial stress to avoid allowed couplings of the magnetic field to the energetically dominant $\Gamma_3$ quadrupolar moments, and so the necessary $\Gamma_5$ strain can be applied without $\Gamma_3$ strain.

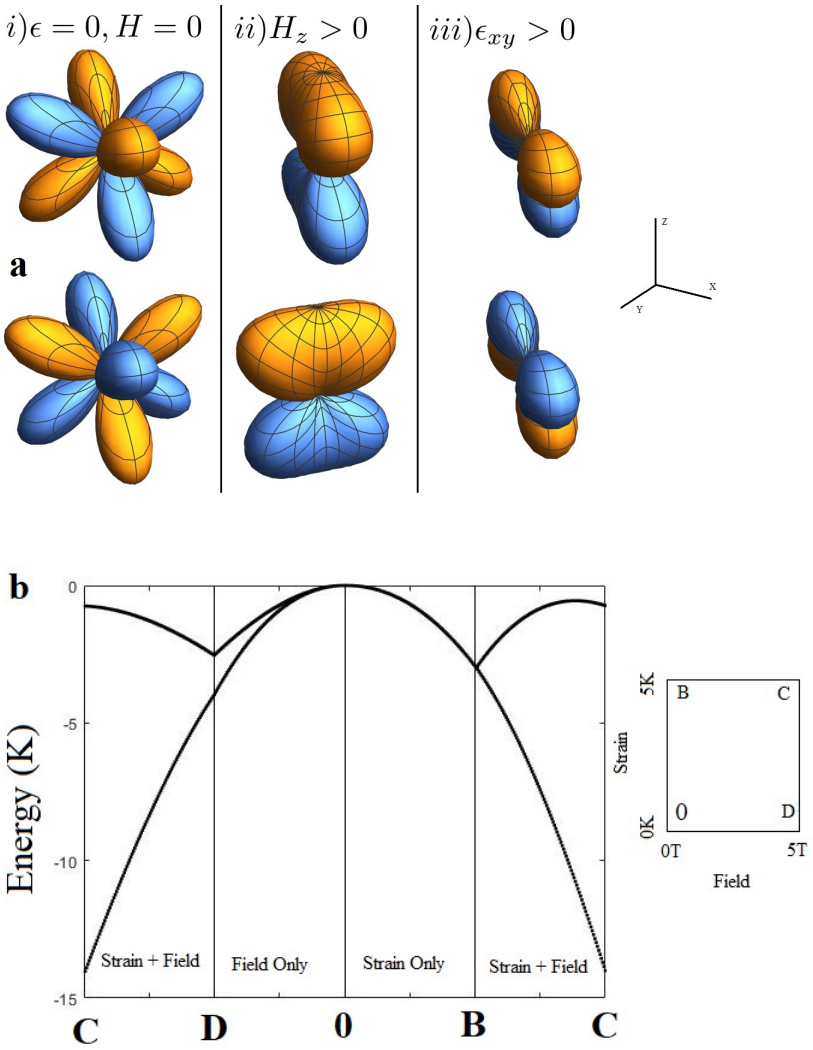


Figure 4.1: (a): Example magnetic charge density of the positive and negative $\Gamma_2$ octupolar moments shown via contours of constant magnetic charge, (i) for $\epsilon, H = 0$, (ii) in the presence of a z-axis magnetic field $H_z$, and (iii) in the presence of a $\Gamma_5$ strain $\epsilon_{xy}$. Note that the two octupolar moments acquire quadrupolar moments (ii) and magnetic moments (iii) (for applied field and strain respectively) of opposite sign, and hence can be split by applied strain and field respectively. (b)Energetic splitting of the ground state doublet for selected linear cuts in the 2D space of applied strain and magnetic field, calculated using the simple $H = H_{CEF} - \epsilon Q - HJ$ for $Q$ and $J$ representing 111 quadrupole and magnetic moments, respectively ($H_{CEF}$ taken from Ref. [13]). Strain-based splitting in the absence of field is negligible when considering experimentally relevant strain amplitudes. While splitting exists at finite magnetic field, it is negligible compared to that achieved with combined strain and field.

To use said field to probe the octupolar moment, we choose to use the AC Elastocaloric Effect, as pioneered by Ikeda et al [23, 33]. Stress and magnetic field were applied in parallel along the 111 axis (see Appendix A for geometry). In the measurement, an AC stress is applied to the sample at a frequency such that the sample cannot thermalize with the surrounding cell ($277.\overline{7}$ Hz here), and is considered to be approximately adiabatic (Appendix C). Provided strain splits the doublet or otherwise reduces entropy in an isothermal environment, the temperature must then shift in the isentropic environment to compensate for any such loss of degeneracy. The adiabatic elastocaloric temperature oscillation is given by

$$\left(\frac{dT}{d\epsilon}\right)_S = -\frac{\partial S}{\partial \epsilon}\frac{T}{C_\epsilon} \tag{4.1}$$

To measure the temperature oscillation, an AC current is applied to a thermometer attached to the sample at some frequency, and the thermometer voltage is measured with a lock-in amplifier attuned to the sum frequency of the current and strain to isolate the strain-induced change in the thermometer resistance, i.e. the strain dependent temperature fluctuation, as the primary experimental output. A commercial CS100 strain cell from Razorbill Insruments was used to induce strain, measurable via the change in sample length $\Delta L/L$; this generally overestimates the total uniaxial strain, but in a consistent manner (see Appendix B).

Uniaxial stress then naturally creates strains of $\Gamma_1$ and $\Gamma_5$ character. $\Gamma_1$ strain, equivalent to the effect of pressure, will generally have a lesser effect on $\frac{dT}{d\epsilon}$ than the symmetry-breaking $\Gamma_5$ absent any phase transitions, with dependence of thermodynamic properties (such as entropy or free energy) on $\Gamma_1$ strains often being dominated by the linear term (absent a $\Gamma_1$-strain-induced phase transition); this then creates a constant, strain-independent background on $\frac{dT}{d\epsilon}$, which causes small deviations from the dominant effect associated with the coupling to octupole desgrees of freedom (to be discussed below), and can be ignored in simple models which accurately predict much of the system's behavior. In the following analysis, we use $\epsilon$ to refer to the $\Gamma_5$ strain contribution, where $\Delta L/L$ is proportional to, but greater than, the $\Gamma_5$ strain.

### 4.3.2 Expectations

The energetic splitting (and thus the change in entropy) as a function of strain is expected to be minimal in the absence of field, but to grow large as field is increased. As a crude indicator of expectations, we suggest the simple Landau model

$$F = \frac{a}{2}O^2 - \lambda_1 H\epsilon O - \lambda_2 H^3 O \tag{4.2}$$

where $O$ represents the octupolar moment and $H$ is the magnetic field oriented along the 111 crystallographic axis. This model is relevant for sufficiently high temperatures above any octupolar (or competing) phase transition, where $a = a_0(T - T*) > 0$, provided again that the strain and magnetic field do not couple to competing order parameters, and for sufficiently small values of $H$ and $\epsilon$. Absorbing some constants into $\epsilon$ for simplicity yields

$$F = \frac{a}{2}O^2 - \lambda H(\epsilon - H^2)O \tag{4.3}$$

where it should be noted that the octupolar moment will be zero not at zero applied strain, but at some finite strain wherein the two allowed couplings cancel; the choice of relative sign between the two bilinear octupole couplings is then experimentally motivated, as this finite strain of cancellation is found to be, in the convention used herein, positive. Minimizing this yields $O = \frac{\lambda H(\epsilon - H^2)}{a}$ and thus $F = -\frac{\lambda^2 H^2(\epsilon - H^2)^2}{2a}$. We can then define an octupolar strain susceptibility

$$\chi_O = \left.\frac{\partial O}{\partial(H\epsilon)}\right|_{H\epsilon, H^3=0} = \frac{\lambda}{a} \tag{4.4}$$

We note here that susceptibilities are traditionally defined in the limit of vanishing conjugate field, generally corresponding to zero order parameter. Here, we seek to measure primarily using one component, $H\epsilon$, of the full conjugate field, $H\epsilon - H^3$. The traditional constraint then requires the limit where the total field $H\epsilon - H^3 = 0$, a limit wherein the higher-order terms in $O$ are necessarily negligible. It is then additionally desirable, however, that the derivative be evaluated where the $H\epsilon$ field is zero, or

more specifically that $H = \epsilon = 0$, to avoid any potential minor distortions invoked by allowed couplings of the form $H^2O^2$ or $\epsilon^2O^2$. Achieving both limits, that of zero for both our total $H\epsilon - H^3$ conjugate field and the $H\epsilon$ field we measure with, is however somewhat experimentally unfeasible. Given the inequivalence of these two limits in this scenario, we suggest the traditional limit of vanishing total field, or equivalently vanishing order parameter, to be more physically relevant, as will be discussed in more detail below.

$S$ can then be solved for, followed by $\frac{dS}{d\epsilon}$

$$S = -\frac{\partial F}{\partial T} = \frac{d\chi_O}{dT}\frac{\lambda H^2(\epsilon^2 - H^2)}{2} \tag{4.5}$$

$$\frac{\partial S}{\partial \epsilon} = \frac{d\chi_O}{dT}H^2(\epsilon - H^2) \tag{4.6}$$

Thus, for small perturbations from the zero-octupole point, and sufficiently far away from any phase transition, where the variance in heat capacity is likely small, the elastocaloric signal is anticipated to be linearly dependent on strain, with a slope that is quadratic in magnetic field. $\chi_O$, as defined, will then have a $(T-T^*)^{-1}$ temperature dependence typical of such susceptibilities, and the measured elastocaloric signal $\frac{dT}{d\epsilon}$ should have $(T - T^*)^{-2}$ dependence, in regimes where the heat capacity does not significantly change and the Landau formulation holds.

## 4.4 Experimental Results

As a starting point for examining the validity of the simple model, the elastocaloric signal $\frac{dT}{d\epsilon}$ was measured with and without field at low temperature (2.5K, Figure 4.2b). In the absence of field, the signal is weakly linear w.r.t. strain, likely representing the small but non-zero $\Gamma_5$ quadrupolar susceptibility. The CEF splitting is finite, so this will necessarily be present via contributions from excited CEF states, despite being 'forbidden' in the ground state $\Gamma_3$ doublet itself. However, as magnetic field is increased, the slope of $\frac{dT}{d\epsilon}$ as a function of $\frac{\Delta L}{L}$ increases monotonically and dramatically. Thus, the assumption of CEF-forbidden contributions being negligible

relative to the octupolar contribution is made for the remainder of the analysis. Data showing positive and negative fields, and thus ruling out more complicated magnetic effects and hysteresis, can be found in Appendix D.

As was briefly discussed earlier, the zero intercept of the iso-magnetic curves does indeed vary as field is increased, representing a shift in the strain required for cancellation of $H\epsilon$ and $H^3$ couplings with each other as a function of field.

Temperature dependence of $\frac{dT}{d\epsilon}$ for a representative field is then illustrated via Figure 4.2a; as anticipated, the slope of the signal w.r.t. strain (at constant magnetic field) increases dramatically upon cooling. It should be noted that the traces become significantly more curved as their average slope increases, i.e. with decreasing temperature and increasing magnetic field. This is an effect of the lack of symmetry-required equivalence of $\Gamma_5$ quadrupoles of varying signs, which are, as discussed above, induced by applying a strong magnetic field to the octupolar moments. This introduces terms of cubic order and higher of the $\Gamma_5$ quadrupole in the Landau model, which will generally be proportional to $HO$. The simpler Landau picture, however, can then be recovered by looking at the region where these higher order terms are negligible, i.e. the zero of the order parameter, in this case reasonably approximated (but not perfectly matched, due toe the effect of non-symmetry-breaking stress) by the zero of the signal. For further insights, the earlier equations, namely those describing the measured signal (4.1) and the entropy derivative (4.6), motivate taking a strain-derivative in the limit of vanishing octupolar moment.

### 4.4.1 Extracting Susceptibility

Data were then considered in the original ECE vs strain traces across a variety of constant fields and temperatures (see Appendix B). Motivated by the simple Landau paradigm of going to higher-order terms as necessary, these traces were then fit with a 2nd order polynomial, to account for the noted nonlinearity, and the polynomial derivative evaluated at the polynomial's zero intercept, so as to extract the slope in the limit of vanishing order parameter and vanishing higher-order contribution. This quantity is proportional to the temperature derivative of the octupolar susceptibility

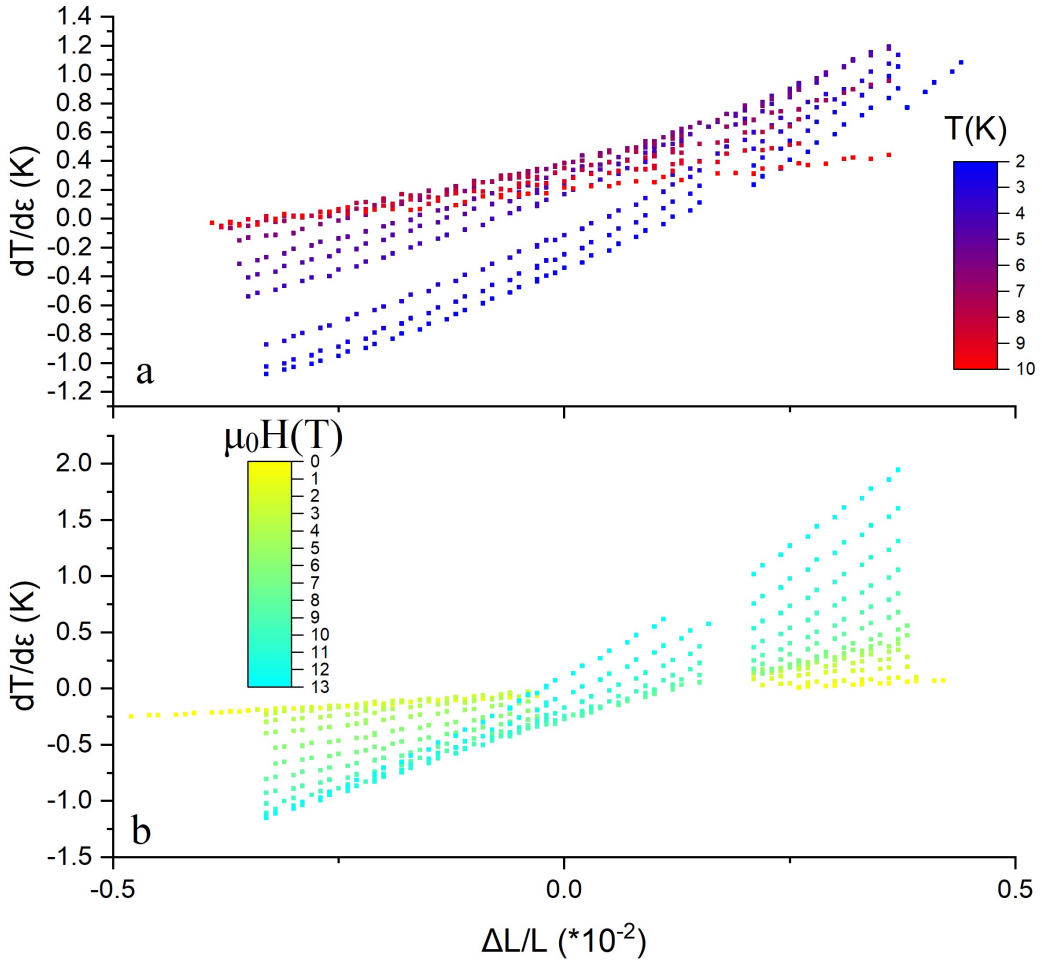


Figure 4.2: Representative data showing (a) $\frac{dT}{d\epsilon}$ as a function of $\frac{\Delta L}{L}$ for a fixed field (here 10T) for various temperatures from 2 to 10K (color bar in legend); and (b) $\frac{dT}{d\epsilon}$ as a function of $\frac{\Delta L}{L}$ for a fixed temperature (here, 2.5K) for various fields from 0 to 14T (color bar in legend). In all cases, H is applied along the [111] axis, and $\frac{\Delta L}{L}$ is the measured strain in the [111] direction in response to uniaxial stress applied along the same direction.

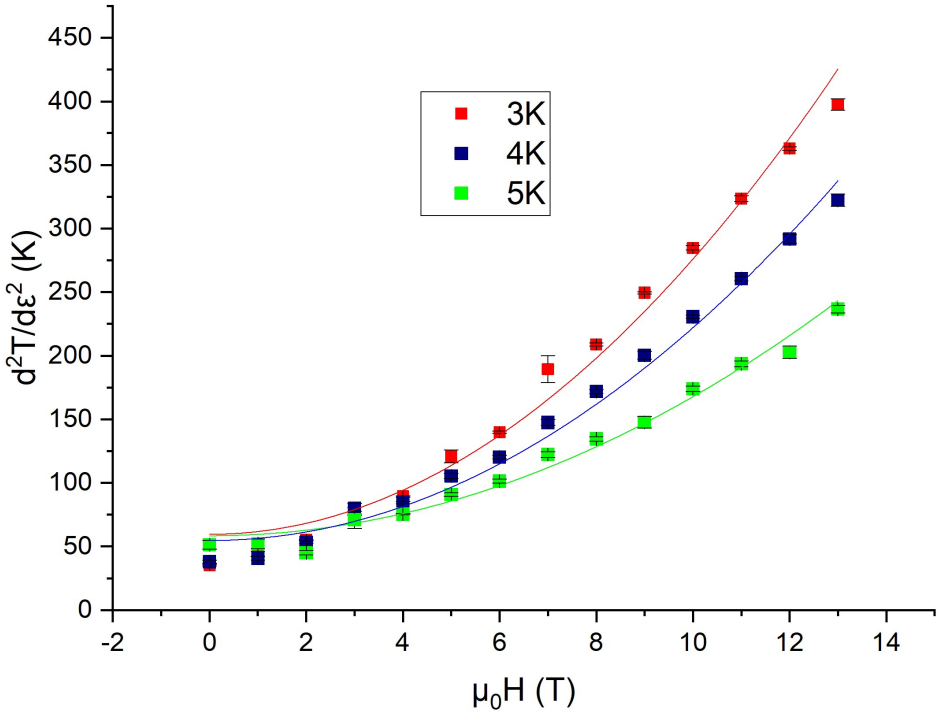


Figure 4.3: Field-dependence of the slope of $\frac{dT}{d\epsilon}$ evaluated at zero ECE signal (i.e. at approximate zero octupole moment; see main text) for 3 representative temperatures. Each curve is fit to a quadratic function with zero slope at zero field (solid lines). Deviations from perfect quadratic behavior are discussed in the main text.

$\chi_O$ multiplied by field squared,

$$\frac{d^2T}{d\epsilon^2} = -\frac{\partial^2 S}{\partial \epsilon^2}\frac{T}{C_\epsilon} = -\frac{T}{C_\epsilon}\frac{d\chi_O}{dT}H^2 \tag{4.7}$$

The extracted fit value for the slope was then itself fit against field, at constant temperature (Figure 4.3). The non-zero intercept is recognizable as the background $\Gamma_5$ quadrupolar susceptibility. It should be noted that the non-zero slope at zero field is an error term, with several possible origins. It is most simply explained by symmetry-preserving strain (pressure) effects on the entropy, which to leading order create a flat background on the signal, thus causing the zero-signal point that is used

to slightly but systematically deviate from the zero-octupole point that would more accurately relate to our simple model; as the slope of the strain dependence increases with increasing field, this flat background shifts the zero in the signal by smaller and smaller distances, meaning this source of error is maximized at zero field. Fits were thus created with an imposed zero slope at zero field, to more accurately reflect the quadratic term dominating the higher-field, and less error-prone, data.

This yields a final result independent of $H$ and $\epsilon$, which can be plotted against T (Figure 4.4):

$$\frac{1}{2}\frac{d^4T}{d\epsilon^2 dH^2} = -\frac{T}{C_\epsilon}\frac{d\chi_O}{dT} \tag{4.8}$$

To extract the temperature-dependence of $\frac{d\chi_O}{dT}$, it is necessary to multiply the experimentally measured $\frac{d^4T}{d\epsilon^2 dH^2}$ by $\frac{C_\epsilon}{T}$. While a more precise refinement would require taking heat capacity in the limit of zero octupolar moment, i.e. at finite strain and magnetic field, an approximation can nevertheless be made using values of the heat capacity measured with zero field and strain, wherein the $\Gamma_3$ doublet will remain essentially un-split (as near the zero in octupolar moment), under the assumption that strain and field do not strongly affect background heat capacity contributions, such as those from phonons and excited CEF states. Heat capacity at constant pressure ($C_P$) can then further be used to approximate the constant strain equivalent ($C_\epsilon \approx C_V$) [33]. The final result can then be taken to demonstrate a susceptibility (right-hand axis, Figure 4.4) increasing with decreasing temperature. The maximum in the signal observed near 2.5K is then attributed to experimental limitations, such as the heat capacity approximation and the limited adiabaticity, or to physics beyond the scope of our limited model, such as the Kondo screening known to be important at lower temperatures [13].

## 4.5 Conclusion

In summary, a signal proportional to the octupolar susceptibility was extracted via the elastocaloric effect by taking advantage of the unique constraints of a localized $Pr^{3+}$ electronic system with $\Gamma_3$ CEF ground state. These constraints allowed a composite

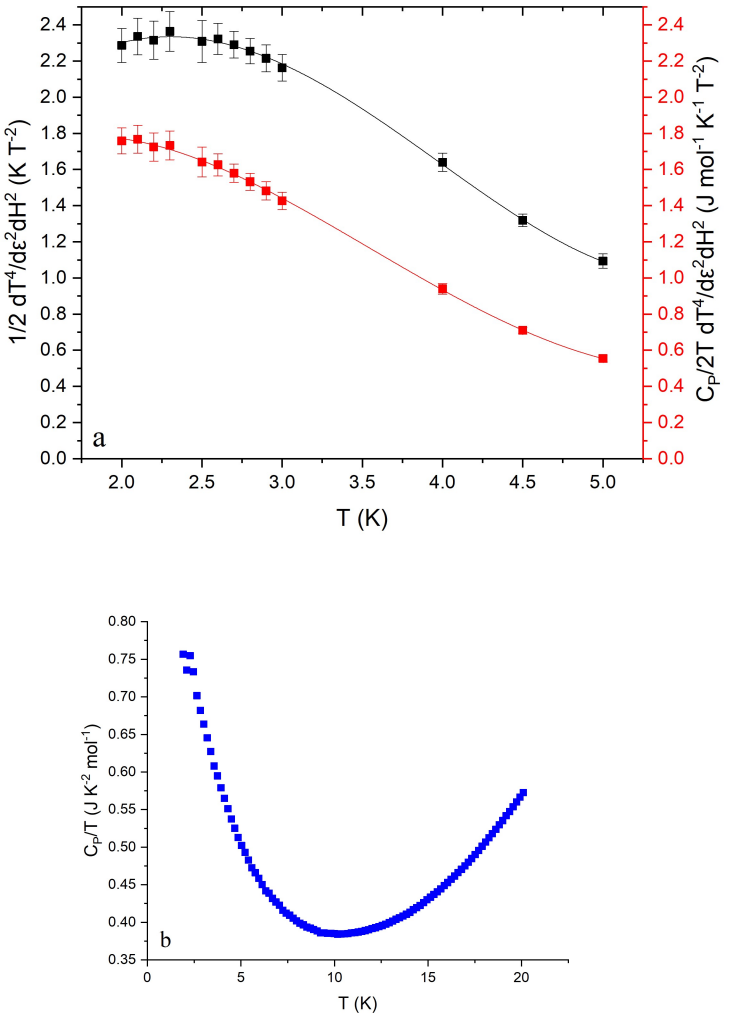


Figure 4.4: (a): Extracted $\frac{1}{2}\frac{d^4T}{d\epsilon^2 dH^2}$ (left axis) and $\frac{C_P}{2T}\frac{d^4T}{d\epsilon^2 dH^2}$ (right axis) as a function of temperature. Lines are a guide to the eye. (b) $C_p$ as a function of $T$ for zero strain and zero field. As discussed in the main text, this measured value of the heat capacity closely approximates the value that should be used in conjunction with the measured $-\frac{1}{2}\frac{d^4T}{d\epsilon^2 dH^2}$ (equation 4.8) to evaluate the octupole susceptibility. The strong temperature dependence of the experimentally obtained $-\frac{C_P}{2T}\frac{d^4T}{d\epsilon^2 dH^2}$ indicates strong octupolar fluctuations in this material.

field to probe the octupole without significant background contributions from the order parameters with direct bilinear couplings to the applied strain and magnetic field. A simple Landau model provided a reasonably successful prediction of the effects of these two fields on the signal, allowing them to be extracted from the final result to yield physically intrinsic quantities dependent only on temperature.

## 4.A Adiabatic Condition

The adiabatic condition describes the extent to which the assumptions underpinning interpretation of the data are accurate, and can be measured via frequency dependence ([23]); a plateau indicates the desired condition of good thermal contact between the thermometer and the sample and thermal decoupling from the broader cell, where very low frequencies allow coupling to the cell which dampens the signal and very high frequencies decouple the thermometer from the sample. If a plateau is absent in favor of a more well-defined maximum, the adiabatic condition is not fully achieved, reducing the signal amplitude. However, so long as the cutoff frequencies for decoupling from the strain cell and sample remain relatively constant, this is simply a constant multiplicative factor decreasing the amplitude, and does not interfere with the dependence of the amplitude on other factors, such as strain, temperature, and magnetic field. Given the functional form defined by Ikeda et al [23], movement of the cutoff frequencies would be evidenced by movement of the frequency of maximum signal. Figure 4.5 then demonstrates the frequency dependence traces, for which movement of the maximum is not observed to be significant w.r.t. the inherent noise of the data. Given the predominant factor in such frequencies moving would likely be the heat capacity, this suggests the sample heat capacity is not changing significantly as strain and magnetic field are applied, consistent with the use of a fairly high-order coupling and the generally lower energy scales of higher-order multipoles like octupoles. With the frequency dependence not varying significantly across parameters, the frequency can then be chosen near the maximum to avoid potential noise sources; in this case $277.\overline{7}$ Hz was used.

The phase of the ECE signal here presents the standard behavior: a monotonically

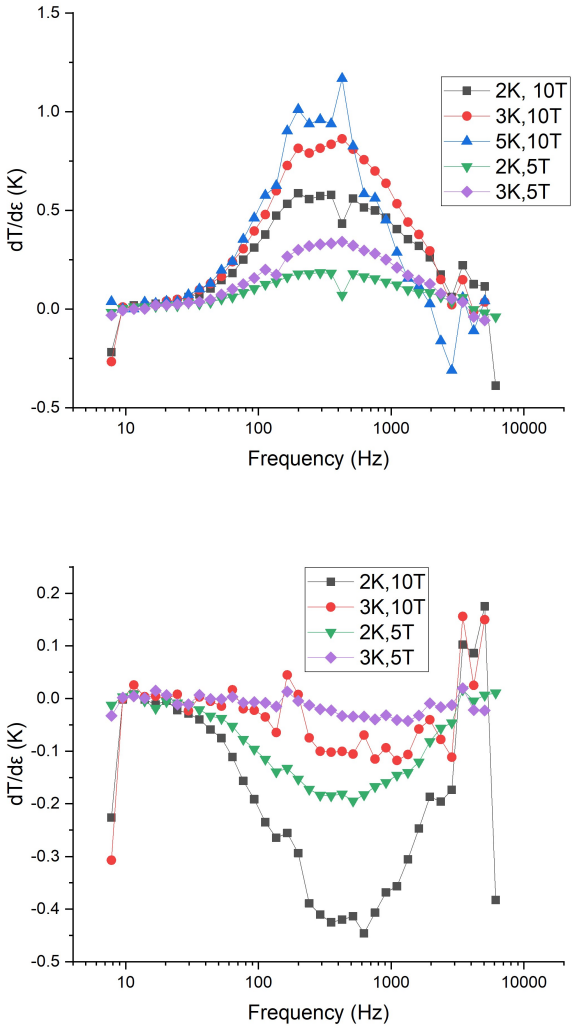


Figure 4.5: In-phase ECE signal as a function of frequency, for a variety of temperatures, and magnetic fields, at $\frac{\Delta L}{L}$ values of approximately .0029 (top) and .0005 (bottom); no significant dependence of the functional form on these parameters, beyond its amplitude, is observed. The signal is dominated by noise for sufficiently low fields and high temperatures. Functional dependence of the amplitude at a constant strain, rather than at the zero-signal strain used elsewhere, is of a non-trivial form, and not of interest here. Note again that the zero-strain point is crudely approximated herein, due to its irrelevance to the underlying analysis.

decreasing function, with a zero at approximately the frequency of the maximum in all cases. However, as can be seen by light manipulation of equation 2.5, this zero is universally at $a = 0$, which itself corresponds to $\omega^2 = \frac{1}{\tau_i \tau_\theta}$, the frequency which is the geometric mean of the inverse of the two relevant timescales, or, equivalently, the geometric mean of the two relevant cutoff frequencies. As this is also the universal maximum of the $T_\theta(t)$ function w.r.t. frequency, the phase thus cannot further elucidate the quality of the adiabatic condition, and is of little interest here.

## 4.B Time Reversal Symmetry Breaking

To rule out time reversal symmetry-breaking impurities and potential magnetic hysteresis, magnetic field was swept at a constant strain, to demonstrate the even character of the dependence on magnetic field (Figure 4.6). As can be seen in the Landau-derived formula for $\frac{dS}{d\epsilon}$ below, this can have a somewhat complicated functional form dependent on the strain; hence, after demonstrating this paramagnetic character, other forms of data collection, most notably sweeping strain under constant field, were preferred.

$$\frac{dS}{d\epsilon} = \frac{d\chi_O}{dT} H^2(\epsilon - H^2)$$

Data from positive and negative strain values are presented to demonstrate contrast; the function changes shape quite rapidly near 0 field as strain is altered, while asymptotic high-field behaviors that are more consistent across strains exceed the low-field limits of a Landau model.

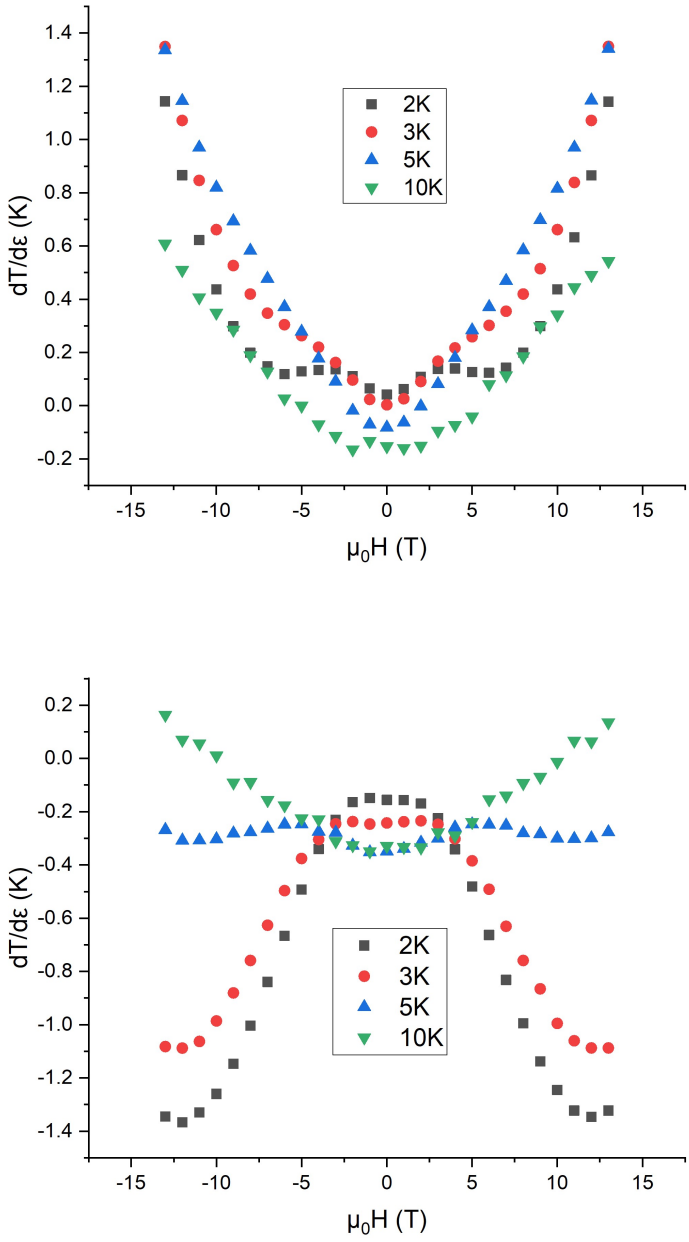


Figure 4.6: ECE signal as a function of magnetic field at a variety of constant temperatures and $\frac{\Delta L}{L}$ of approximately .0025 (top) and -.0033 (bottom); no hysteresis or other evidence of intrinsic time reversal symmetry breaking is observed, though the functional form is non-trivial and varies significantly with strain

# Chapter 5

# Quadrupole ECE Measurements

## 5.1 Preface

The following chapter represents an as-yet unpublished paper in the process of publication, titled "Elastocaloric Measurements of Quadrupolar Fluctuations in $PrTi_2Al_{20}$" The authorship includes Maja Bachmann, Matthew E. Sorensen, Linda Ye, and Ian R. Fisher, with Maja Bachmann and Matthew Sorensen having contributed equally to this work.

## 5.2 Abstract

The AC elastocaloric effect, wherein strain is applied at a finite frequency and the resulting temperature fluctuation is used to probe the strain derivative of entropy, has been used to great effect in tetragonal systems [23, 33]. Here, the adaptation of such techniques to cubic systems is discussed, with particular focus on the symmetry differences intrinsic to strain in the two systems. Resulting differences in expectations for elastocaloric effect measurements are outlined. Results are presented from elastocaloric effect measurements on the cubic ferroquadrupolar-ordered compound $PrTi_2Al_{20}$. Dependencies on temperature and strain are compared to expectations, and limitations of the measurement noted. Improvements are proposed to allow for more exact quantitative comparison.

## 5.3 Introduction

Electronic nematic phases, or phases in which the electrons break rotational symmetries without breaking translational symmetries, have been widely examined as both present and potentially relevant in high-temperature superconductors and as a potential or proven order parameter in many localized 4f or 5f systems. While a potential role for nematicity has been suggested for cuprate superconductors [34], it is well-documented in many iron-based superconductors [35, 36], with FeSe in particular realizing only a nematic phase outside of the superconducting state [37]. In 4f and 5f systems, nematic order parameters, such as quadrupoles, are often the natural result of orbital degeneracy imposed by the CEF potential surrounding the 4f ion, including simple examples of a Jahn-Teller effect.

Symmetry-breaking strain has proven to be a highly useful tuning parameter within tetragonal systems, both as a conjugate field [33] and a transverse field [23] to a nematic order parameter. Susceptibility measurements, using strain to measure a nematic susceptibility, have proven particularly useful, by bypassing domain physics and generally allowing an examination of an ordered state above an ordering temperature. The elastocaloric effect, in particular, has been recently employed to great success as a strain-based thermodynamic probe in iron pnictide systems [33].

It is then natural to ask how such techniques might be applied to systems of other symmetries, such as cubic materials. Effects of symmetry-breaking strains have been somewhat less thoroughly studied in systems of higher symmetry. Here, we motivate and demonstrate the application of symmetry-resolved strain measurements on the cubic intermetallic compound $PrTi_2Al_{20}$, and discuss how the interpretation of such data necessarily differs from the simpler tetragonal case.

## 5.4 Irreducible Representations of Strain in Cubic and Tetragonal Systems

Symmetry-resolved strains have been used to great effect to probe and understand nematic order parameters in tetragonal systems. In straining these systems, a simple

Table 5.1: The six independent strain tensor components in the basis of irreducible representations, for $D_{4h}$ and $O_h$

| $D_{4h}$ | |
|---|---|
| $A_{1g}$ | $\epsilon_{zz}, \frac{\epsilon_{xx}+\epsilon_{yy}}{\sqrt{2}}$ |
| $B_{1g}$ | $\frac{\epsilon_{xx}-\epsilon_{yy}}{\sqrt{2}}$ |
| $B_{2g}$ | $\frac{\epsilon_{xy}+\epsilon_{yx}}{\sqrt{2}}$ |
| $E_g$ | $(\frac{\epsilon_{yz}+\epsilon_{zy}}{\sqrt{2}}, \frac{\epsilon_{zx}+\epsilon_{xz}}{\sqrt{2}})$ |

| $O_h$ | |
|---|---|
| $A_{1g}$ | $\frac{\epsilon_{xx}+\epsilon_{yy}+\epsilon_{zz}}{\sqrt{3}}$ |
| $E_g$ | $(\frac{2\epsilon_{xx}-\epsilon_{yy}-\epsilon_{zz}}{\sqrt{6}}, \frac{\epsilon_{yy}-\epsilon_{zz}}{\sqrt{2}})$ |
| $T_{2g}$ | $(\frac{\epsilon_{xy}+\epsilon_{yx}}{\sqrt{2}}, \frac{\epsilon_{yz}+\epsilon_{zy}}{\sqrt{2}}, \frac{\epsilon_{zx}+\epsilon_{xz}}{\sqrt{2}})$ |

bilinear coupling between a nematic order parameter and strain is often the dominant interaction, particularly above any extant ordering temperatures. This often allows the nematic component of more complex order parameters to be isolated and examined more carefully via the use of strain, probing nematic fluctuations directly and exclusively even in the presence of other interactions, such as magnetism.

It is then of interest to apply similar techniques and ideas to systems of different symmetries, such as the cubic systems we discuss here. Despite being of higher symmetry, however, the symmetry-imposed constraints on the effects of strains, based on their irreducible representations, are ultimately somewhat less stringent in cubic systems than their tetragonal equivalents, and behaviors forbidden in the latter must be accounted for and even expected in the former. More directly, the bilinear interaction between the strain and nematic order parameter no longer dominates, even well above any ordering temperature. This is perhaps best illustrated by briefly examining the symmetry decomposition of a given strain in both tetragonal and cubic systems.

As can be seen in Table 5.1, if one could apply a uniaxial strain $\epsilon_{xx}$ along the 100 axis in a tetragonal system, one will necessarily apply strains in two 'symmetry channels', $\epsilon_{A_{1g}}$ and $\epsilon_{B_{1g}}$.

$$\epsilon_{xx} = \frac{\epsilon_{A_{1g}} + \epsilon_{B_{1g}}}{\sqrt{2}} \tag{5.1}$$

The symmetry-breaking component of the strain belongs to $B_{1g}$, a one-dimensional irreducible representation. Practically, this means the system must behave similarly under a $B_{1g}$ strain of either sign; the difference between a positive and negative $B_{1g}$

Figure 5.1: Compressive and tensile strains in a tetragonal system, projected onto the basis of irreducible representations, via symmetric ($A_{1g}$, grey) and symmetry-breaking ($B_{1g}$, red/blue) components. The equivalence of the symmetry-breaking components (red and blue) is noted.

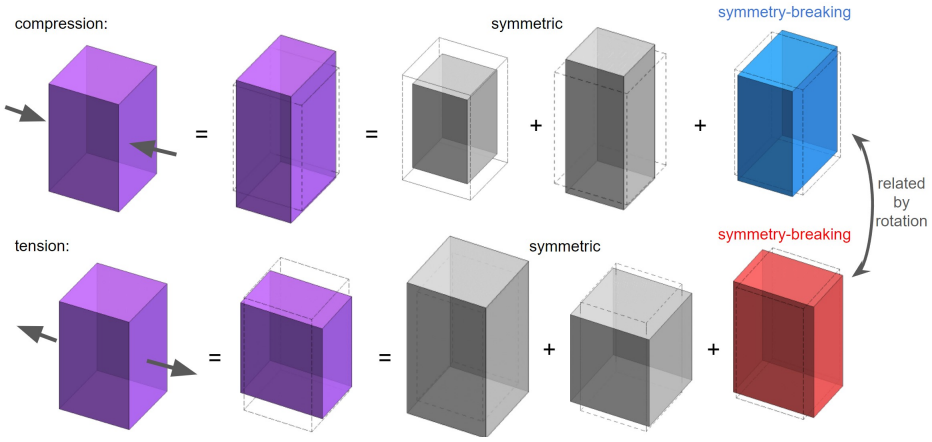


strain is merely a matter of convention, and they are physically indistinguishable. This is easily seen by comparing the two side by side; a rotation of the system turns one $B_{1g}$ strain into the other (Figure 5.1). Among other things, this implies that a $B_{1g}$ order parameter induced by the $B_{1g}$ strain must be odd as a function of the $B_{1g}$ strain; two strains of the same magnitude and opposite sign should invoke two order parameters of the same magnitude and opposite sign. This conveniently implies that all bulk thermodynamic quantities (temperature, entropy, free energy, etc.) must be even as a function of $B_{1g}$ strain. Any deviation from this behavior in any function of strain can then be assumed to be an effect of the $A_{1g}$ strain, rather than the $B_{1g}$ strain, and hence a decomposition of the effects of the two strains ($\epsilon_{A_{1g}}$ and $\epsilon_{B_{1g}}$) can be readily achieved. The $B_{1g}$ strain can couple bilinearly to a $B_{1g}$ order parameter, so it will generally have a much stronger effect than the $A_{1g}$ strain when both are applied simultaneously; $A_{1g}$ strain can only couple to even powers of the order parameter.

Similarly, via Table 5.1, the same strain $\epsilon_{xx}$ in a cubic system will induce strains of two symmetries, $\epsilon_{A_{1g}}$ and $\epsilon_{E_g}$.

$$\epsilon_{xx} = \frac{\epsilon_{A_{1g}} + \sqrt{2}\epsilon_{E_{g,1}}}{\sqrt{3}}$$

Here, the symmetry-breaking component of the strain, the $E_{g,1}$ component, belongs to a two-dimensional irreducible representation, where 1 signifies a direction within that 2D space, and is merely a choice of convention. For uniaxial strains, the relevant component will essentially always be $\frac{2\epsilon_{xx}-\epsilon_{yy}-\epsilon_{zz}}{\sqrt{6}}$, a volume-preserving deformation along the $x$ axis, for an $x$ axis defined as the strain axis. Symmetry does not protect the equivalence of a negative and positive strain here, as can be seen by the varying deformations such strain produces (Fig. 5.2); these shapes cannot be rendered equivalent with any rotation or other symmetry operation, and are thus not required by symmetry to be physically equivalent.

The symmetry constraints on functions of quantities belonging to the $E_g$ representation are somewhat more complicated, with the primary constraint being the 3-fold rotation within the $E_g$ subspace (Fig. 5.3), rather than an equivalence of positive and negative values of the order parameter. The symmetry-required equivalence is then between tensile strains along any primary axis or between compressive strains along any primary axis, but not between compressive and tensile strains along a given axis, even when the $A_{1g}$ strain component/effect is negligible or separated out. The lowest-order allowed terms in a Hamiltonian or Landau expansion imply that one sign of $E_{g,1}$ strain will induce a larger order parameter than a strain of similar magnitude and opposite sign; compressive or tensile strain will have a larger effect, though which causes a greater reaction is system-specific. In more mathematical terms, a coupling of strain to the square of the order parameter now exists for the symmetry-breaking strain, rather than just the $A_{1g}$ strain. This also means that distinguishing the effects of the $A_{1g}$ strain and $E_g$ strains is not as simple, though the $E_g$ strain will still generally have a more noticeable effect given its more direct interaction with a nematic order parameter.

It is worth briefly commenting on the existence of lines within the $E_g$ subspace for which order parameters are equivalent to their negative counterparts, the $y^2 - z^2$ axis within Figure 5.3, and its equivalents generated by the 3-fold rotation. Uniaxial stress along any primary crystal axis will necessarily only distinguish one axis from the other two; i.e., a stress along the x-axis distinguishes x from y and x from z, but does not break the equivalence of y and z. Hence, uniaxial stress will typically generate

Figure 5.2: Compressive and tensile strains in cubic systems, projected onto irreducible representations, via symmetric ($A_{1g}$, grey) and symmetry-breaking ($E_g$, red/blue) components. Note that even when the symmetry-preserving $A_{1g}$ component is separated out, the remaining symmetry-breaking $E_g$ strains are not equivalent.

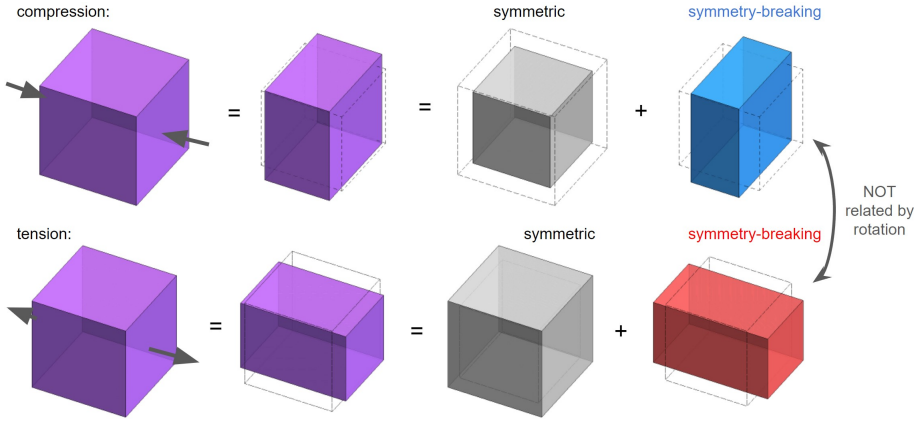


a strain of $2x^2 - y^2 - z^2$ symmetry; a strain of $y^2 - z^2$ symmetry would necessitate breaking additional symmetries. Applying stress along $y$ or $z$ would simply create strain of $2y^2 - z^2 - x^2$ or $2z^2 - x^2 - y^2$ symmetry, rather than the desired pure $y^2 - z^2$ character. This axis of equivalence is thus functionally experimentally inaccessible. The system will also never, barring a coincidence so extreme as to be functionally impossible, choose to order along these axes; the lowest-order symmetry-allowed terms will always favor an order parameter along the $2x^2 - y^2 - z^2$ type axes.

### 5.4.1 Susceptibility and complications

In tetragonal strain cases, the order parameter (quadrupole polarization, for example) is an odd function of the applied strain, and susceptibility can be measured via the slope of said function at the limit of zero strain. The linear relationship/approximation between the order parameter and the conjugate field is then often a reasonable approximation for a fairly wide range of applied strain. In the case of nematic order parameters belonging to higher-dimensional irreducible representations, including any bilinearly-strain-coupling order parameter in a cubic system,

Figure 5.3: A schematic diagram of the $E_g$ subspace, with axes labelled with appropriate basis functions. The locations of specific symmetry-breaking strains within this subspace are noted, with symmetrically equivalent strains having identical colors.

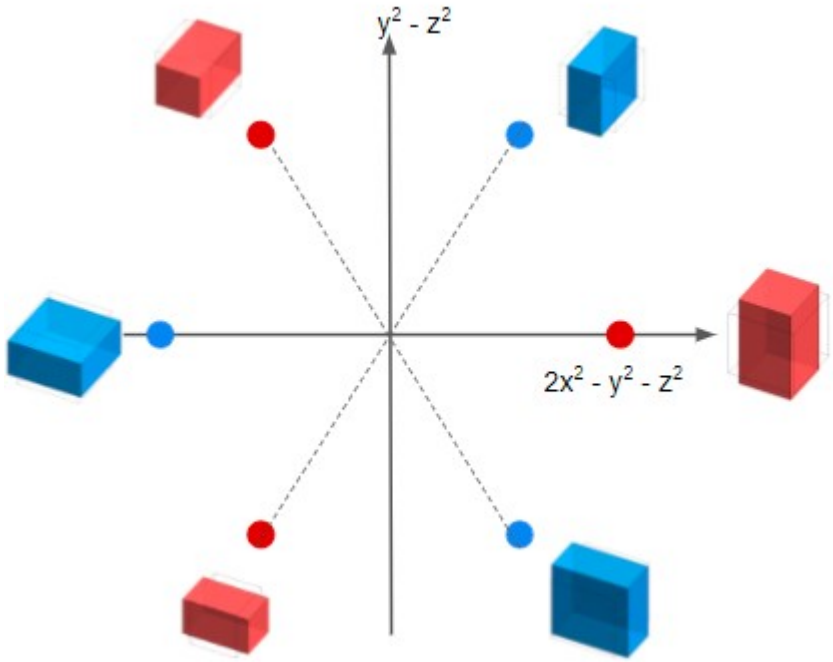


this is no longer a symmetry-protected property. The order parameter as a function of perturbing strain need no longer be odd, and thus the linear regime can be rendered essentially negligible by symmetry-allowed curvature. Most precisely, the second derivative of a nematic order parameter w.r.t. strain will be non-zero even at zero strain. Practically, this might mean that, for example, applying a tensile strain induces a large quadrupole moment, but applying a compressive strain of the same magnitude produces a much smaller quadrupole moment. While susceptibility can still be defined and measured via the derivative of quadrupole w.r.t. strain in the limit of zero strain, its predictive capacity for the value of the order parameter at any given temperature or field, and thus its usefulness, is greatly diminished, and the information is not sufficient to define even a heavily simplified Landau model. Crudely speaking, while the first derivative might represent the strength of quadrupolar fluctuations, the second derivative would contain information on the directional preference

within the 2D plane in which the quadrupolar moment must be represented; without the second derivative, susceptibility information would not even allow a complete description of a ferroquadrupolar ground state. With the behavior thus complicated (Fig. 5.4), a slightly more complex analysis is justified to more adequately describe potential nematic fluctuations and related behaviors.

Figure 5.4: Order parameter vs symmetry-breaking strain for tetragonal vs cubic systems.

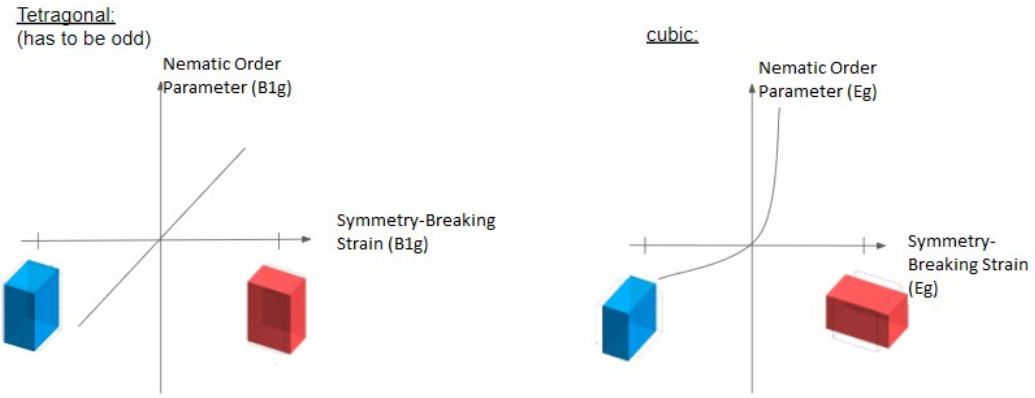


To add some mathematical rigor, a potential free energy can be constructed on the assumption of small strains, including all allowed terms up to linear order in strain and 3rd order in quadrupolar moment, with a 4th order bounding term.

$$F = \frac{a}{2}|Q|^2 - \lambda_1 \epsilon Q_x - \lambda_2 \epsilon (Q_x^2 - Q_y^2) - bQ_x(Q_x^2 - 3Q_y^2) + d|Q|^4 \tag{5.2}$$

Here, $Q_x$ and $Q_y$ represent the value of the quadrupole moment along the two axes of the two-dimensional order parameter space, with $x$ representing the axis in this space corresponding to our applied strain. We constrain ourselves to the singular strain most likely to be experimentally applied, for simplicity and given the difficulty of applying strain spanning the 2D space in one experiment. The terms of third order in $Q$ and/or $\epsilon$, namely those with $\lambda_2$ and $b$, would then influence the curvature of an order parameter vs strain plot, via influencing the preference for the aforementioned differing symmetry-breaking possibilities (red and blue in Fig. 5.3). More specifically, in the zero-strain limit, the second derivative would appear as:

$$\frac{d^2Q}{d\epsilon^2} \propto \lambda_2 - b\frac{\lambda_1}{a}$$

Here $b$ would represent directional preference within the $E_g$ subspace intrinsic to the system, and thus would indicate how the system would order within the subspace if it were cooled under no strain. Alternatively, $\lambda_2$ would represent how that preference might be changed with sufficient applied strain, potentially pushing the system from one preference to the other under sufficient strain if $\lambda_2$ were of appropriate sign.

### 5.4.2 $\Gamma_3$ Doublet as a Model System

$PrTi_2Al_{20}$ is motivated as a material to test ECE measurements in cubic systems by the characteristics of the $Pr^{3+}$ ion. For localized $4f$ electrons, spin-orbit coupling is usually strong enough to make $J$ a good quantum number, with the ground state $J$ value being separated from other $J$ values by thousands of Kelvin. The crystalline electric field then further splits this $2J + 1$ degenerate spin-orbit coupling ground state into smaller subsets based on the local symmetry around the rare-earth ion. In these systems, magnetism is often the dominant order parameter, or there is magnetic order nearby or directly coupling to other order parameters in the phase diagram. For the special case of $J = 4$, realized most readily in Praesodymium, the $\Gamma_3$ doublet is inevitably created by the CEF splitting in cubic systems, and can potentially be the ground state [14]. This ground state is a non-Kramers doublet that, to first order, cannot be split by magnetic field. This allows higher-order multipoles, like the electric quadrupoles that couple to strain, to dominate CEF-constrained magnetic competition. Thus, independent strain-coupling order parameters can be found and readily probed, creating a relatively simple model system for examination of higher-dimensional nematic order parameters.

## 5.5 Elastocaloric Effect

Herein we present data collected via AC Elastocaloric Effect measurements, via the technique of Ikeda et al [23, 33]. Strain is applied at a given frequency, high enough

such that the sample cannot fully thermalize with its surroundings, creating a quasi-adiabatic condition. If the entropy is strongly strain-dependent, the sample will necessarily undergo a temperature change to maintain constant entropy:

$$dS = \frac{\partial S}{\partial \epsilon} d\epsilon + \frac{\partial S}{\partial T} dT = 0 \tag{5.3}$$

$$\left(\frac{dT}{d\epsilon}\right)_S = -\frac{\partial S}{\partial \epsilon}\left(\frac{\partial S}{\partial T}\right)^{-1} = -\frac{\partial S}{\partial \epsilon}\frac{T}{C_V} \tag{5.4}$$

The temperature oscillations of the sample are then measured via a thermometer and lock-in amplifier set to the strain frequency. The desired susceptibility information is then contained within the $\frac{\partial S}{\partial \epsilon}$ term.

Strictly speaking, the technique applies a uniaxial stress, rather than the uniaxial strain discussed above, inducing strain along the orthogonal axes via the Poisson ratio of the material. However, this necessarily induces strain of the same irreducible representations as a uniaxial strain, merely in different proportions than a truly uniaxial strain would. The induced strains for a uniaxial x-axis stress would then be the same $A_{1g}$ and $E_g$ strains of a uniaxial x-axis strain. The $A_{1g}$ strain generally creates a relatively flat background w.r.t. offset strain, allowing the $E_g$ strain dependence to be extracted via the strain dependence of the elastocaloric signal. The sample deformation, $\frac{\Delta L}{L}$, used to quantify the strain (see section 2.2.4), will then represent the sum of these $E_g$ and $A_{1g}$ components.

It is then worth briefly noting that, due to the octahedral crystal habit, the strain here was applied along the [011] crystallographic axis, rather than [100], owing to the edges of the octahedral crystal facets being generally longer than [100] axes in partially-formed octahedra, and given that a certain minimum length is necessary for the elastocaloric measurements (approximately 1mm). This necessarily induces strain of the form $\epsilon_{yy} = \epsilon_{zz}$, and thus still induces an $E_g$ strain of $2x^2 - y^2 - z^2$ symmetry but opposite sign - where as [100] tension would induce a positive $E_g$ strain, [011] tension will instead induce a negative $E_g$ strain. This alternate stress axis then simply reduces the $E_g$ strain by a geometric factor (which varies with temperature via the elastic stiffness coefficients), with a $T_{2g}$ strain $\epsilon_{yz}$ inheriting some of the amplitude.

This $T_{2g}$ strain couples to a quadrupolar moment of similar symmetry, which cannot split the $\Gamma_3$ doublet; as such, the effect on the measurement is negligible, as verified in section 5.5.2.

### 5.5.1 ECE Thermodynamics

In tetragonal systems, ECE in the appropriate channel is proportional to $\frac{d\chi}{dT}$ for a nematic susceptibility $\chi$. This can be demonstrated most simply in the case of a quadrupole order parameter, the onset of which represents a tetragonal-to-orthorhombic phase transition:

$$F = \frac{a}{2}Q^2 - \lambda\epsilon Q \tag{5.5}$$

where $a$ is assumed to be of the form $a_0(T - T*)$ as is typical of Landau models. Minimizing the free energy to solve for the quadrupolar moment $Q$ yields the simple result

$$F = -\frac{(\lambda\epsilon)^2}{2a} \tag{5.6}$$

from which entropy $S = -\frac{dF}{dT}$ can be calculated, allowing the $\frac{\partial S}{\partial \epsilon}$ of the elastocaloric signal to be approximated as

$$\frac{\partial S}{\partial \epsilon} = -\frac{d\chi_Q}{dT}\epsilon \tag{5.7}$$

where the quadrupolar (nematic) susceptibility $\chi_Q = \frac{\lambda}{a}$. The elastocaloric effect is thus expected to be linear w.r.t. strain for some finite strain range over which the simplest Landau model is appropriate, with the slope of this line representing a temperature derivative of the quadrupolar susceptibility.

The cubic equivalent free energy (equation 5.2) evades such simple solutions, as the solution involves a higher-order polynomial with multiple roots, each of which may or may not be the minimum at a given temperature and strain. With the equivalence between positive and negative strains broken, however, the first-order adaptation of the tetragonal is an extra term in $\frac{\partial S}{\partial \epsilon}$. The equivalence in tetragonal

systems mandates entropy be an even function of symmetry-breaking strain, and thus that $\frac{\partial S}{\partial \epsilon}$ be an odd function in strain, with a leading-order linear term and no quadratic term. Without this constraint, $\frac{\partial S}{\partial \epsilon}$ necessarily includes both a linear and quadratic term, giving significant curvature to the measured result. Given the zero-strain point is often a non-trivial point to locate, given the varying thermal contractions of the sample and the strain cell, this makes it especially difficult to isolate the linear component.

### 5.5.2 Expectations and Calculations

With the basic allowed interactions established, it is worth examining how this might affect potential outcomes. Simple mean field calculations can be performed using a model Hamiltonian (computationally simpler than a Landau model), motivated by the method of Taniguchi et al [38] in their approach to magnetic field based measurements of the same material. Such a Hamiltonian then includes similar terms to the aforementioned Landau model:

$$H = H_{CEF} - \epsilon Q_x - \lambda_1(\langle Q_x \rangle Q_x + \langle Q_y \rangle Q_y) - \lambda_2 \epsilon(\langle Q_x \rangle Q_x - \langle Q_y \rangle Q_y) \tag{5.8}$$

where $H_{CEF}$ represents the crystalline electric field for $PrTi_2Al_{20}$, via Sato et al, [16], $\epsilon Q_z$ represents the allowed bilinear coupling between strain and the order parameter, the $\lambda_1$ term represents a (uniform) mean-field coupling within the two-dimensional order parameter space, and $\lambda_2$ represents the allowed coupling discussed in the previous section. With $Q_x$ and $Q_y$ representing quadrupoles of the aforementioned $2x - y^2 - z^2$ and $y^2 - z^2$ symmetries respectively, they are then represented by $\frac{1}{8}(2J_x^2 - J_y^2 - J_z^2)$ and $\frac{\sqrt{(3)}}{8}(J_y^2 - J_z^2)$ respectively. The expected values for the quadrupolar moments can then be calculated using a simple convergence procedure. Values are proposed for the expectation values, $\langle Q_x \rangle$ and $\langle Q_y \rangle$, the resulting Hamiltonian is diagonalized, and the thermal expectation values calculated, with the new values being input into the process once again until the calculated output $\langle Q_x \rangle$ and

$\langle Q_y \rangle$ converge to the inputs; these values are then taken to represent the order parameter for whatever given temperature and strain ($\epsilon$) were used in the calculation. The final Hamiltonian could then be used to calculate a partition function, and by extension an entropy value. Entropy calculated across a range of temperatures and strains could then be used to approximate entropy derivatives with respect to these variables, allowing an expected elastocaloric effect result to be found for a variety of strains and temperatures.

For expediency of calculation, $\epsilon$ was written in terms of Kelvin, incorporating the relevant coupling constant, given the calculation cares only for the product $\lambda\epsilon$ and not for either factor individually. $\lambda_1$ was then set to 2K to create a ferroquadrupolar order at approximately 2.2K, reminiscent of the material in question, and $\lambda_2$ could be varied to see the effects on the order parameter. The resulting behavior across strain, temperature, and $\lambda_2$ values are then most easily seen via plots of the calculated elastocaloric signal vs strain (Figure 5.5). Most notable is the asymmetry of the expected elastocaloric effect as a function of strain. The simplest result then, assuming higher order effects are generally negligible, i.e. $\lambda_2 = 0$, is then a relatively non-symmetric response, with a much larger effect for one sign of strain, induced primarily via the CEF anisotropy. A more symmetric response, rather than indicating that the varying cubic effects are negligible, would then indicate higher-order effects are relatively strong, and cancel out the intrinsic $E_g$ quadrupole anisotropy of the CEF.

Discontinuities in the calculated results are then indicative of spontaneous symmetry-breaking phase transitions, generally inspired by strain pushing the system strongly towards the disfavored order parameter; the symmetry is then spontaneously broken (from tetragonal to orthorhombic) to allow the order parameter to relax within the $E_g$ subspace towards a more energetically favorable order parameter (in Figure 5.3, one of the two red deformations located on either side of the blue deformation along the strain axis, for example, or vice versa).

It is worth noting that the calculation here neglects the effects of $A_{1g}$ strain, necessarily induced in any uniaxial stress measurement. The aforementioned effects of the $T_{2g}$ strain, $\epsilon_{yz}$, can be incorporated into the Hamiltonian on the assumption of similar coupling constants, i.e. $\epsilon Q_x$ becomes $\epsilon(Q_x + Q_{yz})$, where $Q_{yz}$ represents the

$T_{2g}$ quadrupole $(J_yJ_z + J_zJ_y)$, and no additional strain term $\epsilon$ need be added given we assume the two strains scale in parallel. Doing so changes the end result by no more than 1%, verifying the original assumption regarding the negligible effect of a $T_{2g}$ strain of similar magnitude to the $E_g$ strain, owing largely to the $T_{2g}$ quadrupole being CEF-forbidden.

Figure 5.5: Calculation with differing $\lambda_2$ terms for anticipated elastocaloric effect results (see equation 5.8), with temperatures ranging from 10K (red) to 3K (blue), for relevant strain ranges.

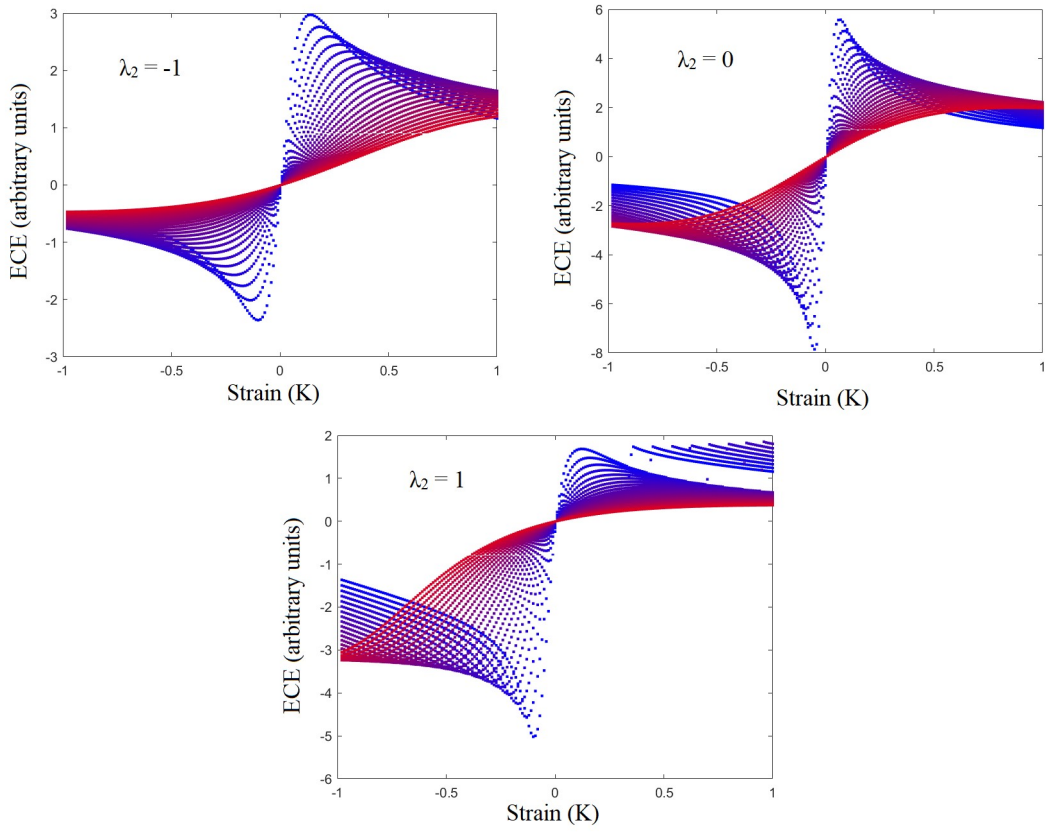


## 5.6 Results

As can be seen in Figure 5.6, the data follow the generally expected trend of a susceptibility-like curve proportional to the applied strain, with the maximum/rollover

Figure 5.6: Elastocaloric effect vs temperature for a variety of offset strains.

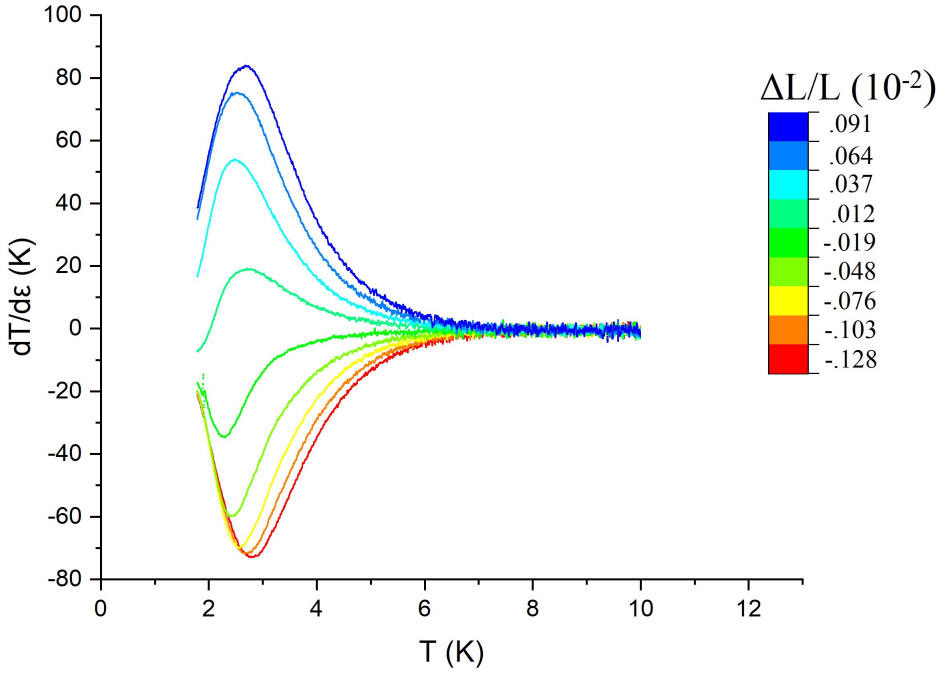


likely being attributable to the onset of the phase transition and/or crossover and ensuing domain formation. While the functional form is not particularly close to a Curie Law for reasons both experimental and theoretical, the result nonetheless indicates that a quadrupole strain-susceptibility can be readily measured in the system, while asymmetry of the curves w.r.t. strain indicates the aforementioned cubic terms. Note that zero strain is an approximation; the most accurate means of identifying the zero strain is generally the zero in the signal, as the elastocaloric response to the symmetry-breaking strain is there mandated to be zero, but the aforementioned $A_{1g}$ background will necessarily shift this, and will generally vary with temperature.

With elastic stiffness coefficients, and thus the relative proportions of $E_g$ and $A_{1g}$ strain, shifting with temperature, it is motivated to probe the strain dependence, rather than the temperature dependence, in deriving any conclusions regarding the material. To this end, the signal was recorded as a function of strain at a variety of

Figure 5.7: Elastocaloric oscillation vs strain, for a variety of (constant) temperatures.

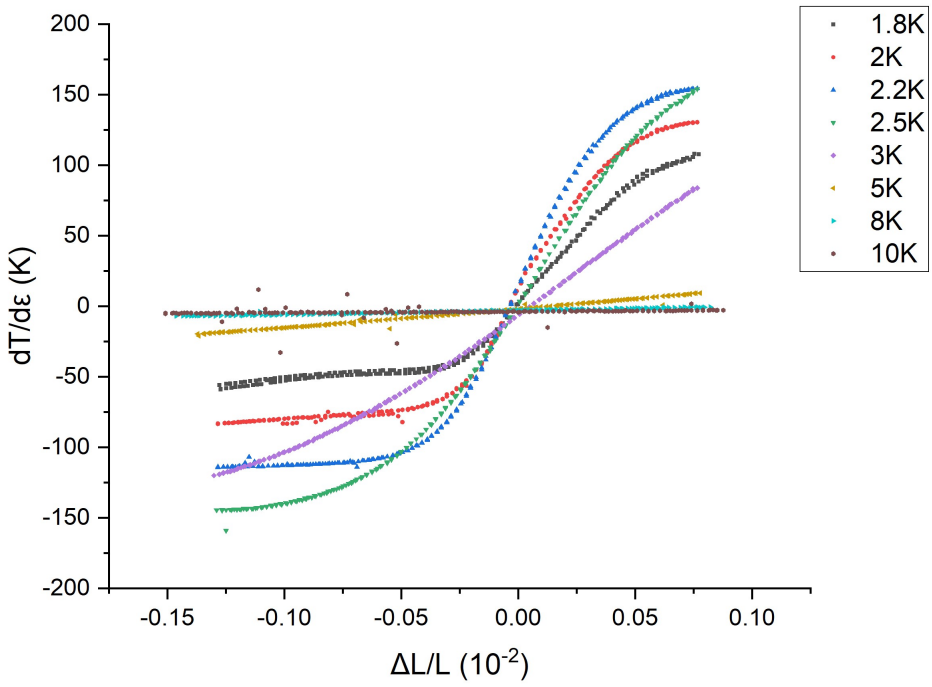


static temperatures (Figure 5.7). The anisotropy in the signal is visible, and can be compared to calculated expectations. Note that the (first-order) phase transition is anticipated at approximately 2K [12], and so measurements at the lowest temperatures may probe domain movement, rendering them less ideal for comparison to the calculated expectations. Based on Figure 5.5, the material is then likely possessed of a $\lambda_2$ coefficient that is small and negative, as the anisotropy is slightly less than the CEF-induced anisotropy predicted by the simplest model; the signal on the dominant side has only 35% higher amplitude than that of the disfavored side at 2.2K, where both maxima are most visible, as opposed to roughly 54% in the simplest model at 3K. More precise statements, however, are limited by the imperfect adiabaticity and somewhat limited strain range achieved.

### 5.6.1 Limitations

As can be seen in Figure 5.8, the frequency dependence of the ECE signal undergoes significant changes as both temperature and offset strain are changed. Changes in the maximum of the signal, in particular, necessarily imply changes to at least one of the two relevant thermalization timescales $\tau_i$ and $\tau_\theta$ discussed in section 2.2.6. The resulting shifts then induce a change in the magnitude of the thermal transfer function $T_\theta(t)$ as a function of strain and temperature, both at constant frequency and at the maximum frequency, which are not trivially separated from the dependencies of the intrinsic material response on strain and temperature. Precise quantitative statements are thus difficult to make. This limitation is, however, a tractable problem, with improvements to thermometry and (thermal) contact to the sample potentially allowing $\tau_\theta$ to be reduced, and the frequency dependence resolved into a reasonably flat plateau. In such a scenario, a large swathe of frequencies have approximately equivalent ECE amplitudes, and small perturbations to $\tau_i$ or $\tau_\theta$ do not affect amplitudes of frequencies well within the plateau.

The strain range was additionally insufficient to reach the maximum amplitude in the elastocaloric signal w.r.t. positive strains, limiting the potential to probe the order parameter anisotropy and search for potential phase transitions, whose locations in strain and temperature space would provide information unaffected by the frequency dependence issue. This, however, is also a tractable problem; crystals of adequate size and quality could be strained along the [100] axis, rather than the [011] axis, where the resulting increased $E_g$ strain component for any given total strain would allow greater $E_g$ strain to be applied before the sample begins to mechanically fail.

## 5.7 Conclusions

The data suggests that the strain susceptibility is measurable and diverging. Somewhat lower than expected anisotropy of the $E_g$ order parameter response suggests that the interactions probed by Taniguchi et al [38] may have measurable strain analogues, which could have a significant impact on the behavior under high strain.

Figure 5.8: Frequency dependence of the elastocaloric effect at several temperatures and offset strains. Note the movement of the frequency of maximum signal.

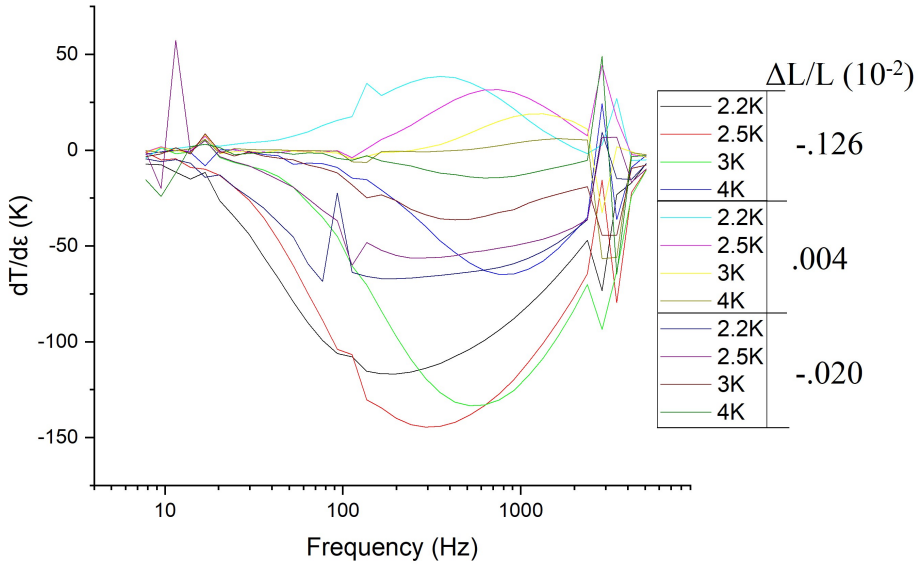


Unfortunately, measurement shortcomings preclude attempting to fit a more precise and specific phenomenological model to describe this behavior, or to more fully probe it across a wider range of parameters. All issues, however, are solvable problems with thermometry or crystal growth, and the technique thus demonstrates potential to illuminate significant information on anisotropic multi-dimensional quadrupolar order parameters. The measurement is adequately sensitive to detect the increasing quadrupolar fluctuations at temperatures well above the ordering temeprature. Observed order-parameter anisotropy, while in this case expected via the known CEF splitting of the material, could potentially be used in other materials to identify the sign of the order parameter, and could even provide significant information on CEF schemes in other materials, given the CEF is a prime driver of anisotropy within the order parameter space. The necessary experimental optimizations are thus highly motivated by the unique information potentially provided by the technique.

# Chapter 6

# Conclusion

## 6.1 Outlook

This thesis has sought to develop techniques to probe higher-order multipolar susceptibilities, most notably those that may not have readily available single conjugate fields, such as the magnetic octupole, and those that exist in multi-dimensional spaces, such as the cubic $\Gamma_3$ quadrupole; many techniques have been discussed, and the elastocaloric effect in particular was utilized to demonstrate the relevant principles. These techniques were developed in the context of the model systems $PrV_2Al_{20}$ and $PrTi_2Al_{20}$, systems possessing the unique $\Gamma_3$ doublet ground state capable of hosting such higher-order multipoles. It is thus worth briefly discussing potential future directions for technique development, study of the specific materials in question, and potential applications for such susceptibility measurements in other materials.

### 6.1.1 Elastocaloric Effect Improvements

Two obvious areas for improvement present themselves in the elastocaloric effect measurements herein used: imperfections in the adiabatic condition, and lack of heat capacity data across the space of potential parameters (most notably strain) with which to normalize the signal.

For the adiabatic condition, as discussed in section 2.2.6, there exist two timescales,

with $\tau_i = \frac{C_s}{K_i}$ representing heat flow within the sample, which sets a lower bound on viable measurement frequencies, and $\tau_\theta = \frac{C_\theta}{K_\theta}$, which represents thermalization of the thermometry within the sample and sets an upper bound on viable measurement frequencies. With $\tau_i$ being primarily intrinsic to whatever material is of interest, $\tau_\theta$ is then the experimental parameter which must be optimized, and specifically minimized, to more perfectly achieve the adiabatic condition. Potential areas for future improvement include thin film thermometry deposited directly onto the sample, via sputtering, lithography, or any of the other usual techniques, as initially suggested by Matthias Ikeda [23] and elaborated upon in unpublished talks; such thermometry could have substantially reduced heat capacity ($C_\theta$) by virtue of greater thinness than any pre-fabricated thermometry, alongside dramatically enhanced thermal conductivity via direct thermal contact across a large surface of the sample.

Heat capacity, used to normalize the elastocaloric data and exactly calculate $\frac{\partial S}{\partial \epsilon}$ via Equation 2.2, is then the other major limitation of the technique. While zero-strain heat capacity can be used as an approximation, as discussed in chapter 4, a more exact correction would require heat capacity as a function of strain. To this end, the work of Y.S. Li et al [39], wherein AC heat capacity is utilized to probe a strained sample, presents an excellent counterpart to the elastocaloric effect. While such a measurement would likely need to be done separately, the pairing of the two measurements would allow a complete entropy landscape, as a function of strain, temperature, and potentially magnetic field, to be mapped out for any given material, fully realizing the potential of the elastocaloric effect to probe strain-induced changes in entropy.

### 6.1.2 Further Material Applications

The techniques herein developed could be quite helpful in elucidating the nature of many 'hidden' orders. $URu_2Si_2$ presents itself as the prototypical example, with the magnetic octupole being one of many proposed order parameters [3]. Other, less-well-studied materials, however, may provide better opportunities, including additional cubic $Pr^{3+}$ compounds. $PrFe_4P_{12}$, for example, has a ground state of some interest;

while some evidence exists of an anti-ferro quadrupolar ordering at approximately 6K [40], other measurements explain a different, high-field ordered state via a $\Gamma_1$ singlet ground state and $\Gamma_4$ excited state [41]. While explanations have been proposed for the quadrupolar order within the $\Gamma_1$ ground state scenario via admixture of the excited state [42], the exact nature of the ground state remains a matter of some contention [43]; susceptibility measurements could help determine the exact broken symmetries, or find evidence of anti-ferro order parameters via behaviors of ferro-type susceptibilities.

$PrOs_4Sb_{12}$, another cubic $Pr^{3+}$ compound, then presents itself as a material with one [44] or two [45] superconducting transitions, depending on the literature referenced. While the susceptibility measurements developed herein are not an ideal probe for the superconducting states themselves, they could be used to identify or rule out fluctuations in specific symmetry channels, potentially narrowing the potential symmetries for pairing mechanisms. Fluctuations in multiple channels, with susceptibilities diverging at different temperatures, could even potentially identify symmetry differences between the two superconducting states, should they both prove intrinsic.

More broadly, susceptibility measurements targeting higher-order multipoles offer a means to systematically examine multipoles and their corresponding symmetry channels. Hidden order parameter candidates can thus be methodically tested and potentially ruled out, providing the sort of detailed symmetry information that has historically been difficult to acquire.

## 6.2 Concluding Remarks

This dissertation aimed to expand the susceptibility paradigm to examine higher-order multipoles, and has offered several methods for doing so. Multiple means of probing the magnetic octupolar susceptibility were discussed, and one, the elastocaloric effect, was demonstrated and proven viable. Measurements of multi-dimensional quadrupoles were demonstrated and, despite current limitations, proven to be viable. This work thus offers foundations for probing more exotic multipoles, and expanding and generalizing one of the most powerful probes of magnetism, the susceptibility.

# Bibliography


[1] Y. Aoki et al. "Octupole ordering in filled-skutterudite SmRu4P12". In: *Physica B: Condensed Matter* 403 (2008), pp. 1574–1576.

[2] S.W. Lovesey et al. "Neptunium octupole and hexadecapole motifs in NpO2 directly from electric dipole (E1) enhanced x-ray Bragg diffraction". In: *Journal of Physics: Condensed Matter* 15 (2003), p. 26.

[3] Katsurou Hanzawa. "Hidden octupole order in URu2Si2". In: *Journal of Physics: Condensed Matter* 19 (2007), p. 7.

[4] Hiroaki Kusunose and Hisatomo Harima. "On the Hidden Order of URu2Si2 - Antiferro Hexadecapole Order and Its Consequences". In: *J. Phys. Soc. Jpn.* 80 (2011), p. 084702.

[5] Jun Kondo. "Resistance Minimum in Dilute Magnetic Alloys". In: *Progress of Theoretical Physics* 32 (1964), pp. 37–49.

[6] A Wörl et al. "Divergent thermal expansion and Grüneisen ration in a quadrupolar Kondo metal". In: *Phys. Rev. Research* 4 (2022), p. L022053.

[7] Koji Inui and Yukitoshi Motome. "Channel-selective non-Fermi liquid behavior in the two-channel Kondo lattice model under a magnetic field". In: *Phys. Rev. B* 102 (2020), p. 155126.

[8] M G Kin et al. "Character of the structural and magnetic phase transitions in the parent and electron doped BaFe2As2 compounds". In: *Phys. Rev. B* 83 (2011), p. 134522.

[9] Samuel Lederer et al. "Superconductivity and non-Fermi liquid behavior near a nematic quantum critical point". In: *PNAS* 114(19) (2017), pp. 4905–4910.

[10] H. Kinder Armin Segmüller R.L. Melcher. "X-ray diffraction measurement of the Jahn-Teller distortion in TmVO4". In: *Solid State Comm.* 1 (1974), pp. 101–104.

[11] Elliott W. Rosenberg et al. "Divergence of the quadrupole-strain susceptibility of the electronic nematic system YbRu2Ge2". In: *PNAS* 116 (15) (2019), pp. 7232–7237.

[12] Akito Sakai and Satoru Nakatsuji. "Kondo Effects and Multipolar Order in the cubic PrTr2Al20 (Tr=Ti,V)". In: *J. Phys. Soc. Jpn.* 80 (2011), p. 063701.

[13] M. Tsujimoto, Y. Matsumoto, and S. Nakatsuji. "Anomalous specific heat behaviour in the quadrupolar Kondo system $PrV_2Al_{20}$". In: *J. Phys.: Conf. Ser.* 592 (2014), p. 012023.

[14] K.R. Lea, M. J. M. Leask, and W. P. Wolf. "The raising of angular momentum degeneracy of f-electron terms by cubic crystal fields". In: *J. Phys. Chem. Solids* 23 (1962), pp. 1381–1405.

[15] Daisuke Okuyama et al. "Crystal Structure in Quadrupolar Kondo Candidate PrTr2Al20 (Tr = Ti and V)". In: *J. Phys. Soc. Jpn.* 88 (2019), p. 015001.

[16] Taku J Sato et al. "Ferroquadrupolar ordering in PrTi2Al20". In: *Phys. Rev. B* 86 (2012), p. 184419.

[17] K Araki et al. "Magnetization and Specific Heat of the Cage Compound PrV2Al20". In: *JPS Conf. Proc.* 3 (2014), p. 011093.

[18] Minoru Koseki et al. "Ultrasonic Investigation on a Cage Structure Compound PrTi2Al20". In: *J. Phys. Soc. Jpn.* 80 (2011), SA049.

[19] Mingxuan Fu et al. "Unveiling Quadrupolar Kondo Effect in the Heavy Fermion Superconductor PrV2Al20". In: *J. Phys. Soc. Jpn.* 89 (2020), p. 013704.

[20] Akito Sakai, Kentaro Kuga, and Satoru Nakatsuji. "Superconductivity in the Ferroquadrupolar State in the Quadrupolar Kondo Lattice PrTi2Al20". In: *J. Phys. Soc. Jpn.* 81 (2012), p. 083702.

[21] Masaki Tsujimoto et al. "Heavy-Fermion Superconductivity in the Quadrupole Ordered State of PrV2Al20". In: *Phys. Rev. Lett.* 113 (2014), p. 267001.

[22] Paul C Canfield et al. "Use of frit-disc crucibles for routine and exploratory solution growth of single crystalline samples". In: *Philosophical Magazine* 96:1 (2015), pp. 84–92.

[23] M.S. Ikeda et al. "AC elastocaloric effect as a probe for thermodynamic signatures of continuous phase transitions". In: *Rev. Sci. Instrum.* 90 (2019), p. 083902.

[24] A. S. Patri et al. "Unveiling hidden multipolar orders with magnetostriction". In: *Nat. Commun.* 10 (2019), p. 4092.

[25] M. Tsujimoto, Y. Matsumoto, and S. Nakatsuji. "Anomalous specific heat behaviour in the quadrupolar Kondo system PrV2Al20". In: *Journal of Physics: Conference Series* 592 (2015), p. 1.

[26] M. C. Shapiro et al. "Symmetry constraints on the elastoresistivity tensor". In: *Physical Review B* 92(23) (2015), p. 235147.

[27] M. C. Shapiro et al. "Measurement of the B1g and B2g components of the elastoresistivity tensor for tetragonal materials via transverse resistivity configurations". In: *Rev. Sci. Instrum.* 87(6) (2016), p. 063902.

[28] Clifford W. Hicks et al. "Piezoelectric-based apparatus for strain tuning". In: *Review of Scientific Instruments* 85 (2014), p. 065003.

[29] Frederic Freyer et al. "Two-stage multipolar ordering in Pr(TM)2Al20 Kondo Materials". In: *Phys. Rev. B* 97 (2018), p. 115111.

[30] SangEun Han, Daniel J. Schultz, and Yong Baek Kim. "Non-Fermi liquid behavior and quantum criticality in cubic heavy fermion systems with non-Kramers multipolar local moments". In: *Phys. Rev. B* 106 (2022), p. 155155.

[31] Masaki Tsujimoto et al. "Heavy Fermion Superconductivity in the Quadrupole Ordered State of PrV2Al20". In: *Phys. Rev. Lett.* 113 (2014), p. 267001.

[32] Matthew E. Sorensen and Ian R. Fisher. "Proposal for methods to measure the octupole susceptibility in certain cubic Pr compounds". In: *Phys. Rev. B* 103 (2021), p. 155106.

[33] M.S. Ikeda et al. "Elastocaloric signature of nematic fluctuations". In: *Proc. Natl. Acad. Sci. USA* 118(37) (2021), e2105911118.

[34] B Keimer et al. "From quantum matter to high-termperature superconductivity in copper oxides". In: *Nature* 518 (2015), pp. 179–186.

[35] Thanapat Worasaran et al. "Nematic quantum criticality in an Fe-based superconductor revealed by strain-tuning". In: *Science* 372(6545) (2021), pp. 973–977.

[36] Hsueh-Hui Kuo et al. "Ubiquitous signatures of nematic quantum criticality in optimally-doped Fe-based superconductors". In: *Science* 352(6288) (2016), pp. 958–962.

[37] Sahana Rößler et al. "Nematic state of the FeSe superconductor". In: *Phys. Rev. B* 105 (2022), p. 064505.

[38] Takanori Taniguchi et al. "Field-Induced Switching of Ferro-Quadrupole Order Parameter in PrTi2Al20". In: *J. Phys. Soc. Jpn.* 88 (2019), p. 084707.

[39] Y.-S. Li et al. "Heat-capacity measurements under uniaxial pressure using a piezo-driven device". In: *Rev. Sci. Instrum.* 91 (2020), p. 103903.

[40] L Hao et al. "Neutron scattering studies of order parameters and excitations in antiferro-quadrupolar phase of PrFe4P12". In: *Physica B* 359-361 (2005), pp. 871–873.

[41] Takashi Tayama et al. "New High-Field Ordered State in PrFe4P12". In: *J. Phys. Soc. Jpn.* 73(12) (2004), pp. 3258–3261.

[42] A Kiss and K Kuramoto. "Model for multiple ordered phases induced by magnetic field in PrFe4P12". In: *Physica B* 378-380 (2006), pp. 248–249.

[43] Tian Le et al. "Fermi surface gapping in the hidden order state of PrFe4P12 by point-contact spectroscopy". In: *Sci. China Phys. Mech. Astron.* 65 (2022), p. 237412.

[44] M-A Measson et al. "Double superconducting transition in the filled skutterudite PrOs4Sb12 and sample characterizations". In: *Phys. Rev. B* 77 (2008), p. 134517.

[45] B Andraka and K Pocsy. "Evidence for intrinsic superconductivity at Tc1 in PrOs4Sb12". In: *J. Appl. Phys.* 111 (2012), 07E115.